A numerical study of the frictional dependence on the sliding velocity

Andreas Birkeli

1st September 2009

Contents

1 Motivation **5**

2 Theory **7**
2.1 Elementary theory on dynamic and static friction 7
2.1.1 Historical 7
2.1.2 The adhesion theory of friction 8
2.2 The rate and state variable friction laws 9
2.3 An experimental study of the real area of contact between a block and a substrate 12
2.4 Elastic instability transition 12

3 Modelling **19**
3.1 The physical system 19
3.2 The slider 20
3.3 The base 22
3.4 The slider-base interaction 23
3.5 The slider-piston interaction 23
3.6 Applied load on the slider 24
3.7 The equation of motion for the slider particles 24

4 The numerical setup **27**
4.1 The sliding velocity v 27
4.1.1 Initialization of the simulations 28
4.2 The numerical algorithm 29
4.2.1 Initializations of the system 29
4.2.2 Loop over iterations 30
4.2.3 Calculate the averaged dynamic coefficient of friction and ϵ 34
4.3 The physical and non-dimensional parameters for the simulations 35
4.3.1 Choosing the physical parameters 36

5 The topography of the base **39**
5.1 An analytical study of simple rough surfaces 39
5.2 Numerical test of the A_r dependence on N 42

6 Geometric friction **47**
6.1 Introduction 47
6.2 Analytical analysis of the $\mu(t)$ dependence for the model . . . 47
6.3 Testing the simulation program 49

7 Geometric sliding friction **57**
7.1 Introduction 57
7.2 Measuring μ 57
7.2.1 The $\mu(t')$ curve 57
7.2.2 Averaging methods for μ 60
7.3 Problems with oscillations in the piston slider interface 62
7.4 The early simulations of the dependence of μ on v 65
7.4.1 An early $\mu(v)$ simulation 66
7.5 Geometric sliding friction for a more realistic system 71
7.5.1 The spikes for low g. 75
7.6 Summary 88

8 Sliding friction with adhesion **89**
8.1 Introduction 89
8.1.1 Introducing adhesion at the junctions in the model . . 90
8.2 Constant adhesion 91
8.3 Time dependent adhesion 94
8.3.1 Stability problems when introducing time dependent adhesion 95
8.3.2 The simulation results 96
8.4 Summary 99

9 Conclusions and discussions of possible improvements to the slider model **101**
9.1 The dependence of μ on the the sliding velocity 101
9.2 The behavior of μ at low sliding velocity 102
9.3 Discussion of possible improvements to the slider model 103

Chapter 1

Motivation

Friction between materials is a practically important problem that has been studied for centuries. The laws of friction was first found by Leonardo da Vinci, but was later later rediscovered by Amontons and are known as Amonton's laws of friction [1]. The first law explains a linear relation between the force needed to obtain steady sliding and the normal force, where the constant of linearity is the coefficient of friction μ. Although this law gives a macroscopic description of the consequences of frictional interactions, the effects that determines the size of μ is not well understood in a physical point of view. Friction occurs over several length scales. It includes interactions at the molecular or atomic level, the interaction at so called asperities in contact, i.e. junctions and the macroscopic effect of many such junctions on the materials in contact.

Experiments conducted in the last century hows a velocity weakening effect on μ for small sliding velocities [2]. Other experiments shows that the maximum static frictional force increase with the time of stationary contact [3, 4]. For low sliding velocities an increase in the real area of contact A_r has been observed, and this has been shown to be because of asperity creep [11, 12]. Empirical formulas for the behavior of μ has been constructed and are known as *the rate state variable friction laws*.

In this project I address the questions of how the frictional force depend on the sliding velocity. Can asperity creep give a velocity weakening effect on μ for low sliding velocities, and a transition between static and dynamic friction?

In this project I will study a physical system where a block is pushed by a piston on a rough base. I will develop a discrete element method with next-nearest neighbor interactions, and interactions between the slider and the base. I will simulate sliding at different sliding velocities and study the resulting friction laws of the relation between the sliding velocity and μ. Two

different models for adhesion is also introduced to study the effect of adhesion on μ with and without time dependence of A_r.

I am most interested in the velocity dependence of μ. I don't try to predict the correct value of μ for the slider system since that would require to take into account several more frictional interactions than studied in this project.

Chapter 2

Theory

2.1 Elementary theory on dynamic and static friction

2.1.1 Historical

The laws of friction have been known as Amonton's laws of friction [1]

$$\begin{array}{ll} F \propto N & \text{(1st law)} \\ F \text{ is independent of the apparent area of contact, } A & \text{(2nd law),} \end{array} \tag{2.1}$$

where F is the force of friction and N is the normal force. From Amonton's time through the time of Coulomb the importance of roughness on friction was recognized, and friction was assumed to be caused by various interactions at the points of contacts between surfaces, called *asperities*. The asperities was viewed as acting as either rigid or elastic springs. In the first case friction was assumed to be caused by the gravitational work done when asperities rode up on another. In the other case the elastic bending of asperities which was expected to increase with load was used as an explanation of the frictional force. The difference between static and dynamic friction was also recognized, and Coulomb noticed particularly for wooden surfaces that the static frictional force increased with the time of contact. He explained the observation by imagining that the surfaces was covered by bristles. When the two surfaces came in contact, the bristles interlocked, a process that became more pronounced with increasing time of contact. Coulomb found that the coefficient of friction μ is usually nearly independent of N, A, the surface roughness, and the sliding velocity v as long that it is not too high or too low.

The weakness of these early theories is that they failed to describe frictional wear and to account for the energy dissipated during friction. Asperity shearing is today expected to be important in both these cases. In addition the early models could not give a correct explanation of why μ is independent of the apparent area of contact.

2.1.2 The adhesion theory of friction

The modern concepts of friction is generally attributed to Bowden and Tabor [5, 6]. They envisioned all real surfaces as having a topography. Most real surfaces have a roughness of many different length scales, thus when a block is put on a substrate, the actual contact area will not be the whole apparent or geometric area A of the contacting surfaces. The block only touches the substrate at a few points, called asperities or junctions. The sum of all these asperities is the real area of contact A_r, and it is generally much smaller than A. When the block is lowered towards the substrate the first contact between the two will be a single junction where the perpendicular pressure will become so high, i.e. it exceeds the Yield strength of the softest material in contact, that it will give rise to a local plastic deformation. They assumed that when the block is lowered further, more junctions would form until A_r is large enough so that the load N is balanced by the contact pressure integrated over A_r. The junctions would now be in a state of incipient plastic flow, i.e. the stress at the junctions equals the penetration hardness p of the softer material in contact, where p is the maximum stress the material can bear without plastic yielding, thus

$$N = pA_r. \tag{2.2}$$

p is a material property which has been measured for a large number of materials using indentation experiments. Bowden and Tabornow assumed that because of the very high compressive stress at the junctions, adhesion occurred there, welding the two surfaces together. In order to initiate slip these junctions would have to be sheared through, so that the friction force is the sum of the shear strength of the junctions,

$$F = sA_r, \tag{2.3}$$

where s is the shear strength of the material. Note that the assumption Eq. 2.3 implies that F increases linearly with A_r.

Using the standard formulation of the coefficient of friction μ, Eq. 2.2 and Eq. 2.3, they found that

$$\mu = \frac{F}{N} = \frac{s}{p}. \tag{2.4}$$

Eq. 2.4 is just the ratio between two different measures of strength for a material, being that of the softer if two different materials are brought in contact.

If either Eq. 2.2 or Eq. 2.3 is violated, so is Eq. 2.4 since it relies on these two assumptions. An example of a dramatic exceptions from Eq. 2.4 is the use of various types of lubrication on the interface between the two surfaces.

Even without lubrication layers, Eq. 2.4 in most cases does not predict the correct value of μ. This is because overcoming junction adhesion is usually not the only work done in friction. Asperities often plough trough the surface in contact, or interlock. The deformations resulting from these interactions are not accounted for in Eq. 2.4. Plowing and wear will change the topography of the surfaces, thus even if Eq. 2.2 is true for newly prepared surfaces, it may no longer be true after repeated sliding. It is unlikely that A_r is determined by irreversible plastic deformation the millionth time the same blocks make contact, thus finally mainly elastic deformations will occur in the contact areas. In normally brittle materials like rock, it may be argued that Eq. 2.2 is violated because asperities may fail by brittle fracture rather than plastic yielding. When studying the friction for a given range of materials one therefore need to take into account the deformation mechanisms that are specific to those materials for the given range of conditions. In this case temperature is also a parameter. These complications makes Eq. 2.4 best viewed only as a conceptual framework.

From the above arguments it becomes evident that giving accurate measures of the coefficient of friction is difficult because of the high number of effects that needs to be accounted for.

2.2 The rate and state variable friction laws

In Section 2.1.2 I explained that Eq. 2.4 failed to predict the correct value of μ. Another problem with Eq. 2.4 is that it fails to describe stick-slip motion. If there are variations in the frictional force during sliding, instabilities can occur. Stick slip is caused by a sudden slip with an associated stress drop, followed by a period of no motion where the stress is recharged. When this process is repeated, the behavior is called regular stick slip.

Suppose that a piston pushes a block using a spring off stiffness k, and that that the block is initially stationary. When the piston moves towards the block, the frictional force F between the block and the base increases. Eventually the slider will begin to move. An instability would now occur if

F decreases faster with the slip length u than k, i.e.

$$\left|\frac{dF}{du}\right| > k. \tag{2.5}$$

Such a decrease in F with u is known as slip weakening. Note that the instability Eq. 2.5 is dependent both on the elastic properties of the spring, k, and the friction on the block.

For regular stick slip to occur, a mechanism for the frictional force to regain it's prior level is needed, a mechanism called a *healing mechanism*. This healing mechanism was first found by *Rabinowicz* [3, 4]. Rabinowicz observed that if two surfaces are held in stationary contact,the static coefficient of friction μ_s would increase approximately logarithmically with the time of contact t. Rabinowicz also observed that there is a critical slip distance D_c before μ_s would break down to the dynamic value and that D_c was approximately the size of the contact junctions. Rabinowicz also observed that the coefficient of sliding friction μ_d decreased with the sliding velocity v for steady low v.

The time t two junctions are in contact is inversely proportional to the sliding velocity v, and thus the observations that μ_s increase with t and μ_d decrease with v seems consistent. However, experiments show that a simple velocity dependent relation on friction is not sufficient. In Fig. 2.1 the response of μ_d to a sudden change in v is shown. After a sudden increase in v μ rapidly increases to a higher level, a process called the direct effect, and then decays to a new stable value of μ_d lower than the initial value. The decay in μ_d after the sudden increase in v indicates that μ_d is not only dependent on the v.

Several empirical laws has been constructed, and the one presently in best agreement with experiments [2] is the Dieterich-Ruina law [7, 8]

$$\mu \equiv \mu(v,\theta) = \mu_0 + a\ln\left(\frac{v}{v_0}\right) + b\ln\left(\frac{v_0\theta}{D_c}\right), \tag{2.6}$$

where the state variable θ evolves as

$$\dot{\theta} = 1 - \left(\frac{v\theta}{D_c}\right). \tag{2.7}$$

In the static case $\theta = t$, and Dieterich [7] suggested that θ can be interpreted as the average age of contacts. The critical slip distance D_c is the sliding distance at constant velocity v the over which the contacts between the slider and the base is destroyed and replaced by an uncorrelated set, so that $\theta = D_c/v$. If we now set $\theta_0 = D_C/V_0$ so that μ_0 is the coefficient of friction at

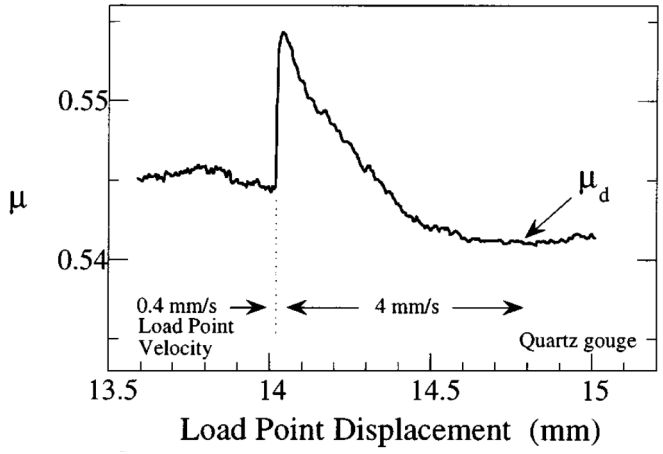

Figure 2.1: Data showing the response to a sudden increase of sliding velocity. Note that the new steady μ_d for $v = 4mm/s$ is lower than the old μ_d for $v = 0.4mm/s$. Figure from *C. Marone* [2]

a steady velocity v_0, we find that the coefficient of friction μ_{ss} at a steady state velocity v is

$$\mu_{ss} = \mu_0 + (a - b) \ln \left(\frac{v}{v_0} \right). \tag{2.8}$$

If we now define μ_d as μ_{ss}, we get that

$$\frac{d\mu_d}{d(\ln v)} = a - b. \tag{2.9}$$

In the static case Eq. 2.7 reduces to $\theta = t$ and thus for long hold times

$$\frac{d\mu_s}{d(\ln t)} = b. \tag{2.10}$$

If the loading mechanism is stiff and a sudden jump in v occurs the time elapsed for the slider to increase it's velocity from v_1 to v_2 is short compared to the age of the contacts $\theta_1 = D_c/V_1$, and thus the age can be considered constant. The frictional jump of the direct effect is therefore given by

$$\Delta\mu = a \ln \left(\frac{v_2}{v_1} \right). \tag{2.11}$$

The slip distance over which friction evolves from the direct effect to the steady state effect is determined by D_c. In laboratory samples D_c is in the micrometer range [9].

Baumberget et al. [10] proposed writing Eq. 2.6 in the form of the Bowden and Tabor equation, Eq. 2.3,

$$F = s(v)A_r(\theta), \tag{2.12}$$

where

$$A_r(\theta) = A_0 \left[1 + \beta \ln\left(\frac{\theta v_0}{D_c}\right)\right], \tag{2.13}$$

and

$$s(v) = s_0 \left[1 + \alpha \ln\left(\frac{v}{v_0}\right)\right]. \tag{2.14}$$

Eq. 2.13 states that the real area of contact A_r is not a constant for a given normal load which was assumed by Bowden and Tabor, see Eq. 2.2. Instead Eq. 2.13 states that A_r will increase logarithmically with the time of contact θ. This has shown to be because of asperity creep [11, 12].

2.3 An experimental study of the real area of contact between a block and a substrate

As presented earlier, the real area of contact A_r between a block and a substrate is generally much lower than the apparent contact area A. The normal load dependence on A_r has been investigated recently be *S. M. Rubinstein et al.* [13] for a block of PMMA on a PMMA base and PMMA on a glass base. A laser sheet was incident on the rough interface at an angle far beyond the angle for total internal reflection from the PMMA-air interface. Thus light can only traverse the interface at the actual points of contact or by tunneling across the surface. Neglecting tunneling effect, th transmitted light is therefore a direct measurement of the net contact area of each point.

In Fig. 2.2 and Fig. 2.3 some of their results for A_r as a function of N is presented. In Fig. 2.2 the two interfaces has an 50nm rms roughness and a large span in A_r/A is obtained. The figure reveals that the relation $A_r \propto N$ assumed in Eq. 2.2 is not valid for a large span in A_r/A, instead a linear relation between A_r and N seems to be valid for a small range in A_r/A. In fig Fig. 2.3 the two surfaces has a 500nm rms roughness and it seems that the relation $A_r \propto A_r$ is a good approximation when $A_r/A \ll 1$.

2.4 Elastic instability transition

In Section 2.1.2 I argued that friction is a combinations of various interactions and effects. In this section I present some simple models of the frictional

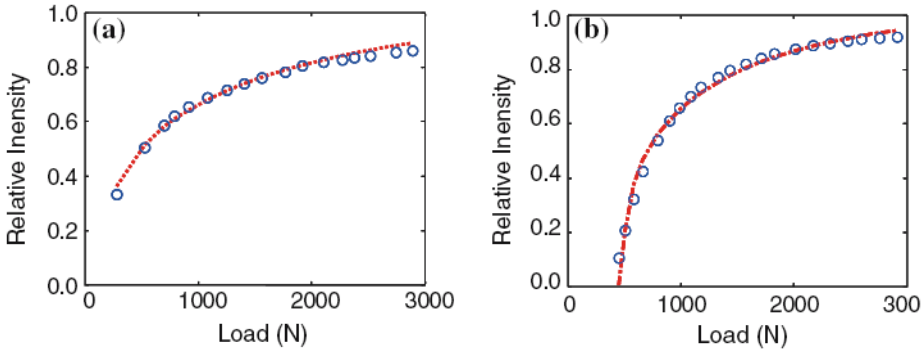

Figure 2.2: Relative light intensity transmitted through the interface as a function of applied load. Measured values are marked with circles. The dashed lines are calculated using a model for the normal load for a fully plastic deformation and a relation between a topography function of the interface and the intensity of the transmitted light. a) PMMA on PMMA b) PMMA on glass. In both a) and b) both sides of the interface has a 50nm rms roughness. Figure from [13]

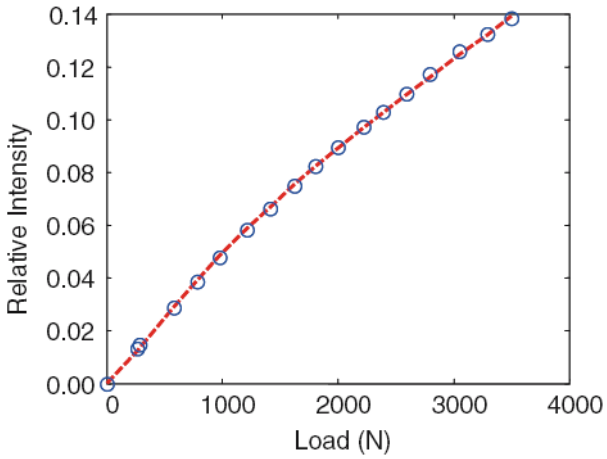

Figure 2.3: Similar to fig. 2.2. PMMA on PMMA where both sides of the interface has a rms roughness of 500nm. Figure from [13]

interactions at the microscopic level. The models illustrate some aspects of friction, such as an elastic instability transition [15]. An elastic instability transition is a discontinuous flipping from one stable position to another which occurs during sliding at low velocities. The models presented assumes that the interactions on the interface between a block and a substrate is elastic.

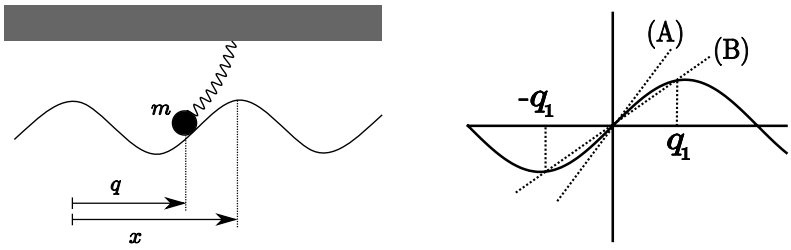

(a) (b)

Figure 2.4: a) The particle with mass m is connected to a slider via a spring with bending stiffness k. q is the position of the particle, while x is the position of the attachment point of the spring on the slider. The potential of the base is U. b) A graphical solution of Eq. 2.19 showing the cases where there is (A) only one solution $q = 0$ and (B) Three solutions $q = 0$ and $q \pm q_1$.

Consider the sliding system in Fig. 2.4(a). A particle with mass m is connected to the slider through a spring with bending stiffness k. The particle travels in the substrate potential $U(q)$, and we assume that the particle is adsorbed on the substrate surface. The coordinates q and x are the distance from the reference point on the substrate to, respectively, the particle and the point on the slider where the spring is attached, see Fig. 2.4(a). The equation of motion for the particle is

$$m\ddot{q} = -U'(q) - m\gamma\dot{q} + k(x - q), \tag{2.15}$$

where the frictional force $m\gamma\dot{q}$ originates from the adsorbate-substrate interaction [14, Sect. 8.2].

The effective potential for the particle is defined as

$$U_{eff}(x, q) = U(q) + \frac{k(x - q)^2}{2}, \tag{2.16}$$

and for simplicity we assume a sinusoidal shape of the potential

$$U(q) = U_0 \cos(2\pi q/a). \tag{2.17}$$

In equilibrium $\ddot{q} = \dot{q} = 0$, and Eq. 2.15is reduced to

$$U_0(2\pi/a)\sin(2\pi q/a) + k(x - q) = 0 \tag{2.18}$$

Suppose that the point the spring is attached to the slider is centered over a maxima in the potential $U(q)$. We can use this point as an reference point

for q and x, and thus we find that

$$U_0(2\pi/a)\sin(2\pi q/a) - kq = 0 \tag{2.19}$$

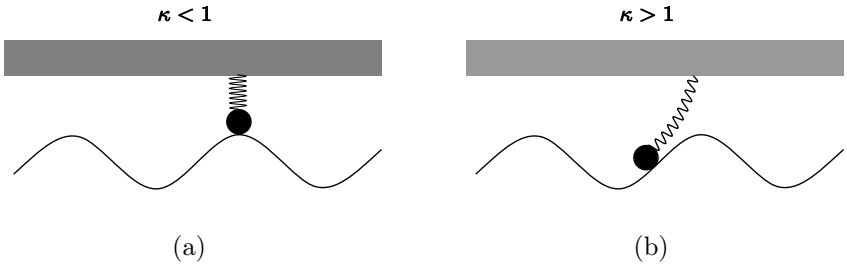

Figure 2.5: a) An illustration of the case $\kappa < 1$. b) An illustration of the case $\kappa > 1$.

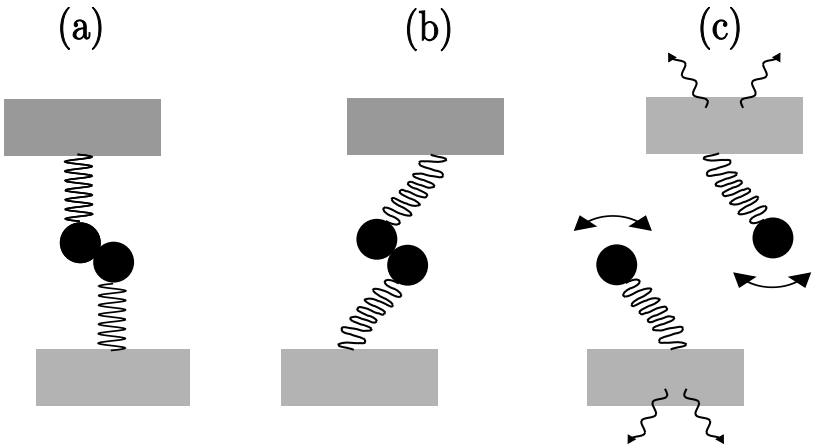

Figure 2.6: a) A slider particle (top) and a substrate particle (bottom) interlock as the two surfaces slides relative to each other. b) Elastic deformation because of the interlocking, and c) a rapid local motion after the interlocking potential barrier is exceeded.

The graphical solution of Eq. 2.19 is shown in Fig. 2.4(b) for the case of a stiff spring (A) and a soft spring (B). The slope of the spring force kq and $U'(q)$ at $q = 0$ is respectively k and $4U_0\pi^2/a^2$. In case (A) $k > 4\pi^2/a^2$ and thus only the solution $q = 0$ is allowed. In case (B) $k < 4\pi^2/a^2$ and the two curves intersects at $q = \pm q_1$ and $q = 0$. Thus in this case there exist three solutions to Eq. 2.19. We introduce $\kappa = 4\pi^2 U_0/(ka^2)$. If $\kappa < 1$, $q = 0$

and thus the spring is not bent. If $\kappa > 1$ we found that three solutions to Eq. 2.19 is possible. However the $q = 0$ solution is unstable since $U''_{eff}(0) = -U_0(2\pi/a)^2 + k < 0$, and thus a small displacement q would make $-U'_{eff}$ increase such that the particle would slide down in the potential well towards $q = \pm q_1$. Thus the particle will occupy on of the positions $q = \pm q_1$. Suppose that the slider moves in the x-direction with a low velocity v. If $\kappa < 1$, see Fig. 2.5(a) the particle will perform a small oscillatory motion with frequency dependent on v superimposed on the horizontal motion vt.The force acting on the block from the substrate will oscillate in time. If we define the kinetic frictional force F_k as the time average of this fluctuating force, $F_k \to 0$ when $v \to 0$.

If $\kappa > 1$, see Fig. 2.5(b) an elastic instability will occur. As the slider moves forward the spring will elasticly deform until q reaches a critical value q_c. At this point the particle will move rapidly forward to another potential well where it will perform a damped oscillation because of γ, this is indicated in Fig. 2.6. Thus even if $v \to 0$ a finite frictional force results after averaging over time. The model presented above considers only one particle,

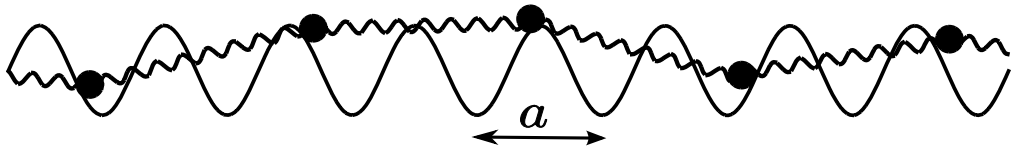

Figure 2.7: The Frenkel-Kontorova model where a chain of point particles coupled with springs is placed on a substrate

but in practice many interacting particles will be present at the contact area between the slider and the substrate. A model that contains some aspects of this situation is the Frenkel-Kontorova model [16]. The model consists of a one dimensional chain of point particles coupled together with springs located on a substrate, see Fig. 2.7. The equation of motion for the particles is

$$m\ddot{q}_i = -U'(q_i) - m\gamma\dot{q}_i + k(q_{i+1} + q_{i-1} - 2q_i) + F, \qquad (2.20)$$

where F is the driving force. The system will perform an elastic instability transition if $\kappa = 4\pi^2 U_0/(ka^2)$ is large enough. The critical value of κ, κ_C, depends on the ratio between the lattice constant a and the distance between two particles, when the spring connecting the is at it's rest length. The ratio between a and b should not be a rational number because of lattice alignment effects.

When $\kappa < \kappa_C$ the particles will be more or less uniformly distributed on the substrate, where some particles are close to the minima in U(q) and some

are close to the maxima. The springs are now so stiff that some particles will move up and others down during sliding in such a manner that there is no net energy barrier towards sliding. And thus an arbitrarily weak external force will induce sliding of the spring system.

If $\kappa \gg \kappa_C$ the force $-U'(q_i)$ is so strong relative the tension in the springs that the particles tends to be distributed close to the bottom of the potential wells. To initiate sliding on this system requires overcoming the potential barrier between the springs, thus producing a non-zero static friction force.

Although these models are very simple, they describe some ideas of the dynamics at the interface between the block and the substrate. Elastic instability transitions occur also in more complex and realistic model systems than the ones studied above [17–19]. Some examples of such models are the model studied by *Matsukawa* and *Fakuyama* [20], and *Caroli* and *Noziéres* [21].

Chapter 3

Modelling

3.1 The physical system

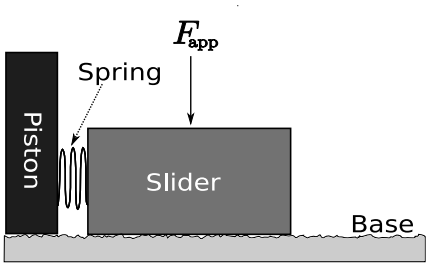

Figure 3.1: A sketch of the physical sliding system. F_{app} is the force from for example a load applied on the slider.

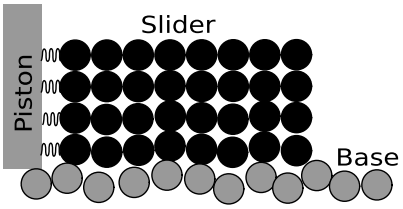

Figure 3.2: The model of the physical sliding system in fig. 3.1. The number of spheres resolving the slider is in this case chosen low (8*4 spheres).

In the study of sliding friction I use the physical system of a piston that pushes a slider placed on a base as an origin. In front of the piston a spring is equipped, and the force from the piston on the slider is transmitted through this spring. The spring is not attached to the slider, so the only forces transmitted from the piston on the slider is when the spring is compressed. The spring is considered soft to prevent that the slider forces the motion of the slider. With a soft spring a displacement in the spring due to variations in the frictional force is allowed. The mass of the piston is chosen so high that the movement of the piston is not affected by the compression in the spring. On top of the slider a load F_{app} may be applied to change the normal force N applied on the slider from the base. A sketch of the sliding system is shown in Fig. 3.1.

3.2 The slider

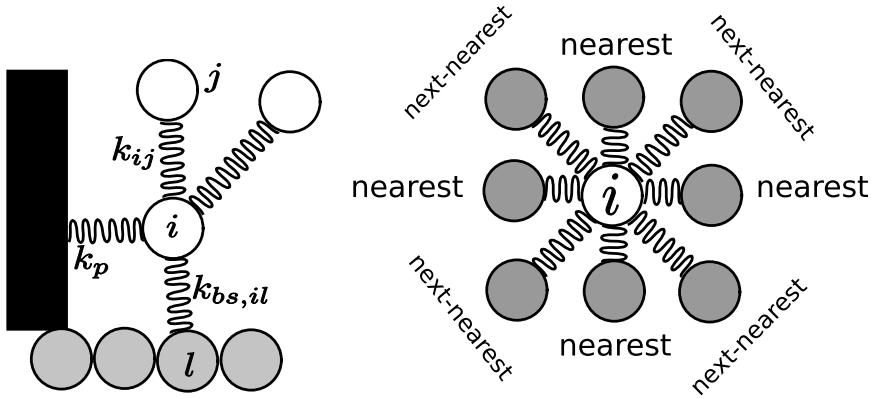

(a) (b)

Figure 3.3: a) The different possible spring interactions on a slider particle i. Only one base slider spring is depicted, however i may interact with several base spheres. The base slider interaction $k_{b,il}$ and the piston slider interaction is presented in respectively Section 3.4 and Section 3.5. b) An illustration of a slider particle i connected to it's neighboring particles. Up to 8 neighbors are possible.

The slider is modeled using a discrete element model [22] with next-neighbor interaction and viscous damping. The elements represents spherical particles that all have masses m and diameter l_0. The elements are arranged on a grid, and each element is connected to it's nearest and next-nearest neighbors with springs. In Fig. 3.2 I have sketched the modeling of the physical system, and in Fig. 3.3(a) the different spring interactions on slider sphere i is shown. The model is two-dimensional, however, since I threat the particles as spheres it may be more correct to say that it is a 3-D model where all motion is restricted to a plane.

In Fig. 3.3(b) I have sketched a slider particle i and it's different neighbors. The nearest neighbor springs have equilibrium length $d_1 = l_0$, and the next-nearest neighbor springs have equilibrium length $d_2 = \sqrt{2}l_0$, and thus if no forces act on the slider, the grid spacing is uniform in the x and y directing. Each spherical element in the slider represents a piece of the slider of size ${l_0}^2$. l_0 is therefore a convenient measure of the resolution of the of the slider model.

The use of both nearest and next-nearest interactions make every element

connected by up to eight neighboring elements. The diagonal springs work as stabilizers on the slider. Without these springs nothing would prevent the slider from tilting forward or backward. I could also have introduced bond bending/rotational springs to stabilize the slider, but I have chosen not to do this to simplify the model and the computations. The nearest and next-nearest neighbor spring interactions have spring constants respectively k_1 and k_2. The internal slider spring force between sphere i and j is

$$\vec{F_{int,ij}} = k_{ij}\left(|\vec{r}_i - \vec{r}_j| - d_{ij}\right)\hat{r}_{ij}, \tag{3.1}$$

where j may be any slider sphere except from i it self, $\vec{r}_i$ and $\vec{r}_j$ is respectively the position of sphere i and j, and $\hat{r_{ij}} = \vec{r}_{ij}/|\vec{r}_{ij}|$ is the unit vector pointing from i towards j.The stiffness k_{ij} is presented in Eq. 3.2 below,

$$k_{ij} = \left\{ \begin{array}{ll} k_1, & j = \text{nearest neighbour} \\ k_2, & j = \text{next nearest neighbour} \\ 0, & \text{else} \end{array} \right\} \tag{3.2}$$

All internal slider springs are damped with a damping term Eq. 3.3

$$\vec{F}_{d,ij} = -\eta_{ij} v_{ij}, \tag{3.3}$$

where η_{ij} and v_{ij} is respectively the damping coefficient and the relative velocity between sphere i and j. The motion of a mass m connected to a spring of stiffness k with damping coefficient η is described by the differential equation

$$m\frac{d^2x}{dt^2} = -kx - b\frac{dx}{dt}, \tag{3.4}$$

with solution

$$x = A\exp\left(-\eta/2m\right)t\cos(2\pi f), \tag{3.5}$$

where x is the position, t is the time and f is the frequency of the oscillation, given by

$$f = \frac{1}{2\pi}\sqrt{\frac{k}{m} - \frac{\eta^2}{4m^2}}. \tag{3.6}$$

The oscillation will be critically damped if $f = 0$. This is obtained for $\eta = 2\sqrt{km}$, and thus η may be written as

$$\eta = q\eta_c, \quad \eta_c = 2\sqrt{km}, \tag{3.7}$$

where q is the fraction of η_c. Similarly for the slider I introduce

$$\eta_{ij} = q\eta_{c,ij}, \quad \eta_{c,ij} = 2\sqrt{k_{ij}m} \tag{3.8}$$

In Eq. 3.1 $\vec{F_{int,ij}}$ is dependent on the stiffnesses k_{ij}, however it would be more convenient to express $\vec{F_{int,ij}}$ in terms of the Youngs modulus E for the material simulated. Young's modulus for for a square lattice with nearest and next-nearest neighbor interactions has been studied by *L. Monette and M.P. Anderson* [23]. For $k_2 = k_1/2$, the lattice behaves as an isotropic elastic material for large systems [23]. Young's modulus E can therefore be related to k_1 [23]

$$E = \frac{4k_1}{3l_0} \tag{3.9}$$

I can now rewrite k_{ij} as

$$k_{ij} = \frac{3}{4} E l_o E'_{ij}, \tag{3.10}$$

where

$$E'_{ij} = \begin{pmatrix} 1 & j = \text{nearest neighbor} \\ 1/2 & j = \text{next-nearest neighbor} \\ 0 & \text{else} \end{pmatrix}. \tag{3.11}$$

Using Eq. 3.1 and Eq. 3.10 I can now express $\vec{F_{int,ij}}$ in terms of E as

$$\vec{F_{int,ij}} = \frac{3}{4} E l_o E'_{ij} \left(|\vec{r_i} - \vec{r_j}| - d_{ij} \right) \hat{r}_{ij}. \tag{3.12}$$

3.3 The base

The model of the base must enable variations in the topography. It is however no point in choosing a finer resolution of the base than the slider, since then the slider spheres would be too coarse to fit in the smallest gaps between the base spheres. I have chosen to model the base similar to the slider, but instead of using a grid of spheres I have only used a single chain of spheres. This chain can be shaped as I want and resolve variations in the topography down to the diameter of each sphere, which I have chosen as l_0. This model opens for the possibility to have both a stationary and a deformable base. For the non-stationary base I can for example use two types of springs. The first type of springs connects the base spheres together on the chain. These spring alone is not sufficient to make the base spheres resist the movement from their initial position. A second type of springs connecting the base spheres to their initial position is therefore needed. I have, however, chosen to use a stationary base. This is because a non-stationary base introduces several new parameters that needs to calibrated. Secondly since I want to simulate a base with higher Young's modulus that the slider, the amplitude in the oscillations in the base should be small compared to the oscillations

internally in the slider. The stiffness of the base also sets restrictions to the size of the time step Δt used in the numerical model. This is presented in more detail in Section 4.3.1. The topography of the base is presented in Chapter 5.

3.4 The slider-base interaction

At every junction a contact force $F_{sb,ij}$ is introduced.

The interactions between the slider and the base occurs at point of contact, i.e. at the junctions. I have modeled the interaction at a junction as a spring that connects the slider sphere i to the base sphere j it is in contact with . The two spheres is in contact when they are closer than the distance l_0 from each other. I choose the equilibrium length of this spring to be $d_{sb} = l_0$. In the simplest case, this spring only exists when the two spheres is closer than l_0 from each other, i.e. the spring only exists when it is compressed. When the two spheres is positioned more than l_0 from each other, the spring is removed. There is also a possibility that i is in contact with several base spheres. Therefore a spring is created between i and all base spheres within a distance l_0 from it. In the more advanced case of friction where adhesion forces is introduced, the springs at the junctions is allowed to be stretched to represent a binding/welding of the particles forming the interface. This is presented later.

The equation for the contact between slider sphere i and a base sphere j is

$$\vec{F_{sb,ij}} = k_{sb,ij} \left(|\vec{r}_i - \vec{r}_j| - d_{sb} \right) \hat{r}_{ij}, \tag{3.13}$$

where

$$k_{sb,ij} = \begin{pmatrix} k_{sb} & |\vec{r}_i - \vec{r}_j| - d_{sb} < 0 \\ 0 & |\vec{r}_i - \vec{r}_j| - d_{sb} > 0 \end{pmatrix}, \tag{3.14}$$

and k_{sb} is the spring stiffness of the slider base interaction when the spring is compressed.

3.5 The slider-piston interaction

The piston is assumed to be of such great mass that it is not affected by the movement in the slider. Such a piston is easy to model and I have chosen to model it as a wall moving with a constant velocity. The force from the piston on the slider is transfered by horizontal springs that works on every trailing end slider particle closer to the piston than the equilibrium length

of the spring, x_{p0}, which I have set to $x_{p0} = l_0$. The piston force on slider particle i, $\vec{F}_{p_i}$ works only in the positive x-direction and is given as,

$$\vec{F}_{p_i} = k_p \max(x_p + x_{p0} - x_i, 0) \tag{3.15}$$

where k_p is the stiffness of each piston slider spring, and x_i is the position of slider particle i.

3.6 Applied load on the slider

The total weight of the slider is

$$w = -mXYg, \tag{3.16}$$

where m is the mass of each sphere, X and Y is respectively the number of spheres in respectively the x- and y-direction, and g is the pull of gravity. To model a load F_{app} applied on top of the slider, I could model a block or piston exerting a vertical force on top on the slider, such that Eq. 3.16 would be modified to

$$\tilde{w} = w + F_{\text{app}}. \tag{3.17}$$

However, instead of applying a load directly on top of the slider, I have chosen to model the effect of different F_{app} by varying g. For example if F_{app} equals the weight of the unloaded slider, $\tilde{w}$ would be $\tilde{w} = 2w$. Doubling the magnitude of g in Eq. 3.16 yields the same result. Thus when I want to simulate a varying F_{app} to obtain a varying normal force N in the simulations, it is the parameter g I am variating. N is related to g through

$$N = -mXYg. \tag{3.18}$$

When I present the simulations the two quantities N and g are sometimes spoken of simultaneously.

3.7 The equation of motion for the slider particles

Using Eq. 3.3, Eq. 3.12, Eq. 3.13 and Eq. 3.15 I find the equation of motion for the slider particles:

$$\begin{aligned} m\ddot{\vec{r}}_i = \; & \tfrac{3El_0}{4} \textstyle\sum_j E'_{ij} \left(|\vec{r}_i - \vec{r}_j| - d_{ij}\right) \hat{r}_{ij} - \sum_j \eta_{ij} \left(\dot{\vec{r}}_i - \dot{\vec{r}}_j\right) + \\ & \textstyle\sum_j k_{sb,ij} \left(|\vec{r}_i - \vec{r}_j| - d_{sb}\right) \hat{r}_{ij} + k_p \max(x_p + x_{p0} - x_i, 0) + \\ & mg\hat{e_y}, \end{aligned} \tag{3.19}$$

where i is an arbitrary slider particle and j is a neighbor particle, see Fig. 3.3(b), and can be either a slider or a base particle. $\hat{e_y}$ is the unit vector in the vertical direction.

Eq. 3.19 can be presented in a non-dimensional form, where the the non-dimensional variables and constants is expressed in terms of the physical parameters which are the physical time parameter t_0, the diameter of each sphere l_0, the acceleration of gravity g, the mass density ρ, Young's modulus E and the viscous damping η. I can express all the physical variables and constants on the form $h = h_0 * h'$, where h_0 is the physical parameter with dimension and h' is a non-dimensional variable or constant. This rule is applied on $\vec{r}_i$, m and t as follows:

$$\vec{r}_i = l_0 \vec{r}_i{}', \qquad m_i = m_i' m_0, \qquad t_i = t_i' t_0, \tag{3.20}$$

where

$$m_0 = \frac{4}{3}\pi\rho(\frac{l_0}{2})^3 \tag{3.21}$$

is the characteristic mass in the system. I don't want $\dot{\vec{r}}_i'$ and $\ddot{\vec{r}}_i'$ differentiated with respect to t, but to t'. This is easily accomplished with the chain rule

$$\frac{d}{dt} = \frac{d}{dt'}\frac{dt'}{dt} = \frac{d}{dt'}\frac{1}{t_0}, \qquad \frac{d^2}{dt^2} = \frac{d}{dt}\frac{d}{dt'}\frac{1}{t_0} = \frac{d^2}{dt'^2}\frac{1}{{t_0}^2}, \tag{3.22}$$

and I get that

$$\dot{\vec{r}}_i = \frac{l_0}{t_0}\,\dot{\vec{r}}_i', \qquad \ddot{\vec{r}}_i = \frac{l_0}{{t_0}^2}\,\ddot{\vec{r}}_i'. \tag{3.23}$$

Using Eq. 3.20 and Eq. 3.23, Eq. 3.19 can be written in terms of the non-dimensional parameters:

$$\begin{aligned} m'\,\ddot{\vec{r}}_i'\tfrac{m_0 l_0}{{t_0}^2} = \quad & \tfrac{3E{l_0}^2}{4}\textstyle\sum_j E_{ij}'\left(|\vec{r}_i{}' - \vec{r}_j{}'| - d_{ij}'\right)\hat{r}_{ij} \\ - \quad & \tfrac{l_0}{t_0}\textstyle\sum_j \eta_{ij}\left(\dot{\vec{r}}_i' - \dot{\vec{r}}_j'\right) \\ + \quad & l_0\textstyle\sum_j k_{sb,ij}\left(|\vec{r}_i{}' - \vec{r}_j{}'| - d_{sb}'\right)\hat{r}_{ij} \\ + \quad & k_p l_0 \max(x_p' + x_{p0}' - x_i', 0) + m' m_0 g\hat{e_y}. \end{aligned} \tag{3.24}$$

I now use Eq. 3.21 in Eq. 3.24 and after some algebraic operations I end up with

$$\begin{aligned} m'\ddot{\vec{r}}' = \quad & \textstyle\sum k_{ij}'\left(|\vec{r}_i{}' - \vec{r}_j{}'| - d_{ij}'\right)\hat{r_{ij}} - \sum_j \eta_{ij}'\left(\dot{\vec{r}}_i' - \dot{\vec{r}}_j'\right) \\ + \quad & \textstyle\sum_j k_{sb,ij}'\left(|\vec{r}_i{}' - \vec{r}_j{}'| - d_{sb}'\right)\hat{r}_{ij} + k_p'\max(x_p' + x_{p0}' - x_i', 0) \\ + \quad & m' g'\hat{e_y}, \end{aligned} \tag{3.25}$$

where the non-dimensional constants are presented in Table 3.1.
Table 3.1 relates the non-dimensional parameters which I use in the simulations to the physical parameters.

k'_{ij}	$=$	$E'_{ij}\frac{2Et_o{}^2}{9\pi\rho l_0{}^2}$
η'_{ij}	$=$	$\frac{6\eta_{ij}t_0}{\rho\pi l_0{}^3}$
$k'_{sb,ij}$	$=$	$\frac{k_{sb,ij}8t_o{}^2}{27\pi\rho l_0{}^3}$
k'_p	$=$	$\frac{k_p 8t_o{}^2}{27\pi\rho l_0{}^3}$
g'	$=$	$\frac{gt_0{}^2}{l_o}$

Table 3.1: The non-dimensional constants in Eq. 3.25.

Chapter 4

The numerical setup

In this chapter the numerical algorithm used to simulate the slider system is presented. In the end of the chapter the challenges with choosing the physical parameters is presented together with the parameters used in the simulations.

4.1 The sliding velocity v

In the sliding system there are several different velocities. Each individual slider sphere has it's own velocity because of the interaction with neighboring spheres. Another measure of velocity is the the center of mass velocity v_{cm} of the slider, resembling the combined velocity of the whole slider.

It may be tempting to use v_{cm} as the sliding velocity, but this choice comes with a complication. v_{cm} may vary in a simulation, and then it would be difficult to extract μ data for a given velocity. I could use a stiff piston slider interaction to reduce the fluctuations in v_{cm}, however this would violate the physical system modeled, where the piston slider spring is considered soft.

The velocity of the piston may also be used as the sliding velocity. Using this velocity as the sliding velocity makes it easier to calculate μ since the velocity is fixed during the simulation. I have therefor chosen to use the piston velocity as the sliding velocity v, and thus v is a parameter that I set for each simulation run.

Although this definition of the sliding velocity simplifies the computation of $\mu(v)$ I must keep control of the fluctuations in v_{cm} since large variations in v_{cm} may give a different value of μ than what smaller variations would. Thus I need to have some measure of how stable the center of mass velocity is during sliding. I have chosen a simple algorithm that does not require much computational resources. Instead of calculating the fluctuations in v

directly, I find the peak displacement in the piston-slider interface

$$\epsilon = \max(x - x_o) - \min(x - x_0), \tag{4.1}$$

where $x - x_0$ is the position of the slider relative the piston. I am not concerned with small variations in ϵ since I expect the frictional forces to fluctuate because of variations in the base. However I must be careful that ϵ does not become too large. The quantity ϵ/v is also important for low v, which gives the time needed for the piston to move the distance ϵ. If ϵ/v is large, the slider may come to a rest before it is hit again by the piston.

4.1.1 Initialization of the simulations

Before I can collect $\mu(v)$ data the piston must push the slider at a velocity v relative the base. The various forces acting on the slider shifts the equilibrium lengths of the springs in the system, and this may lead to unwanted oscillations if this is not taken into consideration when initializing the simulations. It is important to initialize the slider system in such a way that the springs are not far from their equilibrium lengths when the simulations start. I have considered two ways to perform such a initialization.

The first option is to let the slider and piston initially move with velocity v. However this is not straight forward, since the slider becomes compressed because of gravity and friction. For this method to work properly I therefore need to have a good guess of the shifted equilibrium length of the springs given the parameters I chose. In addition the slider should slide for some time such that remaining unwanted instabilities have time to be damped out. The simulation time needed before data collection can begin may be small given that the initial guess of the spring compressions is good.

Another approach is to initially let the slider be at rest, and when the simulations start the slider is accelerated slowly towards v. The springs gradually adapt to the piston and frictional forces when accelerated, and when v is reached the data collection may begin. This method does not require a good guess of the initial displacements of the springs given that the compression of the slider because of gravity is small. The down side with this method is that it requires some simulation time to accelerate the piston.

I have chosen to use the second approach of initiating the slider system. This is because the initial guess needed for the first method is dependent on a lot of variables and is thus not straight forward to evaluate. In this case, the piston acceleration phase needs to be defined. The piston velocity $v_p(t)$ is chosen to increase linearly in the acceleration phase up to v:

$$v_p(t) = \begin{pmatrix} a_p t, & t < t_a \\ v, & t > t_a \end{pmatrix}. \tag{4.2}$$

I don't use $v_p(t)$ directly in the calculations of the spring forces, instead I use the position of the piston

$$x_p(t) = \begin{pmatrix} \frac{a_p t^2}{2} + x_{init}, & t < t_a \\ \frac{a_p {t_a}^2}{2} + v(t - t_a) + x_{init}, & t > t_a \end{pmatrix}. \tag{4.3}$$

4.2 The numerical algorithm

The numerical setup for solving the sliding simulations is schematically presented below.

- Initializations of the system.
- Loop over iterations (time).
    - Calculate the piston position.
    - Find new junctions.
    - Calculate forces.
    - Calculate new positions.
    - Calculate the contribution to the coefficient of friction and ϵ
- Calculate the averaged dynamic coefficient of friction and ϵ

Each element is now present in more detail.

4.2.1 Initializations of the system

After the variables have been declared, the base is built and the highest point on the base is stored.

```
for(i=0;i<num_base_spheres;i++) {
  //base[i][n]: n=0 horizontal position, n=1 vertical position
  base[i][0]= i +"random displacement";
  base[i][1]= Z(i); //Z(i) is a topography function
}
if (base[i][1]>base_peak) base_peak= base[i][1];
```

Now the slider is built, placing the lowest row a distance one sphere diameter l_0' over the highest position of the base. This is done to assure that there is no overlap between the base and the slider which could result in large forces in the beginning of the simulations. Secondly this reduces the risk of placing the slider too high above the base.

```
for(i=0;i<num_slider_particles;i++) {
  //particle[i][n]: n=0 horizontal position, n=1 vertical position
  particle[i][0]= i%X; //X=number of horizontal base spheres
  particle[i][1]= i/X+base_peak; //i/X is an integral division
}
```

4.2.2 Loop over iterations

All variables that needs to be updated is calculated at time t'. The loop then increases the time by Δt.

```
while(time<max_time) {
```

Calculate the piston position.

At the beginning of each iteration, the new piston position is calculated. The piston has two acceleration phases, a linear acceleration phase when $t' < t'_a$, where t'_a is the acceleration time of the piston, and a constant velocity phase with horizontal velocity v' when $t' \geq t'_a$.

```
if(time<t_a) { //acceleration phase
piston_pos = 0.5*a_p*time*time + start_pos;
//a_p is the acceleration of the piston
//start_pos is the initial i.e. t=0 position of the piston
}
else{\\constant velocity phase
 piston_pos = 0.5*a_p*t_a*t_a + v*(time - t_a) + start_pos;
}
```

Find new junctions.

The slider spheres have moved since the last iteration and thus a slider sphere might be close enough to a base sphere to form a junction. This method searches for slider spheres that meets the criteria to form a junction, see Section 3.4, and then creates the junction by combining the spheres forming the junction with a spring. This method does not detach the junctions that violates the junction criteria, since this is performed in the the next method.

```
for(i=0;i<X;i++) { //Only bottommost slider row
  //I find base particles that are close to j
  //too speed up the program so that I don't need
  //to run a loop over every base particle
  for (j:"base particles close to i") {
    if (dist(i,j)<l_0 && "j not already bound to i") {
```

```
      "connecting i and j, and setting up spring
      equilibrium length, spring stiffness, ...";
}}}
```

Calculate forces

This method calculate all forces on every slider particle. The forces is presented in Chapter 3, and I will therefore not give a description of the forces here. The contribution of the different forces on each slider particle is added to a force vector controlling the total force on the particle. The method runs a loop over all slider particles, and for each particle the calculations goes as follows:

- Calculating the gravitational force on i.
- Calculating the piston force on i if i is in contact with the piston.
- Calculating the force on i from it's slider neighbors j
- Calculating the force on i from the base, if i is in contact with the base. If the spring is stretched, the force is discarded and the junction is destroyed.

```
for {i=0;i<num_particles; i++) {
   //particle[i][n] is n=[0,2] position, n=[3,5] velocity,
   //n=[6,8] force, n=9 mass
   //Adding gravity:
   particle[i][7]  =  particle[i][9]*g;
   //Calculating force from piston
   dx= piston_pos + x_p0 - particle[i][0];
   if(dx>0) particle[i][3] += k_piston*dx;
   //Calculating force on i from it's slider neighbors
   for("loop over neighbors j"){
      distance = dist(i,j);
     "calculate spring force, and damping force on i"
   }
   if("contact with base") {
      for("loop over base contacts j") {
         distance = dist(i,j);
         if (distance <eq_length) {
           "calculate spring force on i from j";
         else "Remove spring connecting i and j";
}}}}
```

Calculate new positions

Let $x_i(t)$, $v_i(t)$ and $F_i(t)$ be respectively the position, velocity and force in the direction i for a given slider particle. $x_i(t_0)$, $v_i(t_0)$ and $F_i(t_0)$ are known at time t_0, where t_0 is the current time for this iteration. The task for this method is to calculate the $x_i(t_0 + \Delta t)$ and $v_i(t_0 + \Delta t)$, that is the positions and velocities for the next time step. Δt is the time step separating the iterations, and it is a constant.

The method begins to calculate $v_i(t + \Delta t)$ using a forward Euler scheme

$$v_i(t_0 + \Delta t) = v_i(t_0) + \frac{F_i(t_0)}{m}\Delta t, \tag{4.4}$$

where m is the mass of the slider sphere. It should be noted that the program uses the primed non-dimensional versions of the quantities presented here. Eq. 4.4 treats $F_i(t)$ as being constant over the time Δt which is a truncation of the general Taylor expansion of $v_i(t_o + \Delta t)$ about t_0,

$$\begin{aligned} v_i(t_0 + \Delta t) = &\quad v_i(t_0) + \tfrac{1}{m}\textstyle\sum_{n=0}^{\infty} \frac{F_i^{(n)}(t_0)}{n!}\Delta t^{n+1} \\ = &\quad v_i(t_0) + \Delta t\tfrac{F_i(t_0)}{m} + \tfrac{1}{2}\Delta t^2 \tfrac{F_i'(t_0)}{m} + O(\Delta t^3), \end{aligned} \tag{4.5}$$

where $F_i'(t_0) = \left(F_i(t_0 + \Delta t) - F_i(t_0)\right)/\Delta t$ and $O(\Delta t^3)$ is the truncation error. Comparing Eq. 4.5 and Eq. 4.4 the error in Eq. 4.4 goes as

$$\tfrac{1}{2}\Delta t^2 \tfrac{F_i'(t_0)}{m} + O(\Delta t^3).$$

However this error is only correct for a constant potential. This is not the case of the potential for the slider particles since the potential in the springs generally changes when the slider particle moves.

Now that $v_i(t_0 + \Delta t)$ is calculated, the method continues with calculating $x_i(t_0 + \Delta t)$. Again I chose to use the forward Euler scheme (the reason for this is presented below). The forward Euler scheme estimates the new position $x_i(t_0 + \Delta t)$ by treating the velocity on the interval $[t_0, t_0 + \Delta t]$ as constant. At time t_0 the slider particle is estimated to have velocity $v_i(t_0)$. To calculate $x_i(t_0 + \Delta t)$ I could use a forward Euler formula such as

$$x_i(t_0 + \Delta t) = x_i(t_0) + v_i(t_0)\Delta t. \tag{4.6}$$

However $v_i(t_0 + \Delta t)$ is generally different from $v_i(t_0)$. I therefore expect that the average of $v_i(t_0)$ and $v_i(t_0 + \Delta t)$ would generally be a better approximation of the velocity between t_0 and $t_0 + \Delta t$. I therefore make this modification to eq. 4.6

$$x_i(t_0 + \Delta t) = x_i(t_0) + \frac{v_i(t_0) + v_i(t_0 + \Delta t)}{2}\Delta t. \tag{4.7}$$

Instead of updating v_i and x_i using a forward Euler scheme I could have used a more advanced updating scheme. Such schemes often calculates v_i at up to several sub-steps in time before $v_i(t_0 + \Delta t)$ is calculated. This is an efficient way of reducing the truncation error of the method when it is easy to calculate v_i at such partial time steps. In this case v_i is calculating using F_i which is the sum of all forces in the i direction and thus requires several calculations to evaluate. A second complication is that the calculation of F_i at intermediate time steps would not give a good result if I only moved the current slider sphere at such intermediate steps. This is because the potential also changes when the slider sphere is moved. Thus all slider spheres should be moved to give a good value of F_i. This would require a huge amount of calculations which would make the increased accuracy come with the prize of a huge increase in simulation time. Thus I have instead decided to use the forward Euler scheme with a small enough time step for the calculations.

Calculate the contribution to the coefficient of friction and ϵ

The way I have chosen to calculate the static μ and the dynamic μ_d is described in, respectively, Section 6.1 and Section 7.2.2. μ_d is averaged over a distance d, but the contribution to μ_d is calculated at every iteration. The static μ is calculated at every iteration since I study the time-dependence of it.

```
mu = 0; //used for static friction
//mu_d is the dynamic coefficient of friction measured
//over a distance d.
for(i=0;i<X;i++) {
   //static friction
   mu -= particle[i][6]; //static friction
   //dynamic friction
   particle[i][13] += particle[i][0] - x_old;
   //particle[i][13] stores the horizontal displacement
   //of the slider sphere over the length mu_d is measured over
   dy = particle[i][1] - y_old;
   particle[i][12] -= particle[i][10]*( particle[i][0] - x_old)+
                      particle[i][11]*dy;
   //particle[i][10] and particle[i][11] is respectively the
   //horizontal and vertical force from the base on the slider
   //particle[i][12] stores the work done by the base on the slider
   //over the distance mu_d is calculated over
}

//Measuring the mu_d over a distance d
```

```
if (x_mu-slider_pos>d) {
   //x_mu is the slider position mu_d is measured from
   //while slider_pos is the current slider position
   mu_d = 0;
   for(i=0;i<X;i++}{
      mu_d += particle[i][12]/particle[i][13];
      particle[i][12] = particle[i][13] = 0;
   }
   mu_d /= -(X*Y*m*g);
   //Divide by the average normal force on the
   //slider
   x_mu = slider_pos;
   mu_d_average +=mu_d; //adding mu_d to the global average
                        //for the current velocity
   average_counter++;   //Updating the number of mu_d averaged
                        //over
}
```

ϵ is the maximum difference in the distance betweeen the piston and the slider during the simulation. If the distance from the trailing end of the slider exceeds the maximum distance measured earlier in the simulation, the new displacement is stored. Similarly if the compression of the piston spring is greater than than previously measured, the new compression is stored.

```
//ps_disp is the piston slider spring displacement,
//ps_max and ps_min is respectively the maximum and
//minimum value of ps_disp measured.
if(ps_disp>ps_max) ps_max = ps_disp;
else if(ps_disp<ps_min) ps_min = ps_disp;
```

After all operations at the current time step is finished, the time is updated

```
time +=dt;
```

4.2.3 Calculate the averaged dynamic coefficient of friction and ϵ

When the iterations has ended, the average μ_d for the slided distance is calculated, and ϵ is also calculated.

```
mu_d_average /= average_conter;
epsilon = ps_max-ps_min;
```

k'_{ij}	=	$E'_{ij}\frac{2Et_o{}^2}{9\pi\rho l_0{}^2}$
η'_{ij}	=	$\frac{6\eta_{ij}t_0}{\rho\pi l_0{}^3}$
$k'_{sb,ij}$	=	$\frac{k_{sb,ij}8t_o{}^2}{27\pi\rho l_0{}^3}$
k'_p	=	$\frac{k_p 8t_o{}^2}{27\pi\rho l_0{}^3}$
g'	=	$\frac{gt_0{}^2}{l_o}$

Table 4.1: The non-dimensional constants in Eq. 3.25.

4.3 The physical and non-dimensional parameters for the simulations

In Section 3.7 the relation between the physical and the non-dimensional parameters was found. I have also presented the results here shown in Table 4.1. With the help of Table 4.1 it is possible to find the non-dimensional parameters used by the simulation program for a wide range of physical parameters. However not all such choices of the physical parameters is suitable for the simulation program. In this section some criteria for the choice of the non-dimensional constants is presented. In the following I will use the notation k'_1 for the nearest neighbor interactions of k'_{ij} and k'_2 for the next-nearest neighbor interactions.

Young's modulus E

Ideally I would like to run the simulations for a slider with a realistic Young's modulus E. The slider could for example be soft rubber with $E \approx 0.01$GPa. When E is chosen, I have to decide the size of the slider I want to simulate.

The parameter l_0

The slider model neglects the internal dynamics on length scales less than the size of each sphere l_0, and thus l_0 must not be chosen to large. However l_0 should not be chosen too small either since the elastic spring model may not be a good approximation at very small length scales, for example at atomic or molecular levels. A possible choice for the lower limit of l_0 is the *elastic correlation length* ξ [9]. When a block is at rest on a base the tangential stress fluctuates randomly from one contact area to another and the total tangential stress on the block is be zero. The tangential stress on the particles forming a junction is, however, highly correlated, and thus ξ is on the order of the junction diameter [9]. Simulating systems with $l_0 < \xi$ means that one resolves each junction by several elements/spheres. To obtain

a slider where several junctions occur thus requires a high resolution of the slider, since $A_r/A \ll 1$ for rough surfaces.

The parameter g

The physical system modeled should have $|g| = |g_0|$, where $g_0 = -9.81\text{m/s}^2$. However since I have chosen to simulate a variable applied load F_{app} on top of the slider by varying g, I should have $|g| \geq |g_0|$ in the simulations. The parameter g is therefore varied in the simulations.

The sliding velocity v

The sliding model chosen neglects frictional interactions such as plowing and wear, and is therefore not suited to simulate sliding at large v where I expect such effects to be of importance. Instead I want to study sliding at low velocities and the behavior of $\mu(v)$ when $v \to 0$. The length slided in one second at velocity v is L_v. If L is the length of the slider, I want to simulate sliding at velocities where $L_v \ll L$ up to $L_v \approx L$. Although I am most interested in v giving $L_v < L$ I also show the behavior of μ for $L_v > L$. The non-dimensional velocity is related to the physical velocity through

$$v = v_0 v', \tag{4.8}$$

where $v_0 = l_0/t_0$.

4.3.1 Choosing the physical parameters

Numerical difficulties when choosing realistic parameters

If I for example choose $l_0 = 10^{-5}$ When calculating k'_{ij} in Table 4.1 the ratio $E/{l_0}^2$ would become enormous: $E/{l_0}^2 = 10^{20}\text{Pa/m}^2$. This would result in either a very large stiffness k'_{ij} or a very small t_0. Choosing a very large k'_{ij} would make the system so stiff that it essentially behaves as a rigid body unless a high number of particles were chosen, giving a large system. Increasing the system size increases the number of particles that calculations must be carried out for, and thus the simulation time would increase. Resolving the same physical size of the slider with a higher number of particles is also problematic, because then I would need to decrease l_0, making the ratio $E/{l_0}^2$ even greater.

A third problem is that a small displacement in a stiff spring gives a large force since $F_{ij} = -k_{ij}\Delta r$, where Δr is the displacement from the equilibrium length of the spring. Since the force is only calculated at discrete times t^k,

$\rho = 3.0 * 10^3 \text{kg/m}^3$
$E_0 = 4.0 \times 10^5 \text{Pa}$
$l_0 = 10^{-4} \text{m}$
$t_0 = 3.99 * 10^{-4} \text{s}$
$q = 0.3$

Table 4.2: The physical parameters chosen for the simulations. The sliding velocity and the constant of gravity g is not displayed here since they are variables. Remember that q is the fraction of the critical damping η_c, see Section 3.2

the time step Δt needs to be chosen small to to maintain a stable simulation. Since

$$t^k = k\Delta t = t_0 k \Delta t', \tag{4.9}$$

a small Δt would give a large number of iterations for a relatively small increase in time t^k. A small Δt combined with a high number of particles therefore would require a long simulation time for a relatively small increase in the physical time.

Instead of increasing k'_{ij} I could also decrease t_0. However from Eq. 4.9 we see that this would also require a very large number of iterations for a relatively small increase in the physical time. In addition a small t_0 would make the non-dimensional constant of gravity g' small. Choosing a small g' might be problematic since the slider might begin to jump instead of sliding.

The parameters chosen for the simulations

After trial and error I have found a balance between the simulation time and the physical parameters I would ideally choose. The physical parameters are listed in Table 4.3.1. I have chosen to resolve the slider by 80 spheres horizontally and 40 spheres vertically, thus the dimensions of the slider is 8.0mm long and 4.0mm high. The physical constants chosen gives the non-dimensional spring stiffness $k'_1 = 150$. I want to simulate a base that is stiffer than the slider, and therefore I have chosen the base slider interaction to be $k'_{sb} = 1075$. The reason for choosing k'_{sb} so stiff is to reduce the effect of sphere plowing at high velocities, which is presented in Section 7.4 .

The velocity constant v_0 from this choice of parameters is $v_0 \approx 0.25 m/s$. For a slider of length 8mm a velocity of 250mm/s is considered high, thus $v' \ll 1$ should be used in the simulations. The choice $g' \approx 0.016$ gives $g = 10 m/s^2$, and I have not observed jumping at this value of g', however this may not be true for all shapes of the base. The choice of the topography of the base is presented in Chapter 5

Chapter 5

The topography of the base

5.1 An analytical study of simple rough surfaces

Modeling a realistic base is challenging because most natural surfaces have roughnesses on a wide range of length scales. The geometry of a realistic base is even difficult to quantify [24]. Since the slider is modeled by spheres of diameter l_0, variations in the base cannot be resolved on length scales smaller than l_0. The slider would therefore need to be modeled by a huge amount of spheres if I would create a base with roughnesses of a wide range of length scales. This system would require a lot of simulation time to solve and in addition a lot of work would have been needed to be put into constructing the base. Because of the limited time I have on this project I have decided not to make a realistic shaped base, but instead make a base with a simple rough surface. In this section an analytical study of the dependence of A_r on N is presented for two simple bases.

In Chapter 2 I presented that the relation

$$A_r \propto N \tag{5.1}$$

is expected for contact between surfaces, neglecting time dependent asperity creep, see Section 2.2. Although I don't attempt to crate a realistic base, I try to make a base that fulfills Eq. 5.1. The simplest model of a rough surface is a regular surface such as a triangular wave shaped surface or a wave which has a sinusoidal profile. The dependence of A_r/A on N is presented below for both these surfaces.

The dependence of A_r on N for a triangular shaped base, see Fig. 5.1(b) can be calculated using a simple model based on Hook's law. The base is considered rigid, while the slider is considered a parallel coupling of vertical

springs, see Fig. 5.1(a). The compression of the spring at position x is $f_y(x) = -kh(x)$, where k is the stiffness of the spring and $h(x)$ is the compression at point x. The normal force on the slider is $N = \sum f_y$. The horizontal distance between two parallel spring is dx, and in the limit $dx \to 0$ the sum may be exchanged with the integral

$$N = \int f_y(x)dx. \tag{5.2}$$

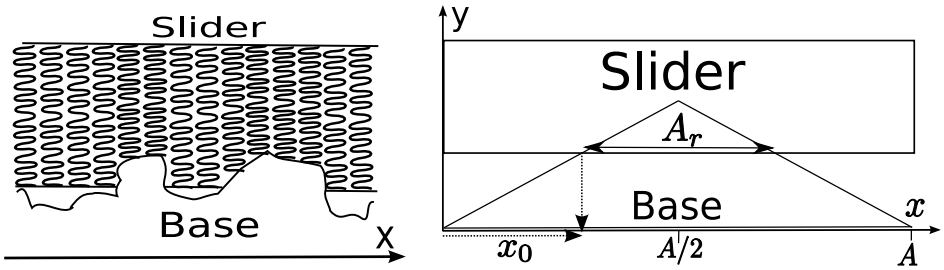

(a) (b)

Figure 5.1: (a) The model of the slider, (b) the triangular base setup.

The triangle in Fig. 5.1(b) has width A and unity height. The area A is just a length in my case since the contact between the slider and the base is on a line. The slider is considered to have length A, and it is placed centered on the triangular shaped base. The triangle of contact between the slider and the base is defined as

$$h(x) = \begin{pmatrix} 2\frac{x-x_0}{A} & x_o \leq x < A/2 \\ 2 - 2\frac{x+x_0}{A} & A/2 \leq x \leq A - x_0 \end{pmatrix}, \tag{5.3}$$

where $A - 2x_0$ is the width of the overlap between the elastic block and the triangle. Using Eq. 5.2 we get

$$N = \int_{x_0}^{A-x_0} kh(x)dx = k\left(\frac{A}{2} - 2x_0 + \frac{2{x_0}^2}{A}\right). \tag{5.4}$$

The maximum in N denoted N^* is obtained for $x_0 = 0$ and has the value: $N^* = A/2$, thus Eq. 5.4 may be rewritten as

$$N/N^* = 1 - \frac{4x_0}{A} + \frac{4{x_0}^2}{A^2}. \tag{5.5}$$

Eq. 5.5 relates N/N^* to x_0, but I want to express A_r/A as a function of N/N^*. This is easily accomplished by the fact that $A_r/A = (1-2x_0/A)$, and inserting this expression for A_r/A in Eq. 5.5 yields

$$\frac{\Delta A}{A} = \sqrt{N/N^*}. \tag{5.6}$$

Eq. 5.6 shows that A_r is not proportional in N. In Fig. 5.2(a) I have plotted the dependence of A_r/A on N/N^* for the triangular shaped base. The simple model used above is not representative for the slider model I have chosen. This is because the diagonal and horizontal springs in the model is neglected. However if the base is modeled with a chain of triangles with a spacing and amplitude small compared to the size of the slider, the resulting deformation of the slider would be small. In this case Eq. 5.6 gives an approximate behavior for the $A(N)$ behavior of the slider model. That said, I don't expect the simulations to give me the result Eq. 5.6 since the modeled slider and base is not smooth as assumed in this analysis.

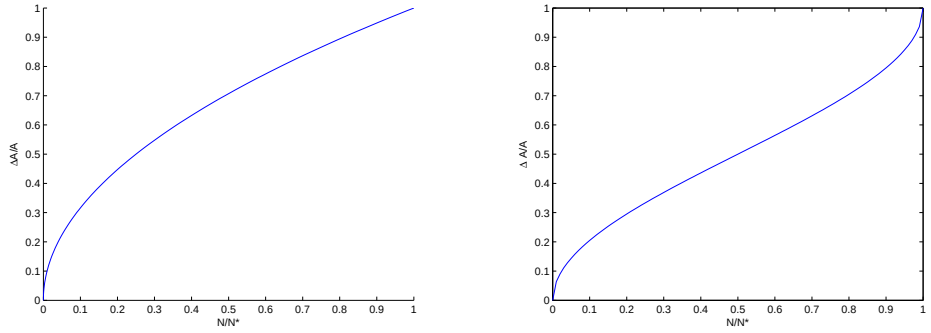

(a) (b)

Figure 5.2: The dependence of $\Delta A/A$ on N for a a) triangular shaped base and b)sinusoidal shaped base. In both a) and b) N^* is the normal force for full contact.

The dependence of A_r on N can be analytically found for a sinusoidal shaped base. The slider is considered an elastic half space [25, Chapter 2.1] with a flat surface, while the base is considered an elastic solid with amplitude Δ and wavelength λ, where $\Delta << \lambda$. The dependence of A_r/A on the mean pressure at the interface $\bar{p}$ is [25, Section 13.2]

$$\frac{2a}{\lambda} = \frac{A_r}{A} = \frac{2}{\pi} \arcsin\left(\bar{p}/p^*\right)^{(1/2)}. \tag{5.7}$$

The contact between the slider and base is strips of width $2a$ at the crests of the sinusoidal wave. In Eq. 5.7 p^* is the mean pressure when $\frac{2a}{\lambda} = 1$, i.e. the pressure at full contact. Note that $N = \bar{p}A$, thus Eq. 5.7 can be written as

$$\frac{2a}{\lambda} = \frac{2}{\pi} \arcsin\left(N/N^*\right)^{(1/2)}, \tag{5.8}$$

where N^* is the normal force for $A_r = A$. Eq. 5.8 does not either fulfill the requirement Eq. 2.2. In figure Fig. 5.2(b) I have plotted the relation Eq. 5.7, and we see that the curve is approximately linear in the range $N/N* = [0.2, 0.8]$.

I could have made further studies of more advanced bases. I have however not chosen to do this because in the simulations I don't use a smooth base, but instead a base composed of spheres. The spheres will introduce a roughness, and the study made in this section may therefore only be valid in the limit where the base is resolved by an infinite number of spheres.

5.2 Numerical test of the A_r dependence on N

A comparison of the numerical results of the sinusoidal and triangular shaped base was originally planned in this section. I planned to choose the base most suited for the sliding simulations based on these results. However when I visualized the slider resting on the triangular shaped base, I became aware of that the sharpness of the triangular base could cause slider spheres to get stuck in the base.

The base spheres are originally spaced by a distance l_0, but to avoid effect of lattice alignment between the slider and the base a small random displacement from l_0 is introduced for the spacing between the slider spheres. A similar random displacement in the y-direction from the sinusoidal shaped base is also introduced. This displacement from the original sinusoidal wave increases the disorder in the base which I think is advantageous when approximating a realistic highly complex shaped base. The random displacement of the base particles may also increase the probability for the slider to get stuck as it could cause pockets/traps in the base. The sinusoidal shapes base has more rounded peaks and I therefore expect the sinusoidal base to be a safer choice. I have therefore decided to discard the triangular shaped base and only measure the dependence of A_r/A on N for the sinusoidal shaped base.

The parameters chosen for the simulations is as presented in Section 4.3.1 The slider is unrealistic soft, but, as I have described earlier, simulating with a realistic Young's modulus requires a large systems and is very time consuming. The sinusoidal shaped base has an an amplitude $\Delta = \mu$m and

a period $\lambda = 60\mu$m. Each base sphere is displaced up to 4μm and 0.5μm respectively in the x and y direction from their original position on the sine wave.

To measure how A_r/A depends on N I measure the number of junctions that occurs at a given N after the slider has had time to come to a rest. In Fig. 5.3(a) I have plotted the ratio A_r/A for different values of g. From

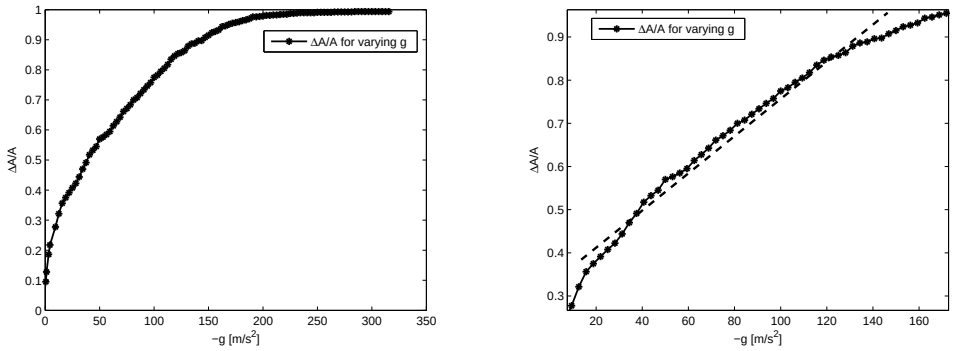

(a) (b)

Figure 5.3: a)Simulation results of the dependence $\frac{\Delta A}{A}$ on N for a sinusoidal shaped base with a random perturbation in the displacement of the base spheres in the x and y direction. b) A zoom in on Fig. 5.3(a). The linear dashed line is inserted to better visualize that $\frac{\Delta A}{A}$ is approximately linear in N for $g \in [20m/s^2, 140m/s^2]$.

Section 3.6 we remember that $N \propto -g$. The figure shows that A_r/A increases with N. However the increase in A_r is not proportional to N. A_r/A increases rapidly with N for low N. A linear approximation for the increase in A_r/A with N may be used approximately in the range $0.35 < A_r/A < 0.85$, see Fig. 5.3(b). A_r/A flatten out when $A_r/A \to 1$.

Analysis of the results

Fig. 5.3(a) is, as earlier explained, obtained by counting the number of slider spheres in contact with the base. At a given N the number of contacts is calculated, and they each give a contribution $1/n$ to A_r/A, where n is the horizontal length of the slider measured in spheres. The slider must rest on at least two slider spheres for $N > 0$. One slider sphere is theoretically possible, as long as the contact is at the same horizontal position as the center of mass

of the slider. This is unlikely to happen, thus two contact points is considered the minimum number of contacts. The minimum value of A_r/A is then

$$\min A_r/A = 2/n, \tag{5.9}$$

and thus obtaining $A_r \propto N$ is essentially impossible using this way of measuring A_r unless $n \to \infty$. Another way of measuring A_r could be to take into account the area of overlap at each junction. However, this would make the result dependent on the model, i.e. spheres would give another result than squares.

In Fig. 5.3(b) the the minimum value of A_r/A is 0.1, which means that $0.1 * 80 = 8$ slider particles is in contact with the base. This result is larger than the minimum value found in Eq. 5.9. The base has a period of 10 particles and thus the contact points between the slider and the base are on average at the topmost base particle for the 8 sine periods of the base under the slider. Although not visible in the figure A_r/A should be able to obtain a lower value that 0.1 because of the random vertical displacement of the base spheres, but this would require even lower values of N than presented in Fig. 5.3(a).

I expect that increasing the random vertical displacement of the base spheres would make A_r/A obtain a lower value for the lowest $N/N*$ values, since the peaks in the base would be more spaced vertically. The result might also have been different if the resolution of the slider and base was increased. If 8 contact points still occurred for the same N when the resolution was doubled, A_r/A would be 0.5.

The rapid increase in A_r with N as seen in Fig. 5.3(a) is in agreement with Fig. 5.2(b). Thus I expect the rapid increase in A_r with N not primarily to be caused by a too low resolution of the base is, but instead by the fact that a sinusoidal shaped base is used.

Discussion of possible adaptions to the base

In the analysis of Fig. 5.3(a) two improvements of the base slider contact is presented: Increasing the resolution of the slider and the base and to increasing the random displacement of the base spheres. An increase in the resolution of the slider comes with the prize that it dramatically increases the simulation time. This is problematic since I need to run simulations for a range of sliding velocities to obtain the dependence of μ_d on the sliding velocity v. For each v I also need to slide over a large enough distance to get a μ_d representative for v.

I expect the simulation time to be approximately linear in the number of particles, thus increasing the resolution of the system with a factor 2 would

increase the number of particles with a factor 2^2 and thus the simulations would require approximately four times more than is the case for the current resolution. Increasing the resolution by a factor f requires an factor f^2 increase in the spring stiffnesses k' to obtain the same E if I don't alter the time step, see Section 4.3.1. This in addition to a decrease in the non-dimensional constant of gravity g' requires new tests and possibly new adaptions which might require much time to perform.

Increasing the random displacement of the base spheres may also be problematic. As I have already described, increasing the random displacements of the base spheres may result in that slider particles get stuck in the base. If a slider sphere gets stuck the elastic model maintaining the shape of the slider could break down and destroy the simulation.

Another possible improvement of the base could be to exchange the sinusoidal shaped base with a more disordered shaped base. However to resolve such a base a larger larger resolution of the base might be needed.

From Section 2.3 we remember that not all experiments carried out by Rubinstein et al. [13] fulfilled Eq. 5.1. The relation was not found for PMMA on glass where both surfaces had a 50nm rms roughness. However the results obtained for the 500nm rms roughness for PMMA on PMMA showed a good agreement with Eq. 5.1. Thus it seems that the magnitude of the roughness influences whether Eq. 5.1 is fulfilled or not. A fully elastic and a fully plastic model was used to make a fit to the experimental results. The best fit for the fully plastic model gave an average stress at the junctions in good agreement with the measured penetration hardness of the material in use. The fully elastic model gave unrealistic results for the radius of and the stress at the junctions using the fitting parameters, indicating that that the plastic model is the applicable one for the PMMA on PMMA material [13]. The model I use for the slider base contact is elastic and may therefore not be a good model when studying the A_r/A dependence on N.

This chapter reveals that modeling a realistic base and introducing realistic contact forces is a challenging task. Even if the adaptions presented above where carried out, the shape of the base would still be very regular compared to the disorder of a realistic base. The model of the base and slider is not made for studying the dependence of A_r/A on N. Since I have a limited time on the thesis I have I have chosen to let the base be as it is.

Chapter 6

Geometric friction

6.1 Introduction

The base and slider is composed of spheres of equal size as presented in Section 3.3. The surface of the base is therefore bumpy with a gravitational potential well between the base spheres. The slider particles at the interface between the slider and the base sinks down in such potentials. The horizontal force from the base on the slider is

$$R = \sum_{i,j} \vec{F_{sb,ij}} \cdot \hat{i}, \tag{6.1}$$

where $\hat{i}$ is the unit vector in the x-direction, and the force $\vec{F_{sb,ij}}$ between slider sphere i and base sphere j is presented in Section 3.4. For the slider system modeled, R is the geometric frictional force, i.e. the force resisting the movement of the slider because of the geometrical shape of the interface. The geometric static coefficient of friction may be defined as

$$\mu \equiv \frac{-R}{N}, \tag{6.2}$$

where N is the normal force on the slider. I also introduce μ_s as the maximum value of μ.

6.2 Analytical analysis of the $\mu(t)$ dependence for the model

Before the static simulations of $\mu(t)$ is presented, an analytical study of the $\mu(t)$ dependence for the slider model is presented. This is a useful tool when testing whether the simulation program works as it should or not.

From Section 2.1.1 we remember that the static frictional force is expected to be proportional to N, neglecting the logarithmic time dependence of the static coefficient of friction μ_s. Thus μ_s should not be dependent on the normal load N. The dependence of μ_s on N can be calculated analytically

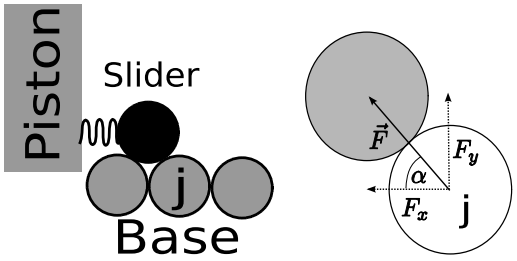

(a) (b)

Figure 6.1: a) The analytical setup, b) the force from the base sphere on the slider sphere $\vec{F}$ may be decomposed into a horizontal and vertical component, respectively F_x and F_y.

for a sphere with diameter l_0 on a base composed of unidistanced spheres of diameter l_0. For simplicity the slider is only considered a single sphere of radius $l_0/2$, placed in the groove between two base spheres, see Fig. 6.1(a). The force from sphere j on the slider, $\vec{F}$, can be decomposed into a horizontal and vertical component, respectively F_x and F_y, see Fig. 6.1(b). F_x and F_y are related by the relation

$$F_x = \frac{F_y}{\tan(\alpha)}, \tag{6.3}$$

where α is the angle between $\vec{F}$ and the negative x direction. The slider sphere will be stuck behind j as long as $F_y < N$. However when F_y exceeds N the slider sphere will begin to move forward. $F_y = N$ is therefore the maximum value of F_y before the slider begins to move. When $F_y = N$ the whole weight of the slider is carried by j and in this case μ_s may be expressed as

$$\mu_s = \frac{F_x}{F_y} = \frac{1}{\tan(\alpha)}. \tag{6.4}$$

From Eq. 6.4 μ_s is expected to be independent on N. μ_s in Eq. 6.4 can be determined by observing that the slider sphere in Fig. 6.1(a) forms an equilateral triangle with the two base spheres it rest on. Here it is assumed that the slider base interactions is stiff such that the slider does not move

significantly before $F_y = N$ is reached. I expect the value of μ_s to be

$$\mu_s = \frac{1}{\tan(\pi/3)} \approx 0.58. \tag{6.5}$$

The simulation code should reproduce the result that μ_s is independent on N. It should give a value of μ close to $\mu_s = 0.58$ just before the slider begins to move. In the simulations a single sphered slider will not be used, but instead a 2*2 slider. However the analytical results obtained above is still valid as long as the compression in the internal slider springs is small.

6.3 Testing the simulation program

To find out whether μ_s is independent on N or not, the test program calculates μ using Eq. 6.2 as a function of time. The slider is placed stationary on the base. The piston is initially in contact with the slider, however the piston slider spring is at it's rest length thus no force is exerted by it on the slider. When the simulations start the piston moves towards the slider with velocity v'_p. Only the primed simulation parameters is presented. This is because the test program is used to calculate μ, and since μ is non-dimensional, a conversion from the primed to the physical parameters is not needed. These simulations are not intended to represent a physical system with realistic density, Young's modulus, etc.

For the test program I use the following spring stiffnesses: $k'_{ij} = 0.05E'_{ij}$, $k'_p = 1.0 \times 10^{-3}$ and the base slider spring has stiffness $k'_{sb} = 0.5$ when compressed, and zero otherwise. The other parameters are: $v' = 1.0 \times 10^{-4}$, $m' = 1$ and $q = 0.3$. g' is varied in the simulations to represent a varying N as explained in Section 3.6. The slider forms a square composed of 2*2 spheres. The base is modeled as a horizontal chain of spheres separated by a distance $l'_0 = 1$. All spheres in the slider and base has the same diameter l'_0.

In Fig. 6.2(a) the $\mu(t')$ curve is presented for $g' = 6.0 \times 10^{-4}$. In the figure $\mu(t')$ does not behave nicely for the lowermost t'. This behavior stems from the fact that although the slider is initially stationary, it is not in an equilibrium position and therefore it will begin to move due to gravity. To avoid this movement in the beginning of the simulation, the slider should be at rest in an equilibrium state before the simulations are started. For this simple setup placing the bottom two slider spheres such as presented in Fig. 6.1(a) would be sufficient for small N. However for a larger slider system internal compression in the slider because of N also needs to be accounted for.

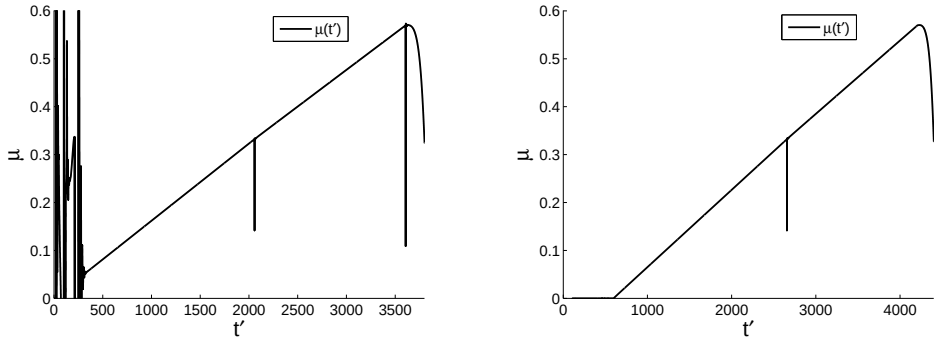

(a) (b)

Figure 6.2: (a)μ vs. t' for $g' = 6.0 \times 10^{-4}$ without the use of the stability algorithm Eq. 6.6 (b) μ vs. t' with the use of Eq. 6.6.

Another option could be to introduce a relaxation time for the system. When the slider falls down and bounce, the potential energy will be converted to internal oscillations in the slider. These oscillations will die of with time because of damping, and eventually the slider will come to a rest.

However for a large slider system, such a relaxation time may take a lot of time. To make the stabilization more effective I have made a simple algorithm that decreases the stabilization time needed. We introduce $\tilde{v_i}$ as the calculated vertical velocity and v_i as the accepted vertical velocity of slider particle i. The vertical force on i is $F_{y,i}$. The idea now is to set

$$v_i = o(F_{y_i}, \tilde{v_i})\tilde{v_i}, \quad t < t_s \tag{6.6}$$

where t_s is a parameter defining how long Eq. 6.6 is in use and

$$o(F_{y_i}, \tilde{v_i}) = \begin{pmatrix} 1, & F_{y,i}\tilde{v_i} > 0 \\ 0, & F_{y,i}\tilde{v_i} < 0 \end{pmatrix}. \tag{6.7}$$

When i moves towards it's vertical equilibrium point it becomes accelerated. Normally it would move past the equilibrium point because of the speed it has gained. However Eq. 6.6 sets the vertical velocity of i to zero when i moves away from the vertical equilibrium point, and thus i reaches it's vertical equilibrium point much faster than when the oscillations is only damped out. Eq. 6.6 is used for a time t_s before it is turned off such that the slider will behave as it is intended and for $t < t_s$ the piston is stationary. In Fig. 6.2(b) Eq. 6.6 is used with $t'_s = 100$. The oscillation seen in Fig. 6.2(a) is now

removed, and we observe that t'_s is less than the time the oscillations elapsed in Fig. 6.2(a).

Fig. 6.2 also shows some μ values that deviate from the general $\mu(t')$ curve. The deviations seen in Fig. 6.3(a) only last for a single iteration in time. They are not frequent, since the time step is chosen to be $\Delta t = 0.02$. It is unclear what causes these deviations. Introducing an average of μ over a number of time steps should remove these irregularities from the plots,

$$\langle \mu \rangle = -\frac{\sum_{n=1}^{M} R_n}{M}, \tag{6.8}$$

where M is the number of iterations averaged over. When using Eq. 6.8 it is crucial to use a small time step since the averaging should happen over a small time. If not the averaging would have an influence of the general behavior seen in Fig. 6.2(b) as well. With the small $\Delta t' = 0.02$ $M = 50$ is used. Thus the data presented will be averaged over $t'_{av} = 1$ which is small compared to the span in t' presented in the figures.

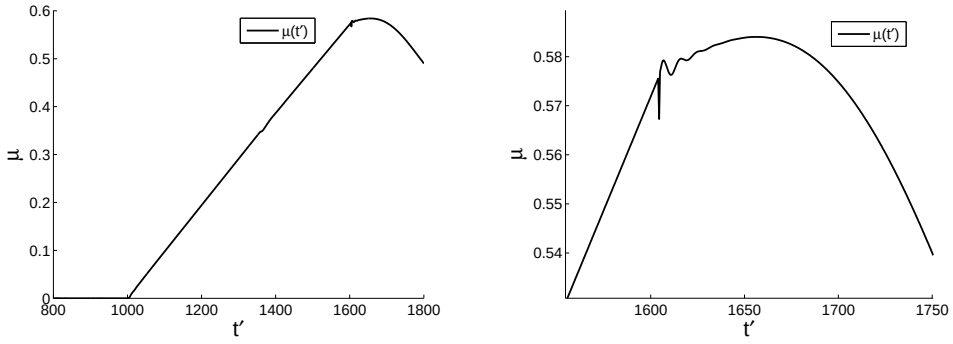

(a) (b)

Figure 6.3: (a) μ for $g' = 1.0 \times 10^{-4}$. (b) Fig. 6.3(a) focused around the largest μ values.

In fig. 6.3(a) the results of the simulation with $g' = -1.0 \times 10^{-4}$ is presented. The figure shows a linear increase in μ with t'. Fig. 6.3(b) is focused on the the peak in μ, and it shows that the linearity in μ is valid up to $\mu \approx 0.58$. In Fig. 6.4 the $\mu(t')$ curves for different g' is presented. The figures show a linear increase in μ up to a critical value in μ which is μ_s. The critical value μ_s μ increases up to before the linearity is no longer present is relatively constant $\mu_s \approx 0.58$, however μ_s decreases from almost 0.58 for $g' = -2 \times 10^{-4}$ down to a little below 0.57 for $g' = -8 \times 10^{-4}$. As seen in

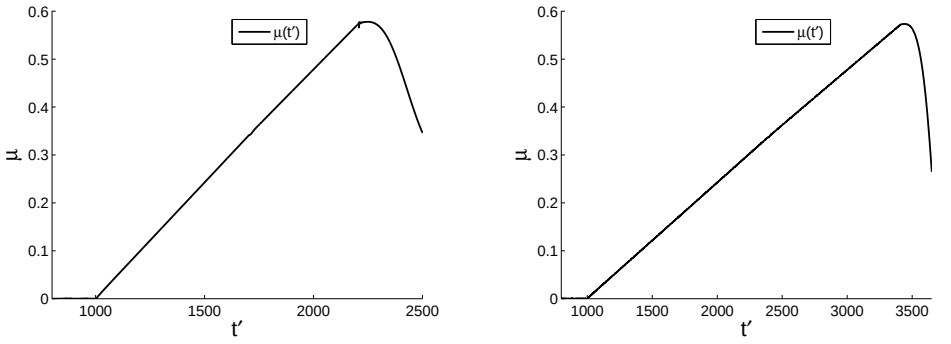

(a) (b)

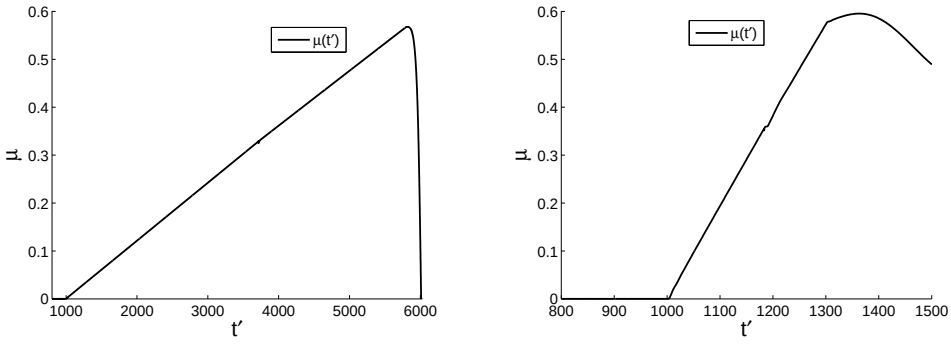

(c) (d)

Figure 6.4: (a) μ for $g' = -2.0 \times 10^{-4}$. (b) μ for $g' = -4.0 \times 10^{-4}$. (c) μ for $g' = -8.0 \times 10^{-4}$. (d) μ for $g' = -5.0 \times 10^{-5}$.

Fig. 6.3(b) a small increase in μ appears when the linearity is no longer valid before μ begins to drop.

Analysis of the results

The linearity of the $\mu(t')$ curve seen in Fig. 6.3(a) and Fig. 6.4 is because of that the simulations are run with a constant piston speed v' that push on a stationary slider. As long as the slider is stationary the compression of the piston slider interface will increase linearly with t'. To keep the slider stationary R and hence μ also increases linearly with t'. When the slider begins to move, the compression of the piston slider interface cannot follow the same linear increase anymore. The point where the linearity in μ is no longer present in the figures therefore shows the value of μ obtained just before the slider begins to move.

In Section 6.2 the slider was expected to begin to move when $\mu = \mu_s \approx 0.58$. This value is in good agreement with the value of μ_s found in Fig. 6.3(a) and Fig. 6.4. g' is 40 times larger in Fig. 6.4(c) compared to Fig. 6.4(d), but the change in μ_s is only minor. However a small but systematic decrease in μ_s with N is observed. When N increases so does the maximum value of the horizontal forces. The deformations of the slider is dependent on the forces acting on it, and thus a large horizontal force will compress the slider so that it wont fit on the base as well as for lower N. The piston also applies a torque on the slider, thus causing the slider to twist. The torque is dependent on R and the torque therefore becomes larger with increasing N. The deformation of the slider and the torque has the effect that the lower rear particle is slightly pushed up on the base particle in front of it. This will give an increase in α in Eq. 6.3, and thus F_x will decrease with the result that the contribution to μ from this slider particle is lowered. The base slider interactions are chosen 10 times stiffer than the internal slider springs, and thus the change in compression of these springs is not considered to cause the decrease. However if $k_{sb} < k_{ij}$ the base slider springs may also give a change in μ with N.

In Fig. 6.5 a comparison of the the result obtained in 6.4(c) with a system where k_{ij} and k_{bs} is 10 times stiffer is presented. The figure reveals that the stiffer system obtains a slightly larger μ_s than the softer slider system. The stiffer system gives $\mu_s \approx 0.58$ which is in very good agreement with the expectation Eq. 6.5. Thus the systematic decrease in μ_s with N seems to be caused by the compressions in the slider springs, since increasing the stiffness of the slider system removed the deviation in μ_s for the highest value of N.

The effect of slider compression is shown in Fig. 6.6, where the slider has height Y and a variable length X. Observe that the length X in the figure

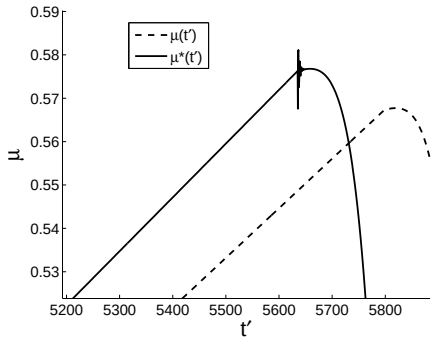

Figure 6.5: $\mu(t')$ is the curve presented in fig. 6.4(c), and $\mu*(t')$ is the result of a simulation for the stiffer system where $k_{ij} = 5E_{ij}$ and $k_{sb} = 0.5$. The stiffer system results in a $\mu_s \approx 0.58$ which is in better agreement with Eq. 6.5.

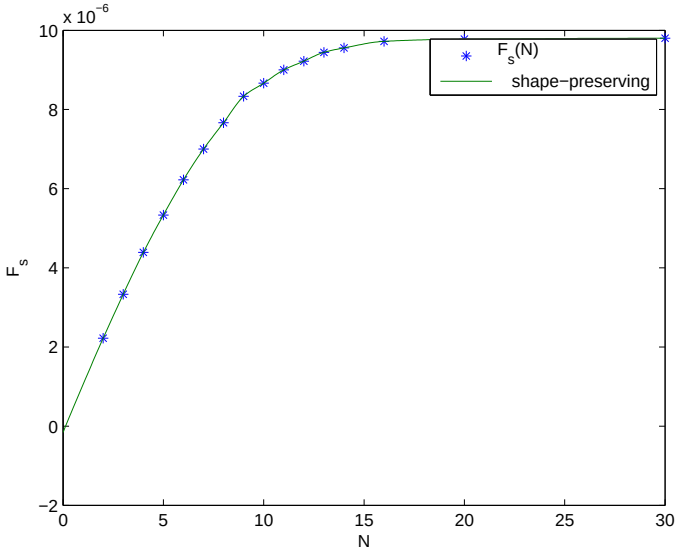

Figure 6.6: Th maximum static frictional force, F_s for different slider lengths, N

is denoted N, which must not be confused with the normal force! Fig. 6.6 reveals that the maximum static frictional force reaches a plateau level for high X, which I expect is because of the elastic compression of the slider. For $X > 15$ F_s is approximately constant, indicating that only the first 15 bottom slider spheres contributes to F_s at the same time.

In Eq. 6.5 it was assumed that when μ_s was reached, μ would drop when the the slider began to move. This is however not the case for the simulation results. Fig. 6.3(b) reveals that μ continues to increase at the very beginning of the movement of the slider before μ begins to drop. The same is also seen in Fig. 6.4. However this effect only gives a minor increase in μ, and thus Eq. 6.5 is a good estimate for μ_s.

The torque on the slider exerted by the piston is an effect that one needs to be aware of. When a large slider is used, it may not be a good idea to use a square slider, but instead use a rectangular slider with larger length than height.

Chapter 7

Geometric sliding friction

7.1 Introduction

In Section 6.1 I presented the expression geometric friction. I used two measures for the static coefficient of friction where μ was the coefficient of friction at a given time while μ_s was the maximum in μ before sliding commenced. The discussion of static friction was mostly for testing the simulation code, therefore from now on I use the notation μ for the dynamic coefficient of friction. In this chapter the dependence of μ on the sliding velocity v for the slider system is studied.

7.2 Measuring μ

7.2.1 The $\mu(t')$ curve

In Section 6.1 I presented the frictional force R

$$R = \sum_{i,j} \vec{F_{sb,ij}} \cdot \hat{i}, \tag{7.1}$$

The same formula may be used in the dynamic case, such that μ can be calculated as

$$\mu = \frac{-R}{N}. \tag{7.2}$$

The $\mu(t')$ measurements for static friction is Section 6.3 was carried out using a base where the base spheres was perfectly aligned on a line with spacing l'_0. It is not easy to obtain stable sliding on such a base, because of lattice alignment effects. I therefore perturb the uniform horizontal positioning of the base spheres with a random displacement up to a maximum denoted $n'_{r,x}$

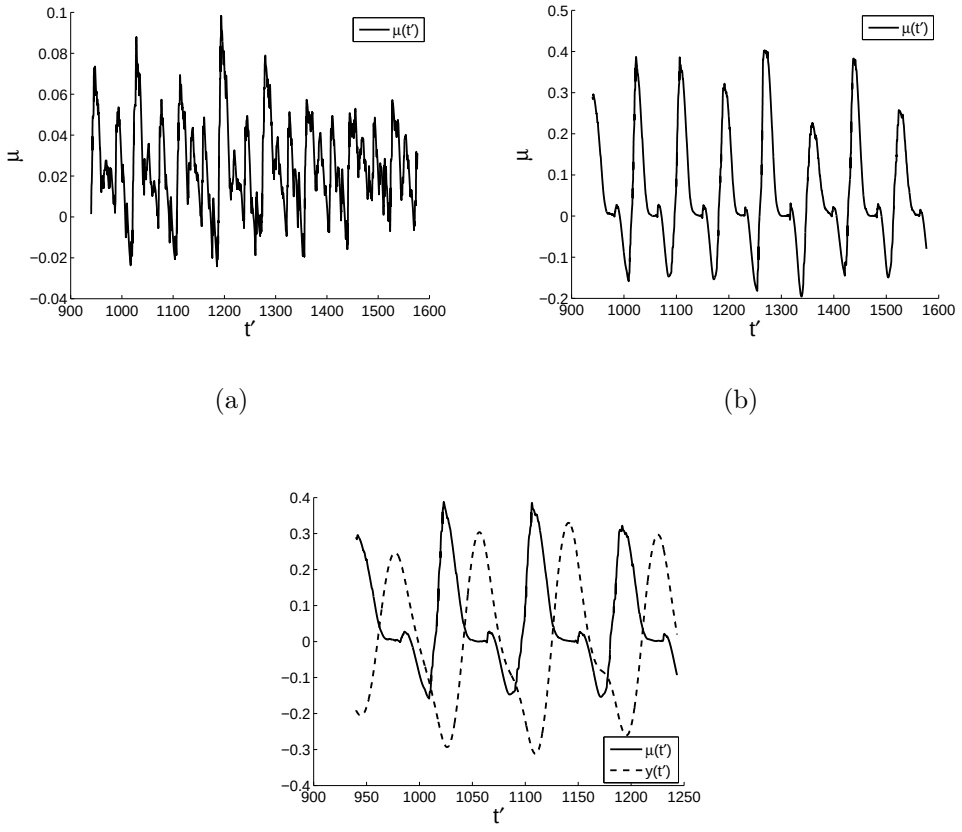

Figure 7.1: (a) μ vs. t' for sliding friction with $n_r = 0.5$ (b) μ vs. t' for sliding friction with $n_r = 0.3$. (c) μ vs. t' for sliding friction with $n_r = 0.3$ plotted together with the averaged vertical motion of the slider at t'. The vertical motion is scaled with a factor 8 to better visualize the connection between it and $\mu(t')$.

in the horizontal direction, and $n'_{r,y}$ in the vertical direction. In this section I want to investigate how μ varies under sliding, and find a way of extract a μ representative for a given sliding velocity. I therefore operate with the primed notation which is the non-dimensional quantities used in the code.

To find out how μ varies with t' I have in Fig. 7.1(a) presented the $\mu(t')$ curve obtained for the parameters shown in Table 7.1. In Fig. 7.1(a) μ varies a lot with t', and thus an averaging of the μ values should be introduced. The figure also reveals that μ attains a negative value for some t'. This is a

$X = 40$	$Y = 20$
$l'_0 = 1$	$k'_{ij} = 2E'_{ij}$
$k'_{bs} = 10$	$k'_p = 0.7$
$v' = 0.012$	$g' = -0.0004$
$n'_{r,y} = 0$	

Table 7.1: The non-dimensional parameters in Fig. 7.1. $n'_{r,x}$ is specified in Fig. 7.1.

strange result since μ should be a positive quantity. When $\mu < 0$, R must be positive, such that the base accelerates the slider. The reason for μ to become negative is easier to understand by analyzing sliding on a base with smaller $n_{r,x}$. In Fig. 7.1(b) the same sliding experiment is carried out with $n_{r,x} = 0.3$. This figure shows an approximate periodic motion of the $\mu(t')$ curve. The time duration of one period is approximately $\Delta t' \approx 80$, and thus the slider slides a distance $\Delta x' = \Delta t' v' \approx 1$, which is the average distance between the slider spheres. In Fig. 7.1(c) the $\mu(t')$ curve for $n_{r,x} = 0.3$ is presented together with the average vertical motion of the slider $y(t')$ found by the algorithm:

$$y(t'_k) = \frac{1}{n}\sum_{i=0}^{n}(r_y(t'_k)_i) - y_0 \tag{7.3}$$

where

$$y_0 = \frac{1}{on}\sum_{i}^{n}\sum_{j=0}^{o}(r_y(t'_j)_i) \tag{7.4}$$

is the mean vertical position of the slider spheres, $r_y(t'_k)_i$ is the vertical position of slider sphere i, while n is the number of slider spheres and o is the length the t'_k array. y_0 is included so that $y(t')$ oscillates around zero. The slider spheres must slide up on the base spheres and then slide back again on the rear side. This periodic vertical motion is seen in Fig. 7.1(c). The figure reveals that $\mu(t')$ increases fast and obtains a maximum when the slider approaches it's lowest point in the periodic motion. I expect the lowest point to be in the groove between the base spheres, thus when the slider spheres slides down on the back side of the base spheres, they eventually bump into the next base sphere which exerts a force $\vec{F}$ to prevent the downward motion of the slider spheres, see Fig. 7.2(a) Note that the horizontal component of $\vec{F}$, F_x now points in the negative x direction. This collision describes why $\mu(t')$ increases and attains a maximum around the minimum in the periodic motion of $y(t')$. We also observe that $\mu(t')$ attains a negative value when the slider spheres is in a negative vertical motion. The slider spheres are now

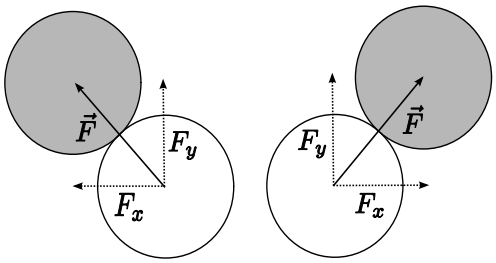

(a) (b)

Figure 7.2: The force $\vec{F}$ exerted by the base sphere on the slider sphere when (a) the slider slides up and (b) when the slider slides down on the back side of the base sphere.

sliding down the rear side of the base spheres, see Fig. 7.2(b). In this case F_x points in the positive x-direction, and thus the slider sphere gains horizontal speed which gives a negative value of μ.

7.2.2 Averaging methods for μ

In Section 7.2.1 we found that μ varies during sliding, and therefore an averaging method should be used to calculate the value of μ representative for the chosen sliding velocity. A simple averaging method could be to take the average of μ over a distance Δx.

$$\langle \mu(x, x + \Delta x) \rangle = \frac{1}{oN} \sum_{j=j_0}^{o} R_j, \tag{7.5}$$

where j_0 is the starting time of the averaging and o is the number of R_j values averaged over or equivalently the number of time steps needed before the sliders moves the distance Δx. Thus Eq. 7.5 gives the average coefficient of friction over a distance Δx.

There is, however, an issue with using Eq. 7.5. For low v I cannot neglect the fact that the some slider spheres may be stationary for a period of time during sliding. This may happen if a slider sphere is trapped in the potential well in the gap between two base spheres. The question now is whether the forces from these temporary stationary particles should contribute to Eq. 7.5 or not. I may end up with that the bottom slider spheres moves in a stick slip pattern where they stop and then move forward again. However the slider as a whole may slide with a well defined velocity v. Thus Eq. 7.5 may

end up with averaging over a significant amount of static forces, and the distinction between the static and dynamic coefficient of friction becomes diffuse. Instead of using Eq. 7.5 to estimate the average of μ, I use another averaging method for finding $\langle \mu(x, x + \Delta x) \rangle$:

$$\int_{x=0}^{x=L} \vec{F} \cdot \vec{ds} = F_d \Delta x. \tag{7.6}$$

Eq. 7.6 states that the total work done on the slider over the distance Δx can be approximated by an average force F_d over the distance Δx. The total work on the slider is the same as the sum of the works done on each slider-particle in contact with the base:

$$\int_{x=0}^{x=L} \vec{F} \cdot \vec{ds} = \sum_{i=0}^{X} \int_{\Delta x_i} \vec{F_i} \cdot \vec{ds}, \tag{7.7}$$

where X is the number of slider-particles on the interface, i.e. the number of slider particles in the x-direction. Δx_i is the horizontal displacement of particle i, which is generally not the same as the total sliding distance Δ_x of the slider since the slider is not rigid. Eq. 7.7 effectively removes the static contribution to F_d, since if the slider sphere i is stationary $\Delta(x_i) = 0$ with the result that $\int_{\Delta x_i} \vec{F_i} \cdot \vec{ds} = 0$. Eq. 7.6 is a weighted mean of the forces $\vec{F_i}$'s where the weights are the displacements over which each force $\vec{F_i}$ works over, and thus the static contributions are removed. From Eq. 7.6 and Eq. 7.7 I can express $\langle \mu(x, x + \Delta x) \rangle$ as

$$\langle \mu(x, x + \Delta x) \rangle = \frac{1}{N \Delta x} \sum_{i=0}^{X} \int_{\Delta x_i} \vec{F_i} \cdot \vec{ds} \tag{7.8}$$

The simulation code cannot evaluate the integral in Eq. 7.8 exactly, since the time is discretized. The integral $\int_{\Delta x_i} \vec{F_i} \cdot \vec{ds}$ can be expanded by the sum

$$\int_{\Delta x_i} \vec{F_i} \cdot \vec{ds} \approx \sum_{j=0}^{o} \sum_{k=0}^{1} F_{ik}(x_i^j)(r_{ik}^{j+1} - r_{ik}^j), \tag{7.9}$$

where o is the number of time steps before the slider has moved the horizontal distance Δx, the index k resembles the components of the vectors, i.e. the horizontal and vertical component. $r_{ik}^{j+1} - r_{ik}^j$ is the movement of slider particle i in the direction k from time step j to time step $j + 1$. Thus I get that:

$$\langle \mu(x, x + \Delta x) \rangle \approx \frac{1}{N \Delta x} \sum_{i=0}^{X} \sum_{j=0}^{o} \sum_{k=0}^{1} F_{ik}(x_i^j)(r_{ik}^{j+1} - r_{ik}^j). \tag{7.10}$$

In Fig. 7.1(b) in Section 7.2.1 we observed a periodicity in the $\mu(t')$ curve for low $n_{r,x}$. The period was approximately the average distance between the base spheres l_0'. Thus $\Delta x > l_0$ should at least be required to get an average representative for the dynamic coefficient of friction at velocity v. In the following the notation $\langle \mu(x, x + \Delta x) \rangle$ is exchanged with μ, where μ is the value obtained by Eq. 7.10 averaged over the total slided distance. Thus μ is the average dynamic coefficient of friction for the whole slided distance at velocity v, also written $\mu(v)$.

7.3 Problems with oscillations in the piston slider interface

When I started to run sliding simulations I had problems with oscillations in the piston slider interface. These oscillations sometimes died out with time, but other times they blew up in time. The oscillations often occurred when the acceleration phase of the piston had ended. The slider often moved away from the piston, but was soon slowed down by the frictional forces before it was hit by the piston again. In severe cases the slider came to a rest before it was hit by the piston again, and the collision with the slider then "launched" the slider forward. Such oscillations made it problematic to collect $\mu(v)$ data since then the slider velocity should not fluctuate too much around v. Although oscillations occur for several choices of the slider system, I present some oscillations occurring for a sinusoidal shaped base with amplitude Δ and period λ. $\Delta x(t')$ is the non-dimensional distance from the rest length of the slider piston spring at time t'. $\Delta x(t')$ for two different simulation runs is presented in Fig. 7.3. The parameters which are the same for both Fig. 7.3(a) and Fig. 7.3(b) is presented in Table 7.2(a), and the differences is presented in Table 7.2(b). In both Fig. 7.3(a) and Fig. 7.3(b) the oscillations dies out with time.

Collecting data under such oscillations is not ideal. A possible solution this problem could be to introduce a time delay before data is collected after the acceleration phase has ended. However, this has consequences for the simulation time, especially for high v where the time step is chosen small. Another problem is that the oscillations sometimes does not die out with

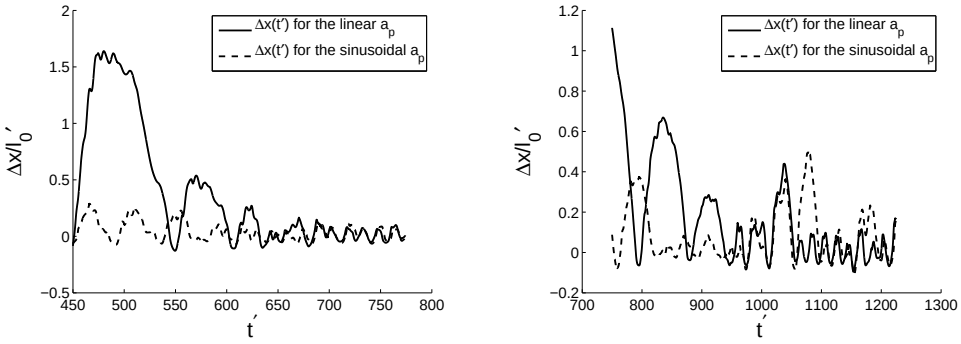

(a) (b)

Figure 7.3: The oscillations in the piston slider interface after the acceleration phase of the piston is completed. The solid line is the oscillations that occurred when $a_p = \text{const}$ was used, and the dashed lines is the oscillations that occurred using Eq. 7.16. The base has a period of (a) $5l'_0$ and (b) $10l'_0$.

$n_x = 30$	$n_y = 15$
$l'_0 = 1$	$k'_{ij} = 75E'_{ij}$
$k_{sb} = 538$ $k_p = 8$	$k_p = 8$
$v' = 0.012$	$g' = -0.03$
$\Delta' = 0.25$	$n_{ry} = 0.05$

(a)

Fig. 7.3(a)	Fig. 7.3(b)
$v' = 0.068$	$v' = 0.05$
$n_r = 0.3$	$n_r = 0.4$
$\lambda = 5$	$\lambda = 10$
$t'_a = 200$	$t'_a = 500$

(b)

Table 7.2: a) The non-dimensional parameters used for both Fig. 7.3(a) and Fig. 7.3(b), and b) the parameters different in Fig. 7.3(a) and Fig. 7.3(b)

time. I have therefore tried to find out the reason for these oscillations to occur.

For simplicity I assume that the frictional force R is not dependent of velocity, and I neglect the internal slider springs . Hook's law

$$F_p = -k\Delta x, \tag{7.11}$$

describes the relation between the force in the piston slider spring F_p and the amount of compression the spring is subjected to Δx. The acceleration of the slider a_s is related to F_p trough

$$F_p - R = Ma_s, \tag{7.12}$$

where M is the mass of the slider. In the acceleration phase the piston moves with a constant acceleration a_p In the acceleration phase F_p is therefore stable when

$$F_p - R = Ma_p, \quad v_s = v_p, \tag{7.13}$$

where v_s and v_p is relatively the slider and piston velocity. If I assume the the slider system fulfills Eq. 7.13 what will happen when v is reached?

When v is reached, $a_p = 0$, and now $F_p > R$, thus the slider will still be accelerated because of the potential energy stored in the piston-slider spring. This may lead to an oscillation in the piston slider interface. Let Δx_{eq} be the displacement giving the value of F_p required by Eq. 7.13. Combining Eq. 7.13 and Eq. 7.11 I get that

$$\Delta x_{\text{eq}} \sim a_p. \tag{7.14}$$

I also introduce a_{rel} as the acceleration of the slider relative the piston given by:

$$a_{\text{rel}} = k(\Delta x - \Delta x_{\text{eq}})/M. \tag{7.15}$$

When v is reached $a_p = 0$ and thus Δx_{eq} instantly drops to a lower value. This is problematic since F_p now accelerates the slider with the acceleration a_{rel} and this may lead to a significant $\dot{\Delta x}$ when $\Delta x = \Delta x_{\text{eq}}$. I expect this to be the cause of the oscillations seen in the slider piston interface when v is reached.

To avoid the oscillation I must avoid that $\dot{\Delta x}$ obtains a large value at $\Delta x = \Delta x_{\text{eq}}$. Δx will move towards Δx_{eq}. If Δx_{eq} is reduced slowly, Δx would follow Δx_{eq} without letting $\dot{\Delta x}$ rise to a high value. Using this observation and Eq. 7.14 I have constructed a new acceleration profile for the piston,

$$a_p = 1 + \sin\left[\left(\frac{2t}{t_a} - 0.5\right)\pi\right], \tag{7.16}$$

where t_a is the acceleration time for the piston. Eq. 7.16 is continuous without rapid changes in a_p, and it has the property that both $a_p(t)$ and $|\dot{a}_p(t)|$ decreases towards zero for $t > \frac{3t_a}{4}$, and that $\dot{a}_p(t_a) = a_p(t_a) = 0$. From eq. Eq. 7.14 we get that both Δx_{eq} and $\dot{\Delta x}_{\text{eq}}$ also decreases towards zero for $t > \frac{3t_a}{4}$ and that $\Delta x_{\text{eq}}(t_a) = \dot{\Delta x}_{\text{eq}}(t_a) = 0$. Since Eq. 7.16 is symmetric the same behavior of Δx_{eq} when t approaches $t = 0$ from above is present. It is important not to choose t_a too small, since $\dot{a}_p(t)$ inversely proportional with t_a.

The property of Eq. 7.16 that Δx_{eq} moves slowly towards zero which is the equilibrium displacement when $t = t_a$ helps to reduce the potential energy in the piston slider spring that may potentially lead to unwanted oscillations. In

the above analysis I have neglected the internal springs in the slider. When the piston pushes the slider, a compression wave will traverse the slider, hence there will be a time delay Δt before the leading end responds to the push of the slider. The decreasing variations in a_p when a_p approaches zero therefore also helps to prevent that too much elastic energy is stored in the slider when the acceleration phase has ended. This of course requires that $t_a \gg \Delta t$.

The dashed lines in Fig. 7.3(b) and Fig. 7.3(a) is the oscillations in the piston slider interface when a_p follows the sinusoidal profile Eq. 7.16. The two figures show that Eq. 7.16 reduces the oscillations after the acceleration phase of the slider has ended. It should be noted that although Eq. 7.16 reduces the oscillations in these two cases, this is not always the case. It is always possible to find a set of parameters which makes it hard to obtain stable sliding. For poor choices of parameters it is also possible that Eq. 7.16 succeeds in reducing the oscillations in the piston-slider interface when the acceleration phase ends and that new oscillations builds up after a period with stable sliding.

A possible third solution to the oscillation problem could be to increase k. This would decrease the energy in the spring at a given load on the slider, since the energy of the spring is expressed as $E_p = k\Delta x^2$. However, making the piston slider springs stiffer is not wanted because then the piston forces the slider to move with velocity v, thus violating the physical system I am modeling.

7.4 The early simulations of the dependence of μ on v

In this section some observations found when first attempting to simulate sliding friction is presented as well as a simulation of the $\mu(v)$ behavior for an early choice of simulation parameters.

When I started to run sliding simulations I thought that it would be easiest to start with a small 2*2 slider and then increase the slider size when the simulations seemed to work well. Getting the 2*2 slider to slide was not easy, and instead of sliding the slider just bounced around. From the static test simulations I knew that I should use a rectangular shaped slider to prevent rotation of the slider during sliding. Thus I chose a longer slider of size 10*5 particles, and with this slider I was able to get a more stable sliding. The roughness of the base relative to a 2*2 slider is much larger than relative to a 10*5 slider. I assume that this is the reason that it is hard to obtain stable sliding for small sliders. A small slider is comparable with

$X = 80$	$Y = 40$
$l'_0 = 1$	$k'_{ij} = 2E'_{ij}$
$k'_{bs} = 10$	$k'_p = 0.7$
$g' = -2.0 * 10^{-4}$	$q = 0.3$
$n_{r,x} = 0.4$	$n_{r,y} = 0$

Table 7.3: The non-dimensional parameters used for the early $\mu(v)$ simulations.

driving a car in a terrain with roughness of the size of the car. Increasing the speed of the car would not result in a more comfortable ride. The 2*2 slider it tilted when riding over the base spheres because of it's short length. The length of the 10*5 slider prevented this tilting, and the increased mass made it slide more easily.

7.4.1 An early $\mu(v)$ simulation

The first study of the dependence of μ on v I performed was done before I had derived the relation between the physical and the primed non-dimensional parameters used by the simulation code. Instead I made live visualizations of the slider, and by trial and error I found a set of parameters that seemed to give a reasonable visually behavior. I was more focused on getting results than to understand what physical system the simulations was run for. This has later shown not to be a good idea since the system I simulated was not realistic and gave me a completely different behavior than what I have found for a more realistic system which is presented later. The work done on the unrealistic system is, however, not a waste of time, since it revealed some important restrictions of the model used to describe the physical system. The non-dimensional constants I chose for the simulations is presented in Table 7.4.1. Choosing l_0,t_0 and ρ as described in Section 4.3.1 the physical parameters are Young's modulus $E = \frac{2}{150}400\text{kPa} \approx 5.33kPa$, which is an unrealistically soft slider. The pull of gravity of this system is $g = \frac{2*10^{-4}}{0.02} * 12.5\text{m/s}^2 = 0.125m/s^2$, which is very small. These values was obtained using Table 3.1.

In Fig. 7.4 I have shown the $\mu(v)$ curve obtained for the simulations with the parameters as described in Table 7.4.1. The figure shows that for low v, $\mu(v)$ increases with v until a maximum, $\mu_{\max}$ is reached, and I denote the sliding velocity corresponding to this maximum $v_{\mu,\max}$. For $v > v_{\mu,\max}$ $\mu(v)$ decreases, and it seems as $lim_{v\to\infty}\mu(v) = 0$.

The fact that $\mu(v)$ decreases for $v > v_{\mu,\max}$ does not agree with what I

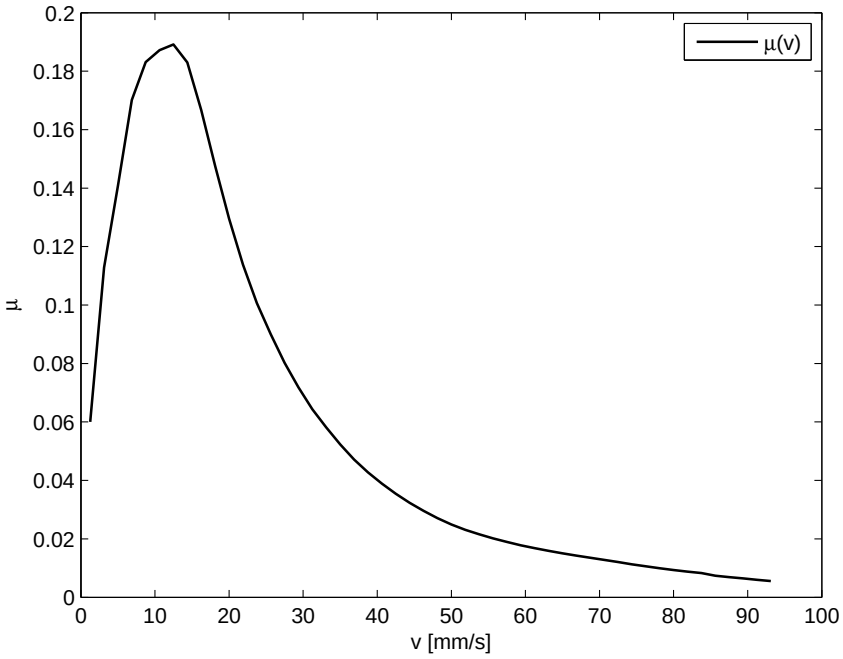

Figure 7.4: The $\mu(v)$ curve for a slider of Young's modulus $E \approx 5.33$kPa and $g = 0.125\text{m/s}^2$

would expect. It is not easy to give an accurate expectation of the $\mu(v)$ curve because of the complexity of the system. Still there is possible to make an expectation based on some approximations.

Let's assume that slider sphere A moves in the positive x direction with horizontal velocity v as shown in Fig. 7.5. When A hits base sphere B a change in A's velocity $\Delta\vec{v_A}$ occurs. If A slides up and above B the time t A has to slide up on B is $t \simeq 1/v$ and thus I expect

$$|\Delta\vec{v_A}| \sim v. \tag{7.17}$$

A may also be obstructed from moving above B. In this case a total decrease in the horizontal velocity $\Delta v_x \geq v$, and thus Eq. 7.17 is also expected. The damping force F_d is dependent on the relative velocity between A and the neighbor sphere C. For simplicity I assume that C moves with velocity v in the horizontal direction. The relation between F_d ad v is found using Eq. 7.17

$$F_d = -\eta_{AC}\Delta\vec{v_A} \sim v \tag{7.18}$$

The energy dissipated by the damping, denoted W_d is dependent on F_d, and

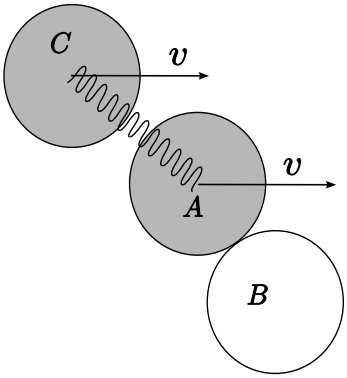

Figure 7.5: The slider sphere A has horizontal velocity v in the positive x direction. A has several neighbors, however only one neighbor C is included in the figure. C also moves with horizontal velocity v. The figure shows A in the moment when it hits base sphere B.

may therefore also be written in terms of v

$$W_d \propto F_d \sim v \tag{7.19}$$

The total work W done on the slider cannot equal the internal energy in the slider. If that was the case the oscillations in the slider would blow up because of the increasing internal translational energy. Thus there must be a transformation of the translational energy in the slider to other states. The only transformation of of energy introduced in the slider system is the damping of internal slider springs. Thus I expect $W = W_{d,internal} + \Delta E_k$, where ΔE_k is the change in the oscillation energy in the springs over the distance W is calculated, and $W_{d,\text{internal}}$ is the total energy dissipated to damping in all internal slider springs. $\Delta E_k = 0$ can be assumed if the oscillations does not blow up with time. The force F_d is applied on C from A, and the larger F_d the larger the change in C's velocity and the energy dissipated between C and other internal particles. Thus I expect that the relation $W_{d,\text{internal}} \sim v$ is valid. Since μ is proportional to the amount of work W done over a distance as described in Section 7.2.2, I expect

$$\mu \sim v. \tag{7.20}$$

I also expect the slope of μ to increase with q. It should be noted that the physical requirement of energy conservation may not be fulfilled in simulations. This is because the forces, displacements and velocities of the particles is only calculated at discrete times and thus the motion of the slider would deviate from the exact result.

Eq. 7.20 is a rough estimate of the $\mu(v)$ dependence. However the $\mu(v)$ curve presented in Fig. 7.4 in the low end of v seems to agree with the expectation Eq. 7.20. Even if Eq. 7.20 was not valid I would still not expect $\mu \to 0$ for $v \gg v_{\mu,\max}$. Such a behavior of μ would be problematic for example for an aircraft coming in for landing, where the relative velocity between the tires and the tarmac is large. If this resulted in a vanishing μ the tires would not spin up but instead only slide. However we know that the frictional forces on the interface between the tires and the tarmac violently accelerates the tires of the aircraft when it touches the ground.

To find the reason for the unexpected behavior of μ at large v, I decided to search for a potential error in the simulations. The error could not be caused by a too large time step causing the collisions to be resolved in too few time steps. This is because the time step is decreased proportionally to v so that a given sliding distance is resolved with an equal amount of points for all v, except for at very low v where this would result in a too large time step. I

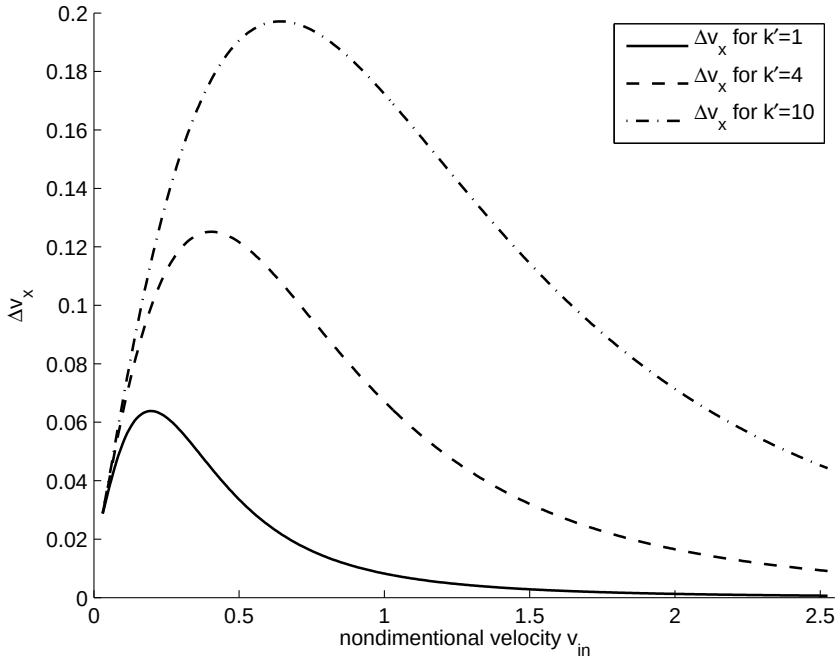

Figure 7.6: The $\Delta v_x(v)$ curves for a given collision setup where one sphere is fixed. v_{in} is the horizontal velocity before collision. The different curves represents different spring constants k' during collision.

decided to make a small test program with the same collision algorithm as in the simulation code. I used this test program to simulate a collision between

a slider sphere A and a fixed base sphere B. With the program I was able to study the change in horizontal velocity Δv_x after collision from the initial horizontal velocity v_{in}. The results of runs with $k' = 1$, $k' = 4$ and $k' = 10$ is presented in Fig. 7.6. The figure shows that Δv_x increases approximately linear with v_{in} for low velocities in good agreement with the expectation Eq. 7.20. This linearity is however not present when v_{in} reaches a critical level,$v_{\text{in,crit}}$ and when $v_{\text{in,crit}}$ is exceeded, Δv_x drops with v_{in}, and Δv_x seems to converge to zero for high v_{in}. The figure also shows that $v_{\text{in,crit}}$ is dependent on k'. The shape of the Δv_x curve shares much of the characteristics as seen in Fig. 7.4.

To find out what caused this drop in Δv_x I made visualizations of the simulations. They revealed that A bounced off B for low v_{in}. When v_{in} was increased so did the compression of the interface between the two spheres with the result that when $v_{\text{in}} > v_{\text{in,crit}}$ A began to plow through B. When the spring connecting A and B is compressed, the force on A from B points radially from A towards B. Thus when the horizontal position of A equals that of B, the force points in the vertical direction. At this point Δv_x cannot increase further, since when the horizontal position of A exceeds that of B, A would gain speed in the horizontal direction. This describes why the maximum in Δv_x is depends on k' since a larger k' gives a larger repulsive force on A at a given compression.

The momentum transfered from the B on A may be expressed as

$$\vec{I} = \int_{t_c} \vec{F}(\vec{r})dt, \tag{7.21}$$

where $\vec{r}$ is the position vector of A relative to B. I expect $|\vec{I}| \sim t \sim v_{\text{in}}^{-1}$ when A plows through B, and therefore $|\Delta\vec{v}|$ decreases with v_{in}. Thus the path of A through B approaches a horizontal line when increasing v_{in}. If A plows through B in a straight line, the work done by B on A during the collision would be zero. This would give no contribution to $\mu(v)$. The observation that A plows through B at high v_{in} therefore explains why $\mu(v)$ drops for high v. It is an important observation that I need to be aware of when choosing the non-dimensional spring stiffnesses of the system. Plowing will occur for any finite stiffness, but the higher I set the stiffness, the higher the value of v required before the plowing problem occurs, as we see in Fig. 7.6

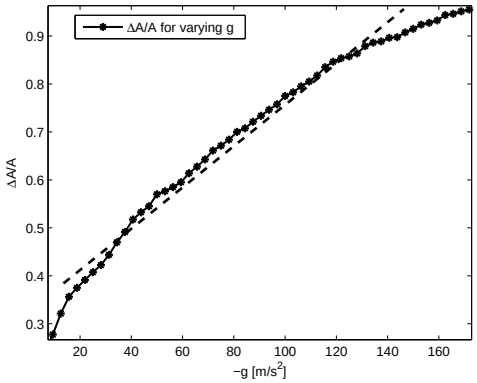

Figure 7.7: The $A_r(-g)$ dependence. The dashed line is inserted to better visualize that A_r may be approximated by a linear expression in $-g$ for $-g \in [20m/s^2, 140m/s^2]$.

7.5 Geometric sliding friction for a more realistic system

In this section I have used the simulation parameters described in Section 4.3.1, that is I choose $E = 400$kPa, $l_0 = 1.0 * 10^{-4}$m and $\rho = 3.0 * 10^3$kg/m^3. I have chosen to resolve the slider by $X = 80$ particles horizontally and $Y = 40$ particles high. This gives me a slider with physical dimensions 8.0mm long and 4.0mm high. The base shape as described in Section 5.2, i.e. the base is stationary and shaped as a sine wave with amplitude $A = 2.5*10^{-5}$m and period 1.0mm. To make the base less regular, I have displaced each base sphere randomly from the sine-shape up to $4.0 * 10^{-5}$m horizontally and $5.0 * 10^{-6}$m vertically. The normal force N represented by g is varied to study how the $\mu(v)$ curve depends on N, and for all simulation I have used $|g| \geq 12.5$m/s^2. In Chapter 5 I presented the relation between the real area of contact A_r and the normal force N. I found that A_r is approximately linear in N for $20\text{m/s}^2 \leq |g| \leq 140\text{m/s}^2$, see Fig. 7.7, and we remember that $N = -Mg$, where M is the combined mass of the slider. The g values chosen cover the interval where the linear approximation of A_r with N may be used, however I have also chosen two values outside this range which are $g = -12.5\text{m/s}^2$ and $g = -156\text{m/s}^2$. To obtain the behavior of μ on v for the slider system, I have run sliding simulations for a range of velocities v, and combined the results to a $\mu(v)$ curve. From theory on friction μ is found to be close to independent of N, a property I hope to find when comparing simulation runs for different N. In Fig. 7.8 I have plotted the

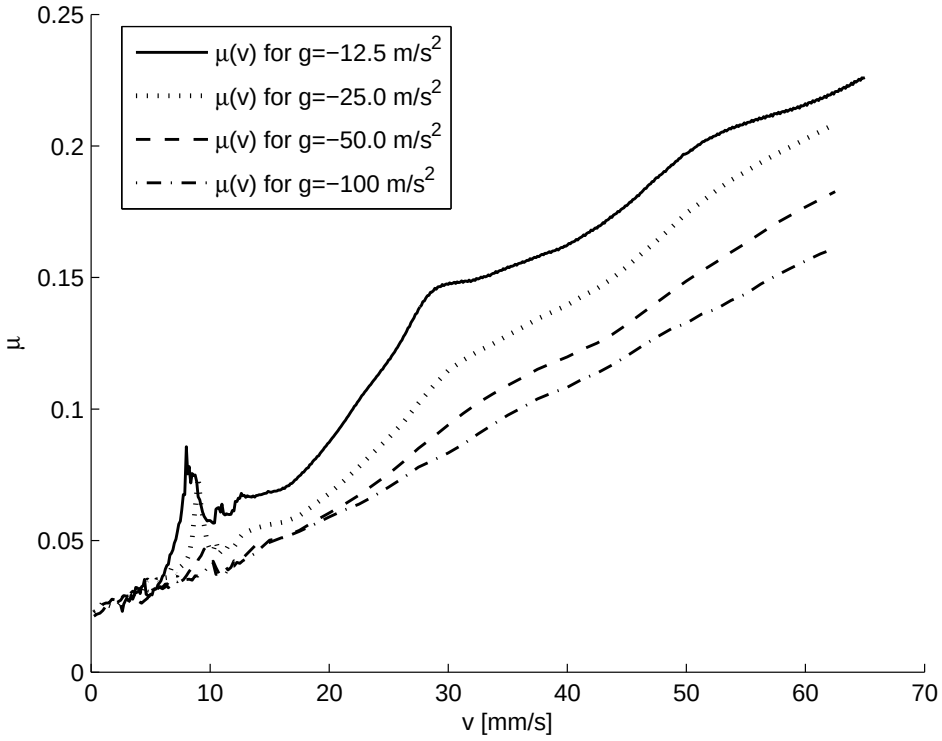

Figure 7.8: The $\mu(v)$ curves for several values of g.

$\mu(v)$ curves for several values of g. The figure reveals that the $\mu(v)$ curves for different N does not overlap as I expected them to do based on theory on friction. For low N the $\mu(v)$ curve has a complex behavior, but it increases with v except at some peaks for low v. For larger N the $\mu(v)$ curve seems to approach a linear shape. This is more clearly seen in Fig. 7.9 where I have shown the results when larger values of N is used than in Fig. 7.8. Fig. 7.9 reveals that the $\mu(v)$ curves overlaps much better for high N, thus it seems that the $\mu(v)$ curve becomes less dependent on N with increasing N.

The peak seen for the two lowest values of N in Fig. 7.8 around $v = 8\text{mm/s}$ is an interesting observation. In Fig. 7.10 I have zoomed in on the region around the peaks. The figure reveals that the peak in μ becomes less visible with increasing N, and for the two highest values of N, only a bump in the $\mu(v)$ curve remains. The position of the peak/bump is slightly shifted towards higher v when increasing N. The peak for $g = -12.5\text{m/s}^2$ curve seems to lie approximately at $v = 8.1\text{mm/s} \equiv v_{\mu 1}$, and looking more closely on the figure another smaller peak on the same curve can be seen at around

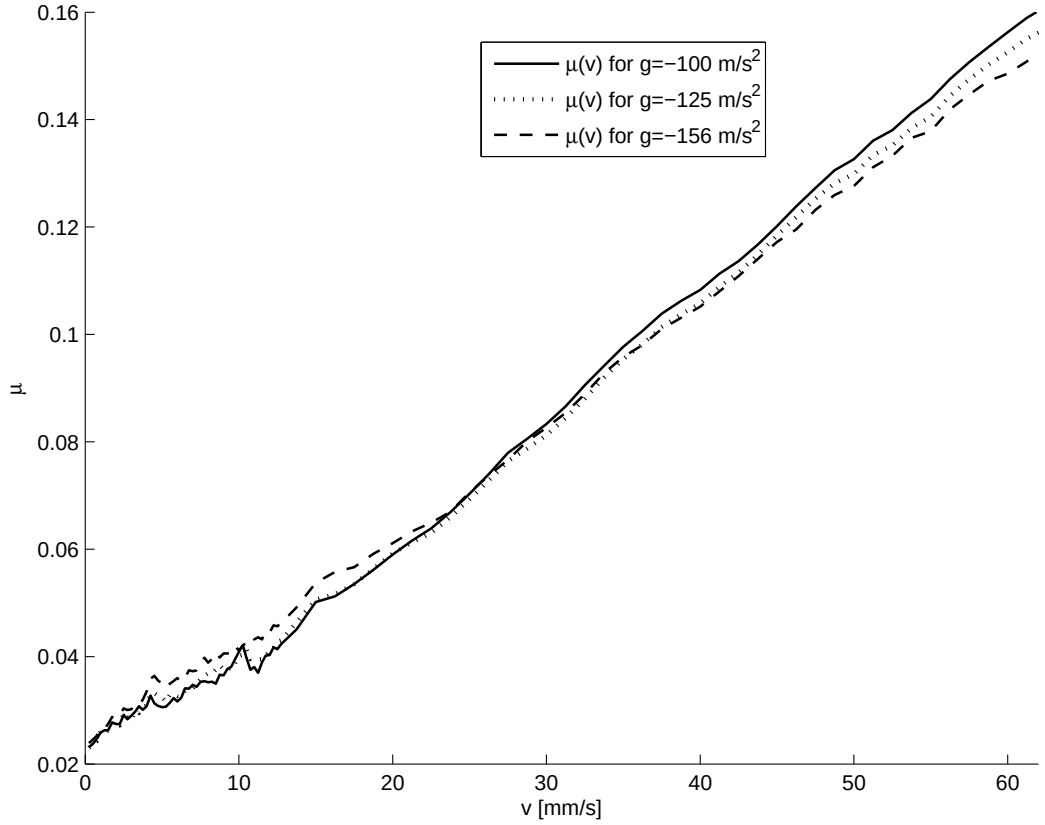

Figure 7.9: The $\mu(v)$ curves for $g = -100\text{m/s}^2$, $g = -125\text{m/s}^2$ and $g = -156\text{m/s}^2$.

$v = 4.2\text{mm/s}$, approximately half the value of the $v_{\mu 1}$. The $\mu(v)$ curve rises fast for $16\text{mm/s} < v < 29\text{mm/s}$ for the $g = -12.5\text{m/s}^2$ curve. It reaches a value greater than for the higher values of N. This increase is ended with a bend reducing the rise in μ with v to approximately the same increase as for the higher normal forces, see Fig. 7.8. This fast increase in μ gradually disappear when N is increased. A more detailed study of the peaks and the reason that the different curves don't overlap is presented in Section 7.5.1.

The $\mu(v)$ curves for the higher values of N seems to be in good agreement with the expectation Eq. 7.20 that μ will increase approximately linear with v. I also expected that the slope of the $\mu(v)$ curve would increase with increasing q. To check if this expectation agrees with the simulations, I have run $\mu(v)$ simulations for q in the range $q = [0.1, 0.6]$ at $g = -50\text{m/s}^2$, a value of g, where $\mu(v)$ begins to have a linear behavior in v. The results is presented in Fig. 7.11. The figure shows that the slope of the $\mu(v)$ curve becomes steeper with increasing q, as expected. The $q = 0.1$ run is only

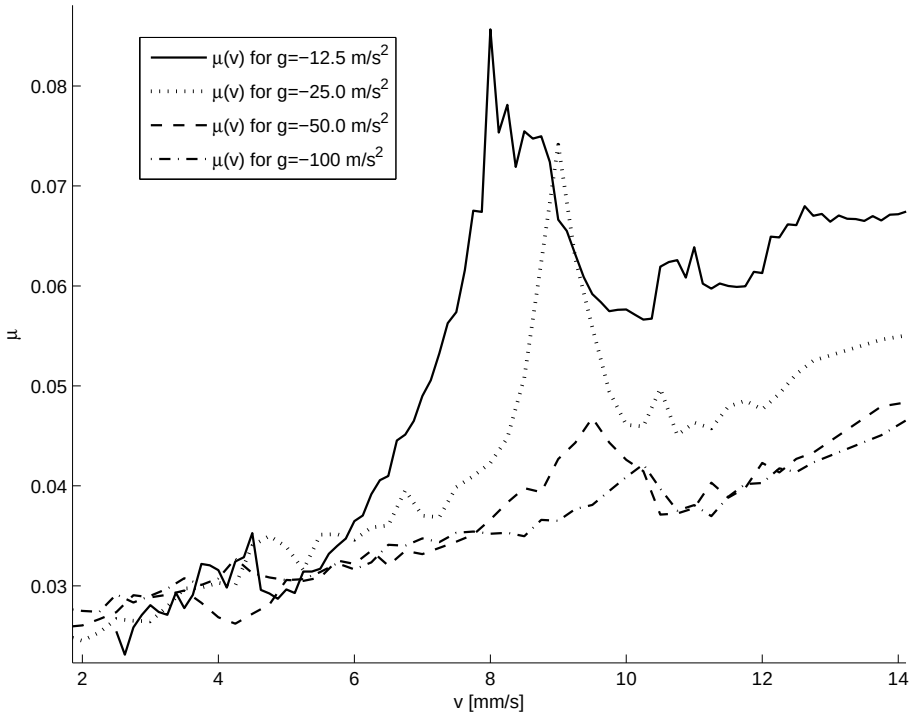

Figure 7.10: $\mu(v)$ around the peak in Fig. 7.8.

included to give a broader range in q and because it seems to agree with the prediction. However at such a low value of q the internal oscillations in the slider may become large, and I don't want to simulate a slider with such a behavior. Thus I will not investigate the shape of the $\mu(v)$ curve for $q = 0.1$ further, even though it shows a velocity weakening effect for low v.

In the low end of v I have searched for a minima level of μ. At very small v, the piston very slowly forces the slider spheres forward past the potential barrier, and then the slider falls down in the next potential well. No rapid motions happens except for the ones occurring when the slider overcomes the current potential barrier. If the same simulation was rerun with half the velocity, the same rapid motion would still occur, and thus I would expect μ to be independent on v for such low v, and therefore a relatively flat minima level of μ for the lowest values of v is expected. It should be noted that such a motion is not considered stable sliding, because the slider may come to a rest after a fast motion before the piston catches up with the slider again, an instability called stick-slip. I have, however, not been able to observe such a lower level in μ. I have run simulations down to $v = 25\mu$m/s, but I have not observed a tendency of a steady value of μ for the lowest values of v. Instead

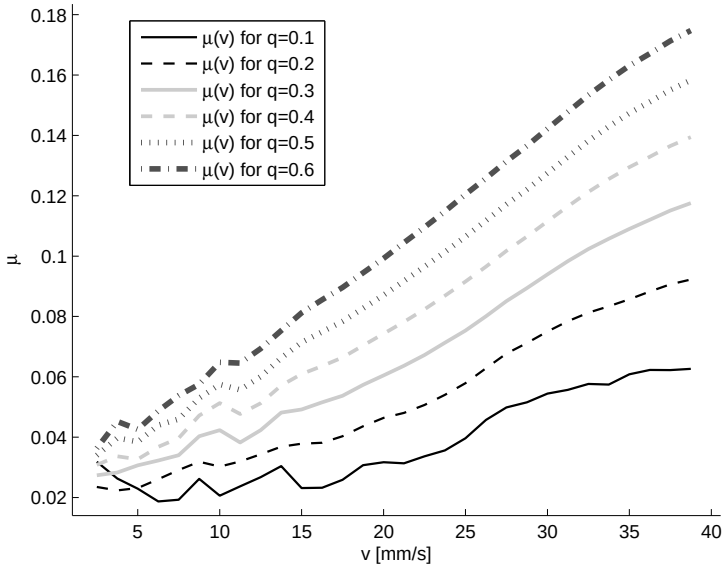

Figure 7.11: The $\mu(v)$ curves for several values of q. All the simulations are run with $g = -50\text{m/s}^2$. The figure shows that $\frac{d\mu}{dv}$ in general increases with increasing q.

I observed the general behavior that μ increases with v, neglecting the spikes. Running simulation at such low values of v is very time consuming. This is because I cannot increase the time step inversely proportional to v for very low v. If I do that, slip motion may not be resolved by a large enough number of time steps leading to numerical instabilities. It may therefore be possible to observe a lower level in μ for $v < 25\mu\text{m/s}$, but I have not spent more time on this.

7.5.1 The spikes for low g.

The peak in the $\mu(v)$ curves seems to increase with decreasing N. In the search for the cause of the peak, I have therefore concentrated the study of the peak for the $g = -12.5\text{m/s}^2$ curve.

Fig. 7.8 shows several interesting behaviors which I have investigated further. The first study of the peak was through a video I made of the system at $v_{\mu 1}$. I noticed that the vertical oscillations of the slider was larger at this velocity than away from the peak. Based on that observation I suspected that the peak in μ was caused by a standing wave occurring at $v_{\mu 1}$. To find out if it was a standing wave that was causing the peak in μ, I studied the

vertical oscillations of the center of mass of the slider. I also compared the oscillations of the center of mass, CM, with the oscillations of the lowermost row in contact with the base and the motion of the top row of the slider. The position of the CM is just the mean of the positions of all the slider particles. To find the position of the bottom and top row, I calculated the average of the position of respectively all bottom and top slider particles.

The motion of the lowermost slider particles is a combination of the interaction with the base-particles and the internal oscillations in the slider. The reason for studying the bottom row motion is because I expect that it will show the average shape of the base, i.e. an oscillation with period l_0, as long as the internal oscillations in the slider is not too large. The CM vertical position is interesting because it tells me how the slider on average responds to the shape of the base. The reason for also to study the vertical motion of the uppermost row is that it is farthest away from the bottom row, and thus it is the row most delayed from the slider base interactions. I expect that a periodic motion of the oscillations in the slider is possible if the three curves have a period that is a integer multiple of each other. I do not expect a pure standing wave because of irregularities in the forces between the base and the slider because of the small random displacements of the base spheres.

In Fig. 7.12 the typical oscillatory motion for the slider at $v_{\mu 1}$ is shown. It is typical because it gives a good representation of the oscillatory motion of the slider over the slided distance. This regular oscillatory motion is, however, not seen for the whole slided distance. After sliding for a time, the standing wave breaks up and a more chaotic behavior is seen. However after a while again, the oscillations builds up to the regular pattern seen in Fig. 7.12 again. To make the regularity of Fig. 7.12 more clearly I have also included a figure comparing the oscillations at $v_{\mu 1}$ and $v = 5.0$mm/s, a velocity where μ in Fig. 7.10 is seen to be relatively low. The comparison is shown in Fig. 7.13. Fig. 7.13 shows that the amplitude of the vertical motion for $v_{\mu 1}$ is several times larger than for $v = 5.0$mm/s. The motion at $v = 5.0$mm/s is also much more chaotic than at $v_{\mu 1}$. The shape of the curves seen in Fig. 7.12 corresponds well with a standing wave. I therefore need to find out what can cause such a standing wave before I can conclude wheter a standing wave is causing the peak or not. For a standing wave to occur there must be a driving force acting on the slider with driving frequency equal to the standing wave frequency of the slider.

A standing wave pattern is present at the peak in μ but not at $v = 5.0$mm/s, thus it seems that the occurrence of the standing wave pattern is dependent on v. The only forces acting on the slider is the force from the base and the force from the piston, and of course the force of gravity which cannot act as a driving force because it is not time dependent. The piston

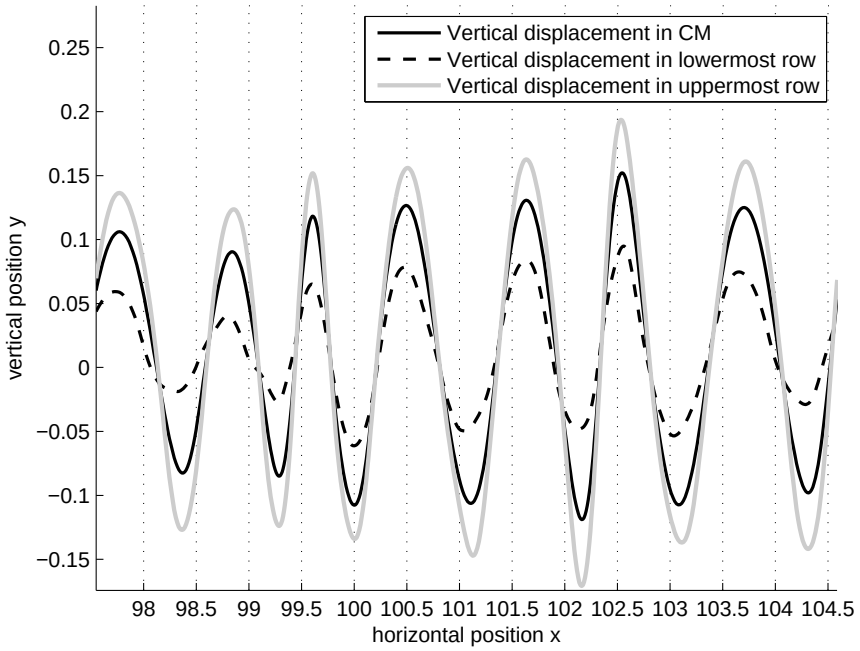

Figure 7.12: A typical image of the vertical displacement of the bottom row, the CM and the top row at $v = v_{\mu_1}$. The vertical displacements are plotted versus the horizontal position of the CM. The first axis is in units of base. The first axis is in units of l_0, i.e. a unity increase in x resembles a slided distance of the l_0. The second axis is in fractions of l_0, i.e. $y = 1$ resembles a vertical displacement of l_0. The three curves shows a clear tendency to oscillate in phase carrying out one period over the length l_0.

moves with a constant velocity and if the base was smooth with a constant μ, any initial irregularities in the force from the piston force would damped out with time. Thus the only candidate left is the force from the base on the slider. The base is composed of identical spheres with a mean spacing of l_0 as earlier described. The spheres is arranged in a sinusoidal wave, but they are displaced with a small random number from the wave to disturb the unrealistic perfect sinusoidal wave. When the slider slides over the base, it must be lifted to be allowed to pass over each of the base spheres. The frequency of the force is the frequency of the collisions between the bottom row slider spheres and the base spheres. This force can act as a driving force, however the random perturbations of the position of the base spheres causes the frequency of the collisions to vary although v is constant. Thus a standing wave may seem to be unlikely. However, since the base spheres

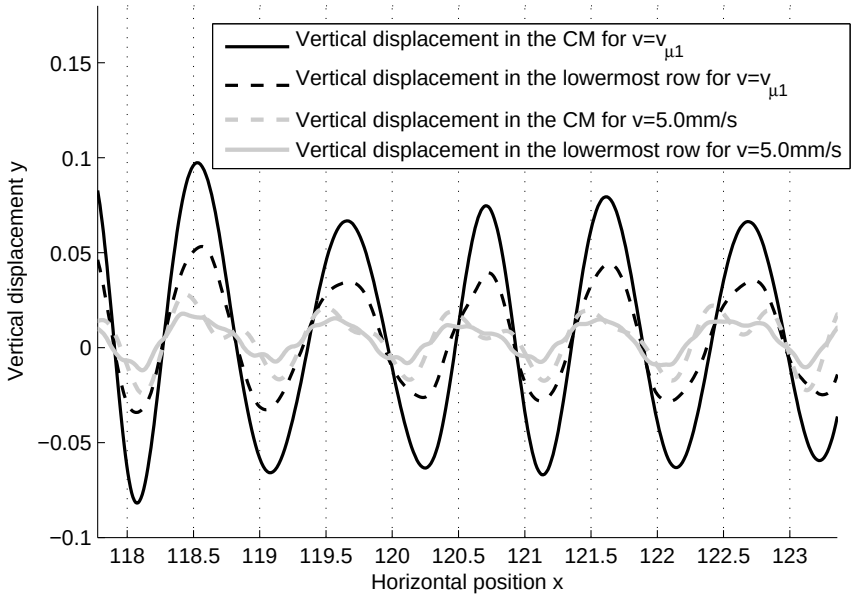

Figure 7.13: A comparison of the oscillations seen in fig. 7.12 compared to the typical oscillations seen for $v = 5\text{mm/s}$. The units of the axis is as presented in Fig. 7.12.

is randomly shifted away from the sinusoidal shaped base, the frequency of the collision of the slider-base-spheres varies around a mean value, and if this value corresponds to the standing wave frequency for the slider, I expect that a standing wave can occur. The inertia of the oscillations in the slider may tolerate small irregularities in the driving force frequency and still maintain the standing wave given that the irregularities are not to large. Looking back on Fig. 7.13 or Fig. 7.12 I observe that the period of the standing wave pattern is in good agreement with the average spacing between the base spheres.

The frequency f of the collisions is given as

$$f \propto v \tag{7.22}$$

since if I increase the speed of the slider I increase the number of base-spheres slided over for a given time, that is I increase f. If the regular oscillatory motion seen in Fig. 7.12 is caused by a standing wave, I would expect that a standing wave would occur at

$$v = nv_{\mu 1}, \qquad n = 1, 2, 3, ... \qquad v = v_{\mu 1}/m, \qquad m = 1, 2, 3, .. \tag{7.23}$$

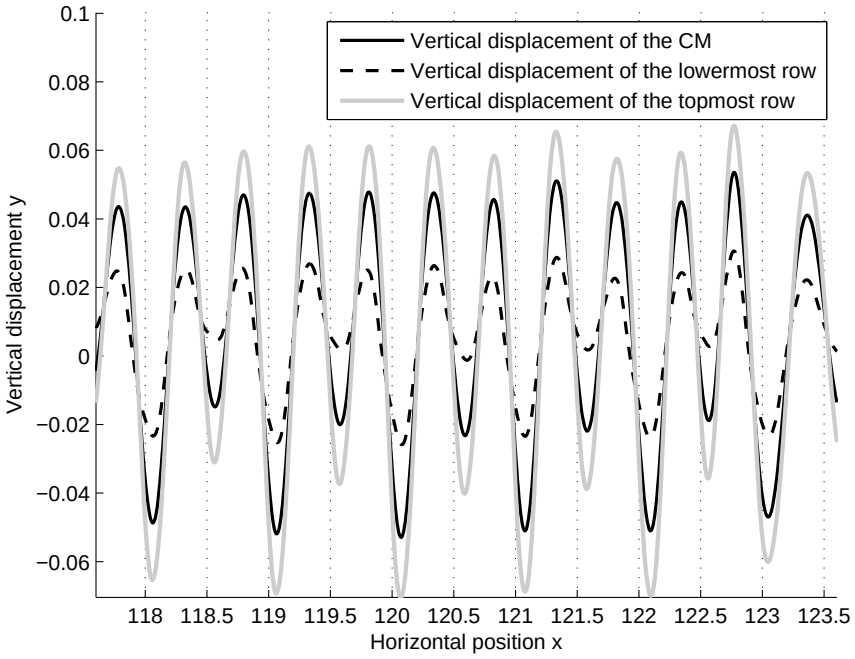

Figure 7.14: The typical behavior of the vertical displacement of the bottom row, the CM and the top row of the slider at $v \approx 0.5v_{\mu_1}$. The vertical displacements are plotted versus the horizontal position of the CM. The three curves shows a clear tendency to oscillate in phase carrying out two periods over the length l_0. The units of the axis is as presented in Fig. 7.12.

using Eq. 7.22. If I neglect the randomness in the base, n is the number of base-sphere slided before the slider CM has completed one period. A standing wave may also occur if the CM undergoes an integer value, m, of periods for each base-sphere slided over. Eq. 7.23 gives an infinite number of possible standing wave velocities, but I expect that the amplitude of the oscillations will die out with increasing m and n. For high sliding velocities the driving force will result in high frequent collisions with the slider. These high frequent collisions will reduce the amplitude of the CM oscillations since they disturb the periodic motion of the CM. For low v the driving force will boost the standing wave every mth period of the CM oscillations, whereas damping always act to reduce the oscillations. Thus I only expect that the oscillations is be important for small values of m and n.

To investigate whether more standing wave patterns could be found I started with searching for a $v = v_{\mu 1}/2$ standing wave pattern, and looking more closely at Fig. 7.10 the small peak around $v = 4.2\text{mm/s} \approx 0.5v_{\mu 1}$ for

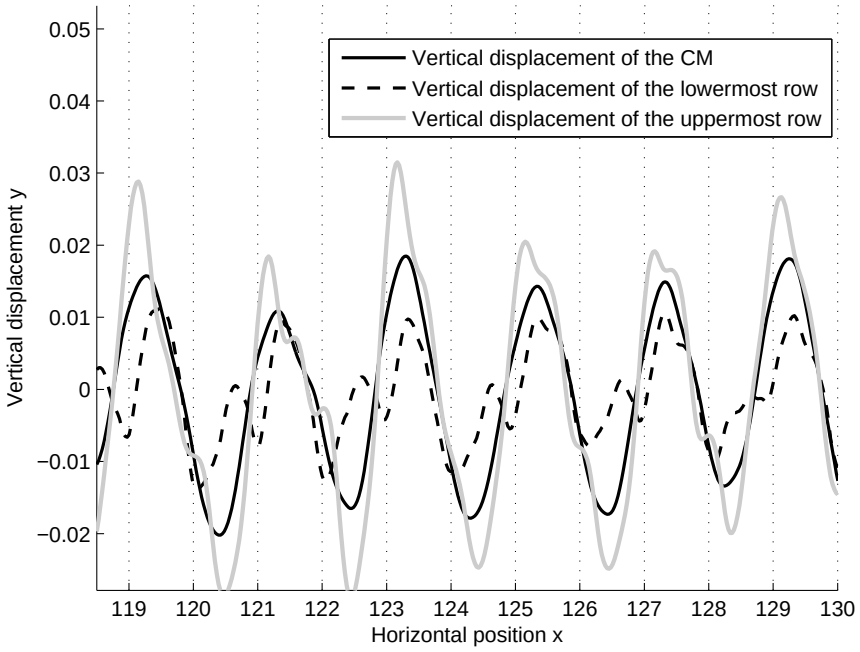

Figure 7.15: The vertical oscillations for a small segment of the slided distance at $v = 17.5\text{mm/s} \approx 2v_{\mu 1}$. The oscillations have a period of approximately $2l_0$ as expected for $v = 2v_{\mu 1}$. The figure is not representative for the whole slided distance since more chaotic behavior is also present. The units of the axis is as presented in Fig. 7.12.

the $g = -12.5\text{m/s}^2$ curve seemed to be a good candidate. A standing wave pattern with $m = 2$ was found at this velocity, and is visualized in Fig. 7.14 with a period corresponding to a sliding distance of $l_0/2$. I have also found a standing wave pattern at $v = 17.5\text{mm/s} \approx 2v_{\mu 1}$. In Fig. 7.15 I have visualized the standing wave pattern found at $v = 17.5\text{mm/s}$ with period corresponding to a sliding distance of $2l_0$. Now that I have found three velocities predicted by Fig. 7.23, I expect there to exist several other velocities giving rise to standing waves as well as the equation predicts.

A standing wave has a relation between the standing wave frequency f_0 and the stiffness k for the slider. We remember from Section 3.2 that the frequency of a damped harmonic oscillator is

$$f_0 = \frac{1}{2\pi}\sqrt{\frac{k}{m} - \frac{\eta^2}{4m^2}}. \tag{7.24}$$

In Section 3.2 I also argued that $\eta = q\eta_c$, where $\eta_c = 2\sqrt{km}$ is the critical

damping, and thus I may rewrite Eq. 7.24 as

$$f_0 = \frac{1}{2\pi}\sqrt{\frac{k}{m}}\sqrt{(1-q^2)}. \tag{7.25}$$

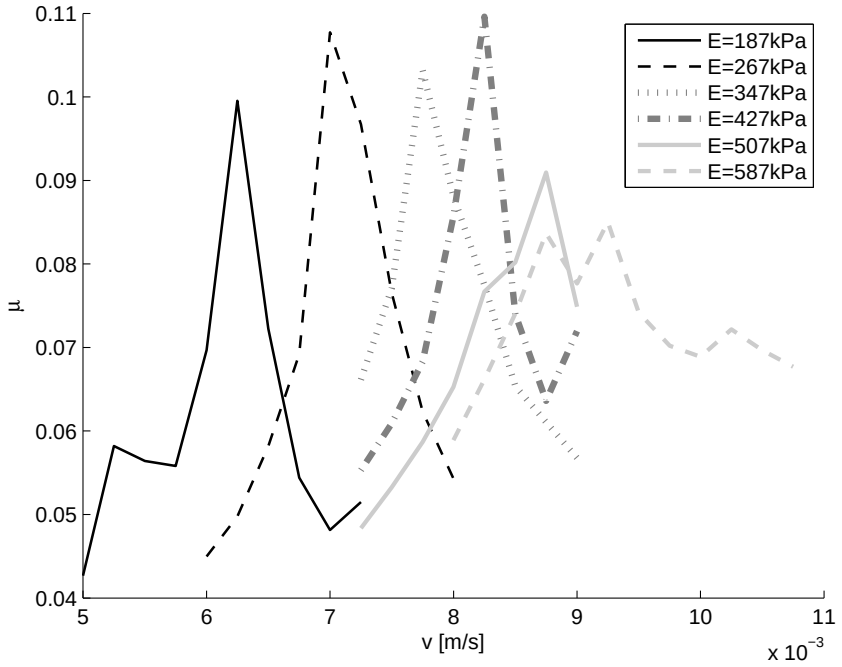

Figure 7.16: $\mu(v)$ plots showing the position of the peaks for different Young's modulus E.

Combining Eq. 7.22 and Eq. 7.25 we observe that the ratio $v/\sqrt{k}$ should be a constant. Thus if a standing wave causes the peak I should be able to obtain a data-collapse if I plot μ versus $v/\sqrt{k}$. Since $k \propto E$, I will plot μ versus $v/\sqrt{E}$ instead. In Fig. 7.16 I have plotted the position of the peaks on the velocity axis for several E. Observe that the peaks are shifted to higher values of v with increasing E. Thus the position of the peaks is dependent on E and f_0 increases with E as I would expect if they are caused by a standing wave. I now try to generate a data collapse to check whether f_0 follows the behavior Eq. 7.25 or not.

In Fig. 7.17 I have plotted the $\mu(v)$ curve versus $E^{-1/2}$. Fig. 7.17 seems to fail to generate a data-collapse, instead it seems that the exponent $-1/2$ has a too large magnitude. It therefore overcompensates for the E dependence by reversing the order of the horizontal position for the different stiffnesses E

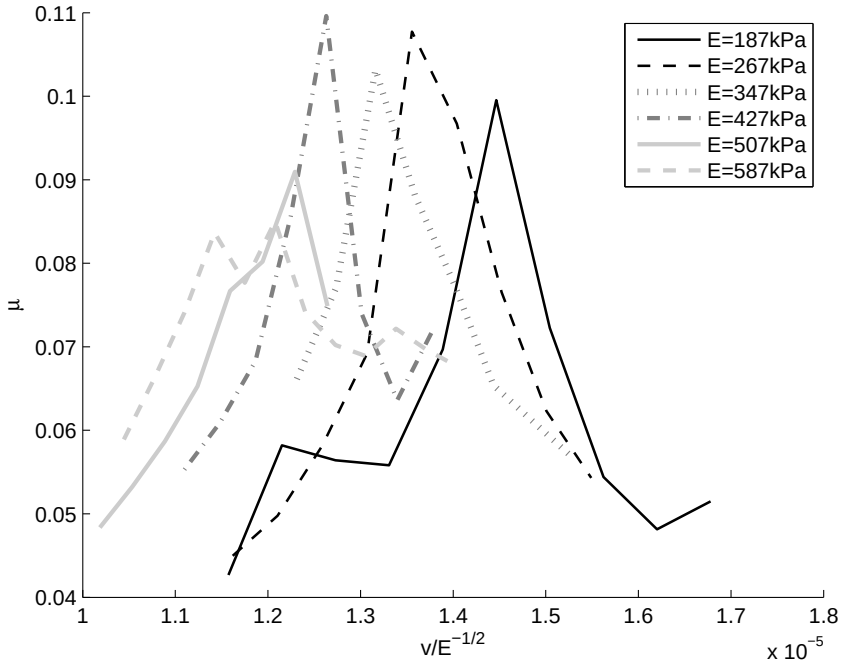

Figure 7.17: The position of the peaks in Fig. 7.16 scaled by $E^{-1/2}$.

relative to Fig. 7.16. I therefore made a second attempt with the scaling $E^{-1/3}$ to see if that would give a collapse. This scaling is presented in Fig. 7.18, and interestingly, this gave a good collapse, for the range in E I have studied. I cannot say that $E^{-1/3}$ is the correct scaling for the position of the peak in μ since that would require me to run simulations with a much wider range in E, but as I have already described earlier running simulations with high E is very time consuming. I cannot choose E too small either because then the system becomes too soft.

Because of the unexpected scaling of position of the peaks, I wanted to do another test. If I now vary q in Eq. 7.25, keeping k constant, the position of the peaks should be shifted towards lower values of v if q is increased. In Fig. 7.19 the dependence of the position of the peak versus q is shown. This figure does not either give the behavior expected from Eq. 7.25. The ratio between the natural frequency for $q = 0.3$ and $q = 0.8$ should be $\sqrt{\frac{1-0.3^2}{1-0.8^2}} \approx 1.59$, and thus possible to see in Fig. 7.19.

After studying the oscillations close to the peak in μ, it became clear that the assumption that the peak in μ corresponds to the velocity giving a standing wave may not be correct. The peak and the standing wave are

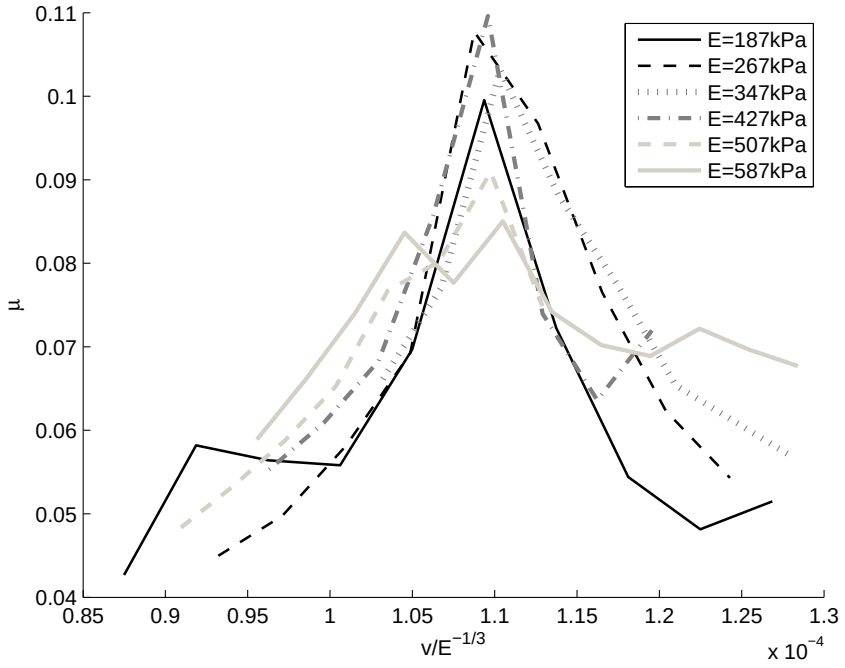

Figure 7.18: The position of the peaks in Fig. 7.16 scaled by $E^{-1/3}$.

related to each other, but does not occur at the same v as I describe below. Let us assume that there is no randomness in the position of the slider, and that we drive the slider at the standing wave velocity. Ideally we would obtain a perfect standing wave. This would result in a given coefficient of friction, but what would happen if I made a small increase in the v? Such an increase would make the natural frequency of the CM oscillations be a little to low compared to the frequency of the collisions between the base and slider spheres. When the lowermost slider row has slided one base particle further and begins to slide up the next one, the CM would not have had time to complete the previous cycle if the CM is oscillating at it's standing wave frequency . Thus the velocity of the CM would point downwards while the lowermost row begins to move up over the next base sphere. After two cycles, the CM would lie even further behind, and so on. Now since the CM is moving downwards at the time the slider needs to move upwards to clear the next base-sphere, the average force on the slider when sliding uphill the base spheres would increase, and thus the the work done on the slider will also increase giving a rise in μ. After a number of cycles the phase difference between the CM and the lowermost slider spheres will force the slider to oscillate with another frequency. A typical pattern seen from the

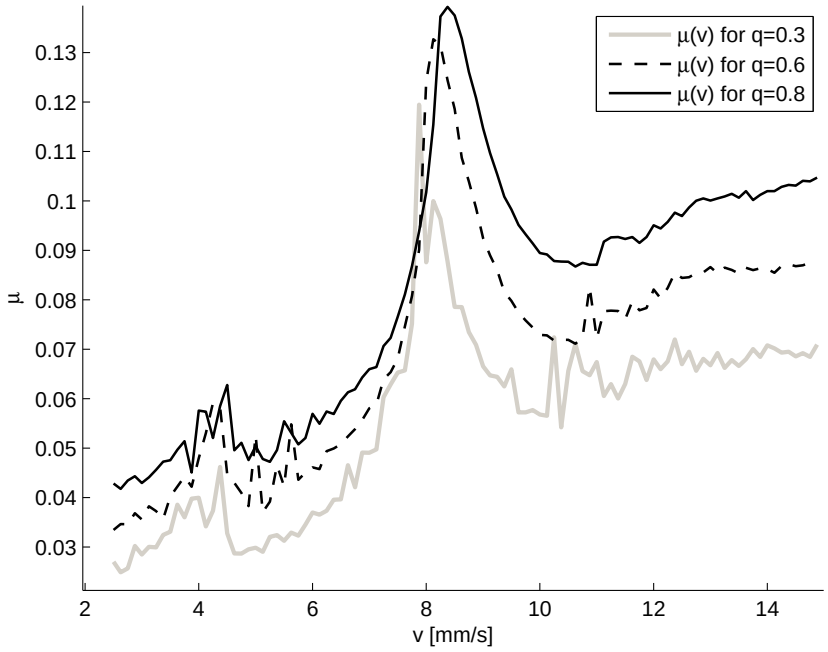

Figure 7.19: The position of the μ peak for different q.

simulations is that the lag of the CM is eventually corrected and the CM is forces into phase with the base. When the slider returns back to oscillate with it's standing wave frequency, the phase difference would then increase again leading to a second correction and so on. To illustrate this behavior I have plotted the oscillatory motion of the slider run at $v_{\mu 1}$ and $v = 7.8\text{mm/s} < v_{\mu 1}$ in Fig. 7.20. The figure illustrates a typical behavior of both the oscillations for $v_{\mu 1}$ and $v = 7.8\text{mm/s}$. The oscillation for the slider at $v = 7.8\text{mm/s}$ is much more stable than the oscillations at $v_{\mu 1}$, and the correction is clearly seen for the $\mu(v_{\mu 1})$ curve indicating that the sliding velocity is higher than the sliding velocity giving the standing wave, thus $v_{\mu 1}$ does not correspond to the standing wave velocity. The above observed behavior is true as long as the sliding velocity is not too much higher than the standing wave velocity. If the sliding velocity is increased further away from the standing wave velocity, the period of the CM oscillations would be too large such that the corrections can no longer help the system maintaining a standing wave behavior.

The velocity v_{μ_1} is dependent on f_0 because f_0 increases the oscillations in the slider. The position of the peak lies above the velocity giving the standing wave frequency f_0. The peak occurs at a velocity where the standing wave behavior is still present and a lot of corrections appear such that the work

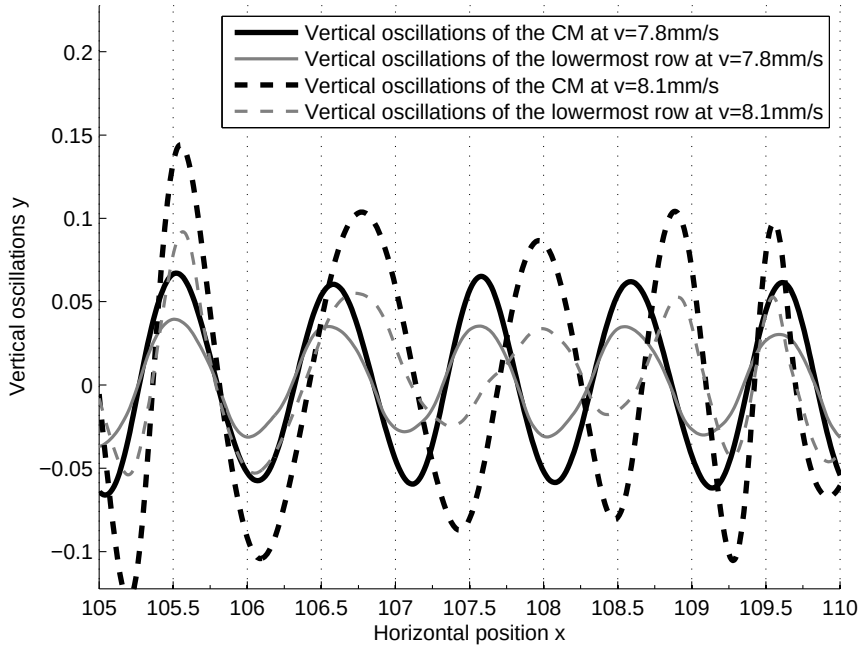

Figure 7.20: The figure shows a comparison between the vertical oscillations for the slider run at $v_{\mu 1}$ and $v = 7.8$mm/s. The black and gray solid lines shows respectively the oscillations for the CM and the lowermost row at $v = 7.8$mm/s, while the black and gray dashed lines shows respectively the oscillations for the CM and lowermost row at $v_{\mu 1}$. The vertical grid is present to clarify that the wavelength of the oscillations at $v = 7.8$mm/s seems to correspond good with the average distance between the base spheres. The wavelength of the oscillations at $v_{\mu 1}$ is longer and does not match the average distance between the base spheres. The phase difference between the CM curve for $v_{\mu 1}$ relative $v = 7.8$mm/s increases as we follow the graphs from left to right, and on the rightmost side in the figure the CM oscillations for $\mu(v_{\mu 1})$ is corrected and brought back approximately in phase with the $v = 7.8$mm/s curve. The units of the axis is as presented in Fig. 7.12.

done on the slider is maximized. The value of q affects the behavior of the slider, and I therefore assumes that it will also have an effect on the distance between the standing wave velocity and the the velocity at the peak in the $\mu(v)$ curve. Thus Fig. 7.19 cannot be used as a measure to see whether the peaks is related to Eq. 7.25 or not, since I have no direct relation between the peak in μ and the velocity giving the peak. The observed scaling $E^{-1/3}$ for the position of the peaks, may also be related to the fact that the peak

does not resemble the standing wave velocity, but I will not pursue this issue further.

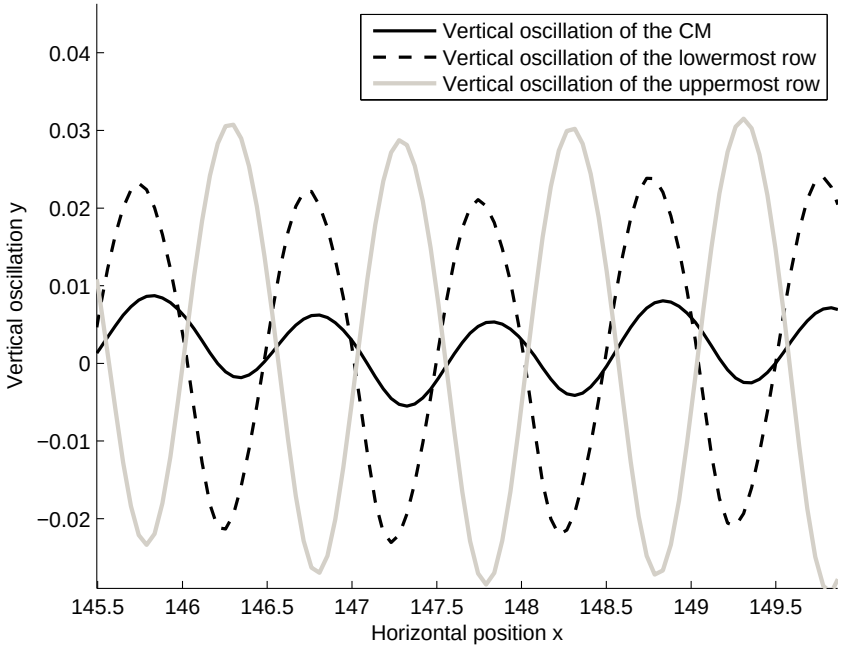

Figure 7.21: The vertical oscillations for a small segment of the slided distance at $v = 0.29m/s$. The oscillations have a wavelength of approximately l_0, the same as I found for $v_{\mu 1}$, but this time the lowermost row an the uppermost row does not oscillate in phase as they did for the standing waves found around $v_{\mu 1}$. Instead the uppermost row lags the lowermost row with a half period. The oscillations in the CM is small compared to the top and bottom row, and is also periodic with a wavelength of approximately l_0, which is the same as the average distance between the spheres in the base. the figure is representative for most of the length slided, but it dies out towards the end of the simulation. The amplitude of the oscillations is only around 10% of the amplitude seen for $v_{\mu 1}$.

Now that the origin of the spike at $v_{\mu 1}$ is understood, I turn over to investigate the bend seen at the greater sliding velocity $v \approx 29mm/s$. It is unlikely that this bend is a result of Eq. 7.23 since it would require a larger value of m than the slightly elevated μ region for $m = 2$ at $v \approx 18mm/s$. I have already argued that the peak is most noticeable for $m = 1$, and that it dies out with increasing m. In Fig. 7.22 the $\mu(v)$ curve for $g = -12.5\mathrm{m/s}^2$

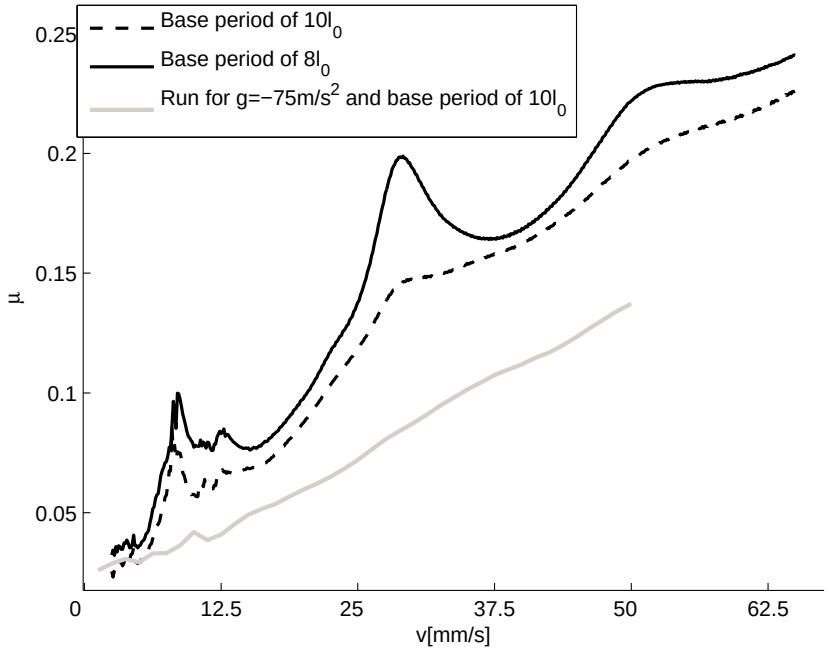

Figure 7.22: The $\mu(v)$ curve for $g = 12.5\text{m/s}^2$ as seen in fig. 7.8 plotted together with a simulation run with the same parameters, except that the base has a wavelength of $8l_0$, and a comparison with the $\mu(v)$ curve obtained for $g = -75\text{m/s}^2$. The $\mu(v)$ curve for the original base with wavelength of $10l_0$ shows a clear peak at approximately $v = 8\text{mm/s}$. Around this peak. At $v \approx 29\text{mm/s}$ a bend in the $\mu(v)$ curve can be seen, and a second less noticeable bend may be seen at $v \approx 53\text{mm/s}$. The $\mu(v)$ curve with base wavelength $8l_0$ enhanced the two bends at $v \approx 29\text{mm/s}$ and $v \approx 53\text{mm/s}$ for the original $10l_0$ base period run.

is shown together with the $\mu(v)$ curve obtained with the same parameters except that the base has a wavelength of $8l_0$. A comparison with a $\mu(v)$ curve with $g = -75\text{m/s}^2$ and an original wavelength of $10l_0$ is also included in the figure. The curve with wavelength $8l_0$ is included since it enhances the bends seen in the $10l_0$ curve at $v \approx 29\text{mm/s}$ and $v \approx 53\text{mm/s}$. The enhancement seems to be at it's greatest at a period around $8l_0$, and choosing a shorter base period decreases the enhancement of the bends.

I have used the same procedure to study the bend at $v \approx 29mm/s$ as I used to study the peak in μ at $v_{\mu 1}$. Since the bend is enhanced to a rounded peak for the $\mu(v)$ curve with base-wavelength of $8l_0$, I started with studying the oscillations at the top $v \approx 29mm/s$ for the $8l_0$ curve. The results of the

simulations revealed a periodic behavior as seen in Fig. 7.21. The oscillations seen in the slider is a higher order standing wave than what is seen around the peak at $v_{\mu 1}$. At $v_{\mu 1}$ the lowermost row, the topmost row and the CM oscillated in phase, while for $v \approx 29$mm/s the top row lags the bottom row with half a period and the oscillations in the CM is very small. To check that this standing wave is the cause for the bends in the $10l_0$ period base, I also ran the simulation again for this default base. When I studied the oscillations, I found the same standing wave as seen in Fig. 7.21. The difference between the $8l_0$ and the $10l_0$ run was that the standing wave existed for almost the whole slided distance for the $8l_0$ run, while it was repetitively created and destroyed for the $10l_0$ run resulting in a larger fraction of the slided length with a more chaotic behavior than for the $8l_0$ run.

7.6 Summary

In this chapther I have found that the dependence of μ on v for geometric sliding friction is approximately

$$\mu \propto v. \tag{7.26}$$

However, for small N, i.e. $|g| < 100\text{m/s}^2$ I have found a more irregular behavior for the dependence of μ on v, and I have in Section 7.5.1 argued that this behavior stems from standing waves in the internal slider springs because of the regularity of the base. Thus there is a transition in μ from being dependent on the spacing between the base spheres for $|g| < 100\text{m/s}^2$ to being more dependent on v for $|g| > 100\text{m/s}^2$. I have also found that Eq. 7.26 is not valid for large compressions of the slider-base springs in which the slider begins to plow through the base spheres, see Section 7.4.1.

In this chapter I have seen that the contribution of the standing wave motion on μ varies with the stiffness of the system E and for example the base period. Thus if I would study how μ depended on other parameters such as E, I would also need to investigate the standing wave motion of the slider system in detail. This makes it difficult to investigate how μ depends on E excluding the standing waves. It would be better to make improvements to the base. Because of the limited time I have on this project I have therefore decided not to investigate how μ depends on for example E.

Chapter 8

Sliding friction with adhesion

8.1 Introduction

Adhesion is the binding between particles creating attractive forces that tends to cling the particles together. Until now I have only allowed compressive spring forces between asperities connecting the slider to the base. Now that I introduce adhesion, I also allow tension in these springs. In Section 2.1.2 I presented the model of Bowden and Tabor [5,6] for the frictional force caused by adhesion

$$F = sA_r, \tag{8.1}$$

where s is a material property and A_r is the real area of contact, and the two were considered independent on time and v. In Section 2.2 I presented the rate and state theory of friction, where

$$\mu = s(v)A_r(\theta), \tag{8.2}$$

where s is dependent on v and A_r is dependent on θ (time). When I run the simulations I want the frictional force to come out as a result of the interactions between the slider and the base. However, I have not constructed a model for plastic deformations in the simulation code, a deformation process that has been found to be important at junctions [13]. In addition I have not chosen l_0 low enough to resolve junctions (remember that junctions has an diameter on the order 10^{-6}m while I use $l_0 = 10^{-4}$m). Therefore I cannot expect adhesion to come out as a result of the model, and instead I must explicitly introduce adhesion to the system. Eq. 8.1 and Eq. 8.2 is formulas for calculating the macroscopic effect of sliding, i.e. the frictional force, and I therefore does not use them to calculate μ in my simulations. Instead I apply a modification of the two equations at each junction. I introduce $A_{\mathrm{r,junction}}$ as the area of contact at a junction. In Section 8.2 I let $A_{\mathrm{r,junction}}$ be a

constant not dependent on time, as suggested by Eq. 8.1, and in Section 8.3 I let $A_{\mathrm{r,junction}}$ be time dependent as suggested by Eq. 8.2. Then I am able to investigate the effect of asperity creep at the junctions versus a constant contact area at every junction.

It should be noted that I denote every bound base slider pair as a junction, and that the area A_r is only calculated based on predefined formulas. It could also have been modified by the overlapping area of the spheres in contact, however then the adhesive force would be dependent on the modeling of the particles, an effect I don't want to introduce.

8.1.1 Introducing adhesion at the junctions in the model

I introduce F_{ad} as the maximum tension in the springs at a junction. The equation I use to relate F_{ad} to $A_{\mathrm{r,junction}}$ is essentially the same as Eq. 8.1

$$F_{ad} = sA_{\mathrm{r,junction}}. \tag{8.3}$$

F_{ad} results in a stretch of the spring

$$d_{\mathrm{ad}} = \frac{F_{\mathrm{ad}}}{k_{\mathrm{ad}}}, \tag{8.4}$$

where k_{ad} is the stiffness of the adhesive spring. When the adhesion limit d_{ad} is exceeded, the bond will break, and the junction is destroyed. The equations of motion found in Section 3.7 is still valid, however $k_{bs,ij}$ in Eq. 3.14 needs to be modified to introduce adhesion. That is I redefine $k_{bs,ij}$ as

$$k_{bs,ij} = \begin{pmatrix} k_{\mathrm{bs}} & |\vec{r}_i - \vec{r}_j| - d_{\mathrm{bs}} < 0 \\ k_{\mathrm{ad}} & 0 < |\vec{r}_i - \vec{r}_j| - d_{\mathrm{bs}}0 < d_{\mathrm{ad}} \\ 0 & else \end{pmatrix}. \tag{8.5}$$

Since the simulation program only use non-dimensional parameters it should be noted that F_{ad} is related to the non-dimensional force F'_{ad} by the relation

$$F_{\mathrm{ad}} = F'_{\mathrm{ad}} \frac{m_0 l_0}{{t_0}^2} = F'_{\mathrm{ad}} \frac{\pi \rho l_0^4}{6{t_0}^2} \tag{8.6}$$

The total adhesive force on the slider is given by the number of junctions and the stretch in each junction. The coefficient of friction μ is therefore the result of a combination of the adhesion and the geometric repulsive forces from the base.

Since I have already discussed the dependence of μ on v for pure geometric sliding friction, it should be possible to extract the effect of adhesion by comparing the simulation runs run with and without adhesion.

The stiffness of the adhesive spring $k_{\mathbf{ad}}$

When I started to introduce adhesion in the simulation code I used $k_{\mathrm{ad}} = k_{\mathrm{bs}}$. Remember that k_{bs} is the spring stiffness of the base slider springs under compression. For this choice of k_{ad} I was however only able to run stable simulations for adhesive forces giving only minor differences from the purely geometric case. For larger adhesive forces the sliding movement became increasingly violent, thus making the sliding unstable.

To find the cause of this problem I tried to estimate the frictional work done because of adhesive forces, based on the work-averaged algorithm Eq. 7.10. The work W done when two spheres slide relative to each other is dependent on the change in the radial distance between the slider and base sphere forming the junction. No work is done if there is just an angular movement. Thus it is easy to calculate the work done to adhesion W_{ad} between two spheres

$$W_{\mathrm{ad}} = \int_{r_0}^{F_{\mathrm{ad}}/k_{\mathrm{ad}}} k_{\mathrm{ad}} r dr = \frac{k_{\mathrm{ad}}}{2} |_{r_0}^{F_{\mathrm{ad}}/k_{\mathrm{ad}}} r^2 = \frac{{F_{\mathrm{ad}}}^2}{2k_{\mathrm{ad}}} \sim k_{\mathrm{ad}}^{-1}, \tag{8.7}$$

where r_0 is the rest length of the spring at the junction. Eq. 8.7 states that $W_{\mathrm{ad}} = \frac{{F_{\mathrm{ad}}}^2}{2k_{\mathrm{ad}}}$ giving that $F_{\mathrm{ad}} \propto \sqrt{k_{\mathrm{ad}}}$ is required to keep W_{ad} constant. Since I am not able to obtain large enough W_{ad} without choosing a too large F_{ad}, I can reduce k_{ad} to obtain larger values of W_{ad}. To enhance the effect of adhesion I therefore set $k_{\mathrm{ad}} = k_1/3$. This was however just meant to be a temporary solution, but I have however forgot to run a new "calibration" of k_{ad} and the simulations presented are therefore run with $k_{\mathrm{ad}} = k_1/3$. From the above explanation it should be noted that the work done to adhesion is dependent on k_{ad} because I introduce a upper limit of the force at a junction, and not on the work done by the tension forces.

8.2 Constant adhesion

The simplest form of adhesion is a binding that occurs at every junction and has a constant value, thus $sA_{\mathrm{r,junction}}$ in Eq. 8.3 equals a constant C The adhesion limit for a junction is then

$$F_{ad} = C, \tag{8.8}$$

In Fig. 8.1 I have plotted the $\mu(v)$ curve with $C = 2.96\mu$N, $C = 4.93\mu$N and $C = 6.41\mu$N in addition to the purely geometric curve. The figure shows that the adhesion increases μ relative the pure geometric friction curve. The figure also reveals the peaks in μ which I have studied earlier. A velocity

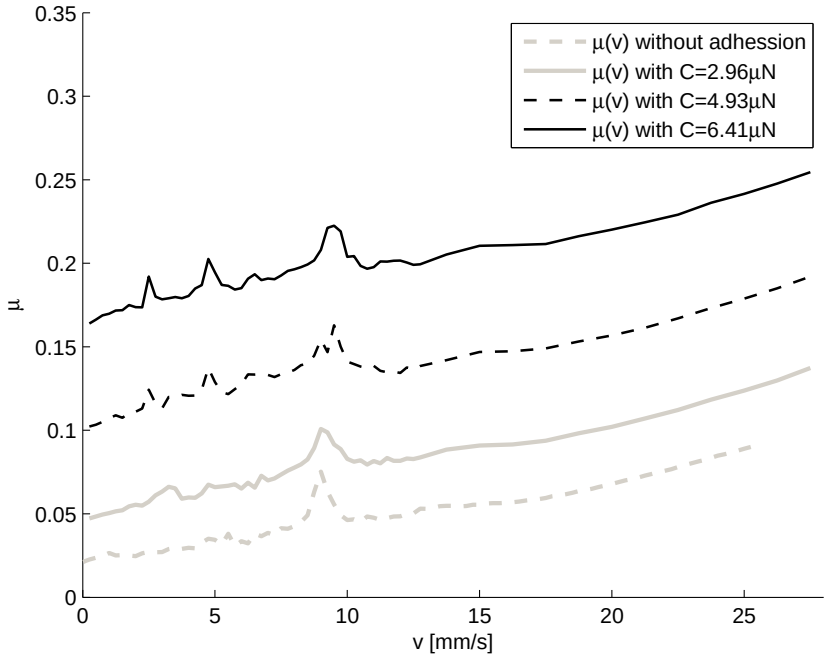

Figure 8.1: The $\mu(v)$ curve with the adhesion term Eq. 8.8 (upper) and for the purely geometric case (lower). $g = -25\text{m/s}^2$ for both runs. The adhesion term seems to give an equal contribution for all v.

weakening effect on μ as found in experiments [3, 4] is however not observed for the $\mu(v)$ curves in Fig. 8.1. Instead it looks like the elevation in μ is more or less constant for all v for a given C. I now introduce $\Delta\mu_C$ as the difference between μ with adhesion constant C and μ for the geometric case. In Fig. 8.2 I have plotted $\Delta\mu_C$ for the different values of C. The figure reveals that $\Delta\mu_C$ is rather constant for the whole range of v studied, except for some bumps which I expect is related to the standing wave phenomenas I have discussed earlier. Remember that the standing waves caused a increase in the vertical displacement of the slider. This gives a larger compression of the slider base interface at the negative displacement of the oscillation than when no standing wave occurrs. This compression enables more junctions to be formed, and thus an elevation in the $\Delta\mu(v)_C$ curve is expected.

In Fig. 8.2 I observe that $\Delta\mu_C$ has a non-linear behavior in C. In Eq. 8.7 I calculated the work done to adhesion, and I found that $W_{\text{ad}} \propto F_{\text{ad}}^2$. To check whether this is consistent with the non-linear observation I calculate $\Delta\mu/C^2$ for the three curves. The result is presented in Table 8.2. Table 8.2 is in very good agreement with the expected adhesive work done in Eq. 8.7, and

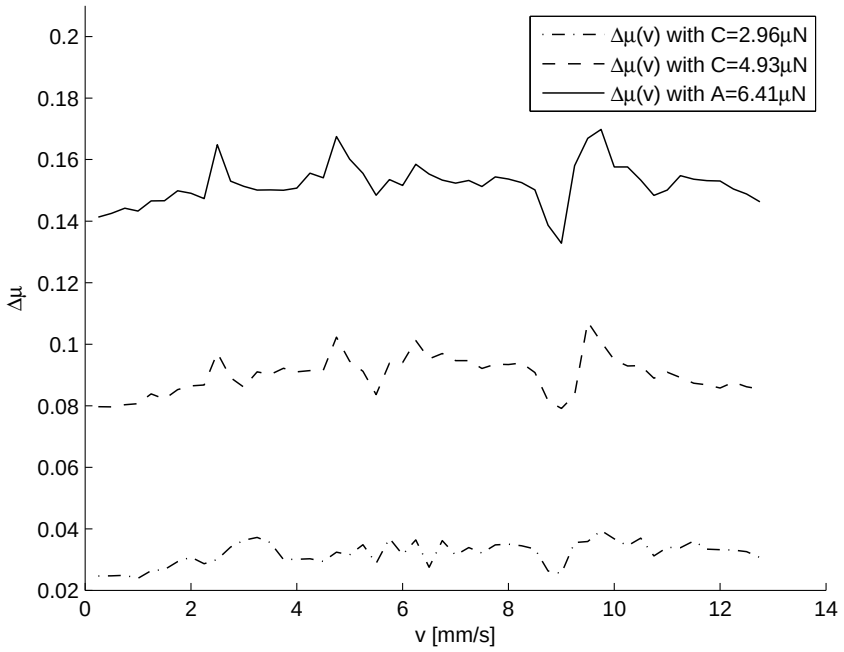

Figure 8.2: The $\Delta\mu(v)_A$ curves for different adhesion constants C

thus the three curves shows the behavior that $W_{\text{ad}} \propto F_{\text{ad}}^2$. However I have not made a sufficient amount of simulation runs to conclude with that this is the general behavior of the $\mu(v)$ dependence. At large C I expect that the large adhesive forces might pull the slider more down in the base compared to smaller adhesive forces, and thus the number of junctions formed during sliding would be dependent on C.

The result that $\Delta\mu$ seems to be rather constant for the range of v is not surprising. The total adhesive work done is dependent of the number of junctions formed during sliding. Each junction gives a contribution W_{ad} as

C	$\Delta\mu$ (mean value)	$\Delta\mu/C^2$
2.96μN	0.0320	$3.65 * 10^9/\text{N}$
4.93μN	0.0900	$3.70 * 10^9/\text{N}$
6.41μN	0.152	$3.69 * 10^9/\text{N}$

Table 8.1: $\Delta\mu/C^2$ for three different values of C.

described in Eq. 8.7. I therefore expect

$$\Delta\mu \propto nW_{\mathrm{ad}}, \tag{8.9}$$

where n is the number of junctions formed over the distance μ is averaged over. Since $\Delta\mu$ is relatively constant over the range in v studied I get from Eq. 8.9 that n is more or less independent on v. The number of junctions is primarily determined by the normal force N, and thus for a given N I expect the number of junctions to be more or less constant when changing v, resulting in a adhesive contribution to μ approximately independent on v.

However for small v, the slider has time to sink down into the base before the next base sphere is hit, and thus one could expect that a larger number of junctions could be formed in this case, leading to a velocity weakening effect on the $\mu(v)$ curve. However, this is not observed for the parameters I have chosen to use.

Now that I have found the contribution to μ for a constant adhesion limit F_{ad} I turn over to the case where A_r is time dependent.

8.3 Time dependent adhesion

The second and more advanced form of adhesion in the slider-base-system is a binding that occurrs at the time t_0 a slider-sphere comes in contact with a base-sphere and then builds up with time. In Section 2.2 I described that the real area of contact has experimentally been found to increase logarithmically with the time of stationary contact [3, 4], and from the rate and state theory of friction I described that $F = s(v)A_r(\theta)$, with

$$A_r(\theta) = A_0 \left[1 + \beta \ln\left(\frac{\theta v_0}{D_c}\right)\right]. \tag{8.10}$$

Although both experiments and Eq. 8.10 suggest a logarithmic dependence of A_r in t I have instead used a exponential function in t for the A_r curve

$$A_{\mathrm{r,junction}}(t) = A_0 \left(1 - exp\left(\frac{t_0 - t}{\tau_0}\right)\right) \tag{8.11}$$

where A_0 is the maximum value of $A_{\mathrm{r,junction}}$, and τ_c is the time it takes before $A_{\mathrm{r,junction}} = (1 - \exp(-1))A_0$. Note that $A_{\mathrm{r,junction}}(t - t_0 = 0) = 0$. I could also have introduced a nonzero value of $A_{\mathrm{r,junction}}(t - t_0 = 0)$, however this contribution is already discussed in Section 8.2, and I have therefore not chosen to introduce such a constant in Eq. 8.11.

The reason for not using the logarithmic time dependence of $A_{\mathrm{r,junction}}$ is that Eq. 8.11 does not diverge for $t - t_0 \to \infty$, thus giving me control of the maximum value A_0. In addition Eq. 8.11 introduces a characteristic buildup time τ_c of the adhesion term that is easy to change. It should be noted that a logarithmic and an exponential function has a major difference, that is $\ln(t)$ and $\exp(t)$ increases respectively slower and faster in t than any power law. That said Eq. 8.11 and a logarithmic increasing function in t share the property for $t - t_0 > 0$ that they are both strictly increasing with a strictly decreasing slope.

With the use of Eq. 8.11 and Eq. 8.3 I get

$$F_{\mathrm{ad}}(t) = F_{\mathrm{ad,max}} \left(1 - exp\left(\frac{t_0 - t}{\tau_0}\right)\right), \tag{8.12}$$

where $F_{\mathrm{ad,max}} = sA_0$, and s is considered a material parameter. Eq. 8.12 has the property that $F_{\mathrm{ad}}(t) \to F_{\mathrm{ad,max}}$ for $t - t_0 \to \infty$ and $F_{\mathrm{ad}} \to 0$ for $t - t_0 \to 0$.

8.3.1 Stability problems when introducing time dependent adhesion

A stability problem occurred when I introduced time dependent adhesion to the contacts between the slider and the base. When the piston started to accelerate the slider the adhesive forces resisted the push of the piston. Eventually the force from the piston overcame the limits for the adhesion with the result that the slider was slung forward. This made it hard to obtain stable simulations. Since the adhesive forces increases with the time of contact, I first tried to turn the adhesive forces off in the acceleration phase of the piston, and turn the adhesive forces on when v was reached. This made it much easier to accelerate the slider, however it also produced an oscillation in the piston slider interface when v was reached. This problem is similar to the stability problem I encountered when I started with sliding friction simulations, described in Section 7.3. From the analysis presented there I know that rapid changes in F_p can cause unwanted oscillations in F_p. It is therefore not a good idea to turn on adhesion at a given time, since that would drastically increase the frictional force, and thus give a rapid increase in F_p. Instead I decided to introduce adhesion over time by multiplying the adhesive force on each junction in the acceleration phase with the the function

$$m(t) = \frac{1 + \sin\left[(\frac{v_p(t)}{v} - \frac{1}{2})\pi\right]}{2} \tag{8.13}$$

Eq. 8.13 gives $m(t=0)=0$ and $m(t \geq t_a)=1$ and m gradually increases for $[t=0, t=t_a]$. Eq. 8.13 is similar to Eq. 7.16 and therefore has the property that the change in $m(t)$ is small near $t=0$ and $t=t_a$. The introduction of $m(t)$ has worked well when running time dependent adhesion simulations.

8.3.2 The simulation results

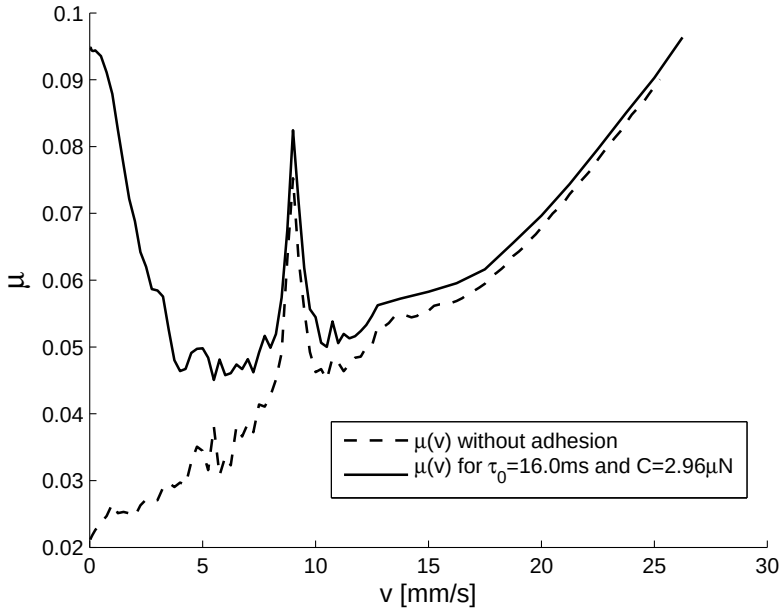

Figure 8.3: The $\mu(v)$ curve with the adhesion term Eq. 8.12 (upper) and for the purely geometric case (lower). $g=-25\mathrm{m/s}^2$ for both runs. The effect of the adhesion term is clearly seen for small v.

In Fig. 8.3, I have plotted $\mu(v)$ with and without adhesion. In the figure I see that the difference between the two curves is greatest for low v. For the high end of v I observe that the adhesion curve approaches the purely geometric friction curve. An interesting observation is that the adhesion term makes μ increase rapidly when v is lowered toward the lowermost simulation values. This is contrary to the purely geometric friction term that can be approximated by a linear increase in v for the range of v I have studied. For the high v the adhesion curve seems to converge towards the purely geometric curve.

I expect the average lifetime of a junction to show the relation $t_{\mathrm{av}} \propto v^{-1}$, since the distance the slider slides in over the time $t-t_0$ is proportional to v.

From Eq. 8.12 we remember that $F_{\mathrm{ad}}(t)$ decays exponentially towards $F_{\mathrm{ad,max}}$ when the lifetime of the junction increase. The slope of Eq. 8.12 with t is

$$\frac{dF_{\mathrm{ad}}(t)}{dt} = \frac{1}{\tau_0} F_{\mathrm{ad,max}} \exp\left(\frac{t_0 - t}{\tau_c}\right), \tag{8.14}$$

and we observe that $\frac{dF_{ad}(t_1)}{dt} > \frac{dF_{ad}(t_2)}{dt} >$, for $t_2 > t_1$ for a given t_0. Thus as $v \to 0$ from above, the slope of $F_{\mathrm{ad}}(t)$ becomes increasingly negative, and $F_{\mathrm{ad}}(t)$ increases rapidly, as seen in Fig. 8.3. In the other end, when $v \to \infty$ $F_{\mathrm{ad}}(t) \to 0$ is expected from Eq. 8.12, and thus $F_{\mathrm{ad}}(t)$ should have negliible contribution to $\mu(v)$. This is seen in Fig. 8.3 where the adhesion curve approaches the purely geometric curve for high v

Varying $F_{\mathbf{ad,max}}$ and τ_0

The adhesion term Eq. 8.12 has two free variables, the strength $F_{\mathrm{ad,max}}$ and the characteristic time of buildup, τ_0. I now present how the $\mu(v)$ curve changes when I make variations in theese two parameters.

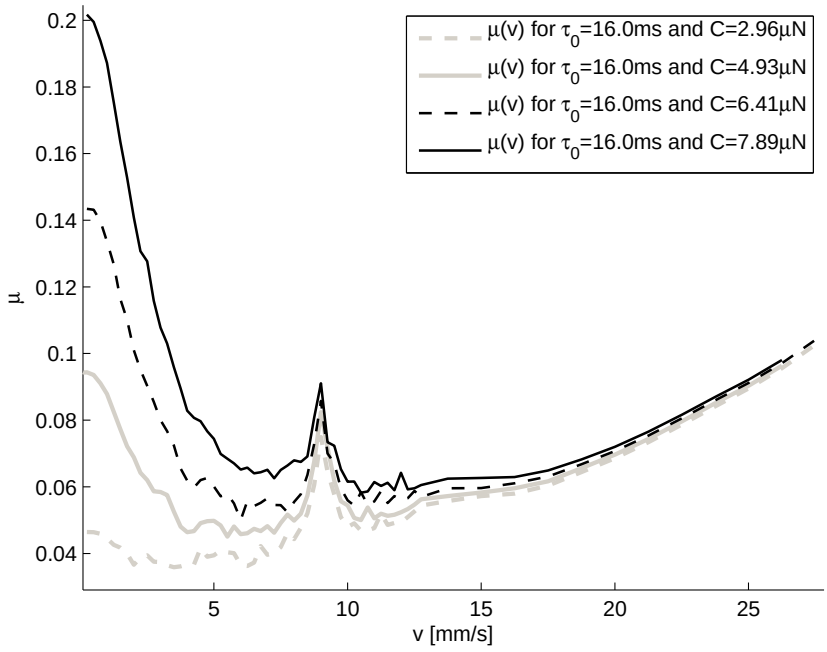

Figure 8.4: The $\mu(v)$ curves for different values of $F_{\mathrm{ad,max}}$. All simulations are run with $g = -25\mathrm{m/s}^2$. Note the geometric standing wave peak at $\approx 8\mathrm{mm/s}$

In Fig. 8.4 I have shown the $\mu(v)$ curves for different values of $F_{\mathrm{ad,max}}$ with $\tau_0 = 16.0$ms. I observe that $F_{\mathrm{ad,max}}$ has an effect on the value of μ obtained for low velocities. From the figure, it is clear that increasing (decreasing) $F_{\mathrm{ad,max}}$ increases (decreases) μ for low v. For the high v limit in the figure, the difference between the $\mu(v)$ curves dies off, and again the curves for different $F_{\mathrm{ad,max}}$ seems to converge towards the purely geometric curve. After the rapid decrease in μ seen for low v a tail in the adhesive contribution to μ is still present, however it gradually disappears as v increases. From Eq. 8.7 we remember that the work done to shear the junction $W_{\mathrm{ad}} \propto {F_{\mathrm{ad}}}^2$. When $v \to 0$ $F_{\mathrm{ad}}(t) \to F_{\mathrm{ad,max}}$, and thus W_{ad} increases with increasing $F_{\mathrm{ad,max}}$ for a given v. This explains why the value μ obtains for low v increases with $F_{\mathrm{ad,max}}$.

In Fig. 8.4 I am, however, not able to observe a plateau value of μ for low v. I would expect such a value to exist since F_{ad} cannot exceed $F_{\mathrm{ad,max}}$. I expect that the reason for not finding such a plateau value of μ is because I have not simulated for low enough values of v, or similarly that τ_0 is chosen too low. I therefore turn over to study the effect on μ when having τ_0 as a free parameter, and check whether I am able to observe such a plateau level for low v with a higher τ_0.

In Fig. 8.5 I have shown the $\mu(v)$ curves for different τ_0. In the figure I observe that τ_c affects how fast μ decays to the purely geometric curve. The lifetime of the tail in the adhesive contribution to μ increases with decreasing τ_0. Thus the difference between the adhesion curve and the purely geometric curve decreases much faster with v for high τ_0 than for the smaller values of τ_0. τ_0 not only determines at what velocity adhesion becomes significant, It also affects the dept in the $\mu(v)$ "well". For the lowermost range in v in Fig. 8.5, the different adhesion curves approach each other, and τ_0 therefore does not seem to affect the maximum value of μ obtained when $v \to 0$. This is better illustrated in Fig. 8.6 where I have zoomed in on the lowermost values of v in Fig. 8.5. The fact that the different adhesion curve approach each other when $v \to 0$ indicate that the value of the exponential $\exp\left(\frac{t_0-t}{\tau_0}\right)$ in Eq. 8.12 is approaching zero, and thus the value of $\mu(v)$ is less dependent on τ_0, and instead approaches a constant value determined by $F_{\mathrm{ad,max}}$. Fig. 8.6 also reveals that the adhesion curves reaches a plateau value for low v, at least down to $v_{\mathrm{min}} = 25\mu$m/s. The plateau is caused by that the average lifetime of the junctions becomes so long that $F_{\mathrm{ad}} \to F_{\mathrm{ad,max}}$.

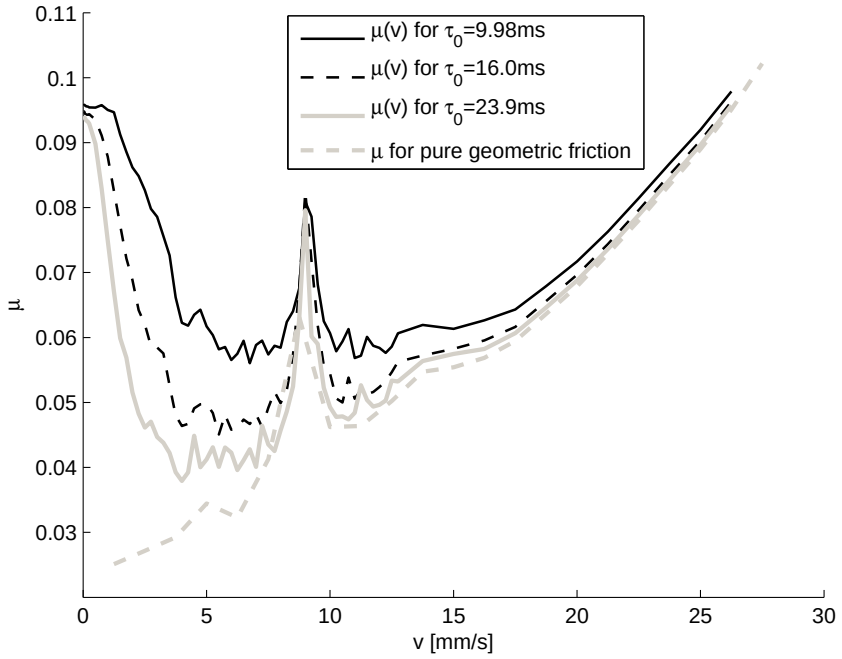

Figure 8.5: The $\mu(v)$ curves for different values of τ_o. All simulations are run with $g = -25\text{m/s}^2$. Again note the geometric standing wave peak at $v \approx 8\text{mm/s}$

8.4 Summary

In this chapter I have studied two different adhesion terms, one that treats $A_{\text{r,junction}}$ as a constant, and one that threats $A_{\text{r,junction}}$ as dependent on time as experiments suggest. For a constant $A_{\text{r,junction}}$ I have found that adhesion gives an approximately constant contribution to μ for v in the range I simulated. I argued that the reason for the adhesive contribution to μ to be constant in v is because that the number of junctions formed during sliding is approximately independent on v.

When I introduced an explicit time dependence of $A_{\text{r,junction}}$ in Section 8.3 I observed the velocity weakening effect on μ for low v. The simulations also revealed that when $v \to 0$, μ reached a plateau level, at least down to the lowest simulated velocity, $v_{\min} = 25.0\mu\text{m/s}$. Such a plateau level has not been seen when constant adhesion and geometric friction was used. For high v the contribution of time dependent adhesion to μ dies out.

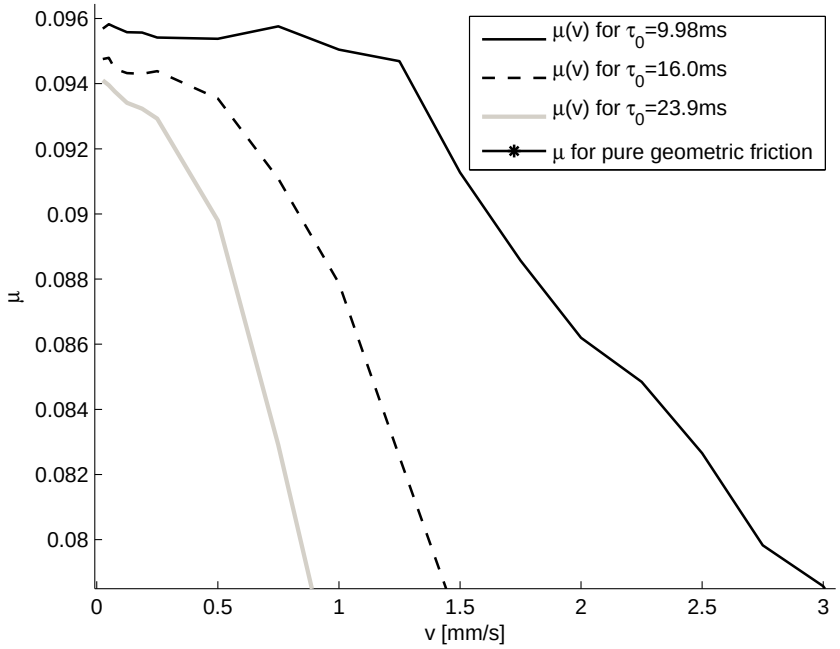

Figure 8.6: This figure is zoomed in on the lowermost sliding velocities in Fig. 8.5. In this region the different $\mu(v)$ curves approaches each other.

Chapter 9

Conclusions and discussions of possible improvements to the slider model

9.1 The dependence of μ on the the sliding velocity

In this project I have found that μ obtains a plateau level for low sliding velocities v. As v increases, μ rapidly decreases and flattens out towards a minima, thereafter increasing approximately linear with v for higher v.

Dry friction sliding has traditionally been considered being nearly independent on the sliding velocity except at high and very low sliding velocities. A velocity independence in μ does not seem to agree with the results I have obtained from the sliding friction simulations, which show that $\mu \propto v$ when the time of contact of asperities is too low for asperity creep to have a noticeable effect on μ. What is causing this disagreement?

The model I have used is a simplification of a sliding friction system. It considers the repulsions caused by asperity collisions, asperity creep and junction adhesion. However, the model does not consider other frictional interactions such as wear and asperity plowing. The model is also two-dimensional, and the stiffness of the slider is unrealistically low. I don't know how these properties would affect the $\mu(v)$ dependence. Thus my results may not show a correct behavior for the dependence of μ on v.

I have found that the slope of the $\mu(v)$ curve increases with the internal damping in the slider. For low damping, the increase in μ with v is not as prominent as for greater damping. Thus it might be that I have chosen the internal damping of the slider too large relative a physical material that

displays a behavior of μ close to independent on v, and that this is causing the disagreement with the traditional view of friction. The choice of the damping coefficient is based more on what I consider practical than on what would be realistic. Running simulations with low damping is problematic since the oscillations in the slider easily become large.

After the rapid decrease in μ for low v, the adhesive tail is still present. Although geometric friction gives a linear increase in μ with v, the adhesive tail gives a decreasing contribution to μ with v. As long as the adhesive tail is present, the sum of the two contributions gives a rather flat $\mu(v)$ curve, neglecting the standing wave spike. For large v where the adhesive tail has died out, the geometric linear increase in μ becomes dominant.

This interval in v where μ seems to be rather independent on μ is not easy to observe because it is not wide compared to the range of v studied and secondly the spike in μ also disturbs the $\mu(v)$ curve in this region. However, the adhesive tail may be enhanced by decreasing τ_0, and thus I expect it to be possible to get a more readily visible flat region in the $\mu(v)$ curve with some adaptions of the parameters used. Thus after a closer look, it seems that the simulations does agree with the traditional view of friction! The results of the simulation may therefore give an explanation of why μ is close to independent on v for low v: After the rapid decrease in μ for very low v, asperity creep gives a decreasing contribution to μ with v while geometric friction becomes increasingly significant. The sum of these contributions makes μ close to independent of μ for an interval in v. It also gives an explains why μ becomes dependent on v for higher velocities, since then asperity creep gives a negligible contribution to μ, and the geometrical friction becomes dominant.

It should be noted that I exclude all other frictional interaction that geometric friction and time dependent adhesion in the above analysis. In the high end of v simulated, I have found that μ increases approximately linear in v. Although this may be correct for an interval in v, I expect plowing and wear of the two surfaces in contact to be significant for the behavior of μ with v for high v. Thus the interactions considered may fail to give the correct behavior of μ for high sliding velocities.

In the next section, the elevation in μ for low v is discussed in more detail.

9.2 The behavior of μ at low sliding velocity

Rabinowicz found in experiments a velocity weakening effect of μ for low sliding velocities [3, 4]. Such a velocity weakening effect of μ for low v is not observed in the simulations run with geometric friction. When I introduced

adhesion in a Bowden and Tabor framework [5, 6] where the real area of contact is considered independent on the time of asperity contact, I could not observe a velocity weakening effect on μ either. It was first when I introduced an explicit time dependence of the area of each junction $A_{\text{r, junction}}$ that I observed the velocity weakening effect on μ for low v. From my results it therefore seems that the Bowden and Tabor framework fails to describe the velocity weakening effect.

The simulations run with time dependent $A_{\text{r, junction}}$ also revealed that when $v \to 0$, μ reached a plateau level, at least down to the lowest simulated velocity, $v_{\min} = 25.0\mu$m/s. I expect this plateau level to be the static coefficient of friction μ_s when only adhesion and geometric friction is considered. Such a plateau level has not been seen when constant adhesion and geometric friction was used. Thus the time dependence of $A_{\text{r, junction}}$ both gives a velocity weakening effect on μ in addition to being able to give a plateau level in μ. The time dependence of the real area of contact represents the effect of asperity creep, and based on my results it seems that asperity creep plays an important role for the transition from the static to the dynamic value of μ. For high v, asperity creep becomes too slow, thus giving an negligible effect on μ. It should be noted that I have described the time dependence of $A_{\text{r, junction}}$ as an exponential equation in t. I would not expect to find such a prominent plateau level for the experimentally found logarithmic dependence on t, since the logarithmic function does not converge for high t. However the slope of the logarithmic function becomes flatter the higher t is, thus a plateau, although not as prominent, would still be possible for low v.

The plateau level of μ as seen for time dependent adhesion in Section 8.3 indicate that it is possible to slide with a very small v without leaving the static regime. Again this might be an effect of using an exponential equation instead of a logarithmic equation in t. Sliding with a static value of μ has, however, been experimentally found to be possible by Rabinowich [3, 4]. Rabinowich found that there is a critical slip distance D_c before the static coefficient of friction breaks down to the dynamic value.

9.3 Discussion of possible improvements to the slider model

For further work with the slider system considered here a development of a 3-D model would be interesting. In the 2-D model when a slider sphere is restricted from moving forward the particles behind it feels very little pull forward. This is different in 3-D since then it exist particles on the sides

which, if not also stuck, would pull on these particles behind a stuck particle. Slip motion in some regions of the slider might now also be observed, and studied in detail.

The slider

The slider I have used in the simulations has a uniform in mass distribution (when not compressed), spring stiffness, and the positions of the spheres is uniformly placed on a grid. Few physical systems displays such characteristics if one does not consider pure crystals, diamonds or models at an atomic level. Introducing some impurities such as a small random contribution to the mass of each element, the spring stiffnesses between the elements, and possibly the rest length of the springs connecting the elements, would therefore make the lattice less regular.

It might also be interesting to add the effect of bond rupture to the slider. For example if the force in a bond internally in the slider exceeds a critical value, it would break.

The base

In this project I have observed that the slider has a standing wave behavior for some sliding velocities. I expected this behavior to be caused by the base being too regular. I would therefore advise to introduce more irregularities in the base, for example by choosing a less regular function than the sinus I have chosen and increasing the random displacements of the base spheres. Increasing the number of spheres resolving the slider and base might be advantageous for this purpose, since then a more complicated shaped base is easier to resolve.

The base slider interaction

The contact between the slider and the base has been modeled by elastic springs. A fully elastic model is however not in good agreement with experiments [13], and a model for plastic deformations might therefore be advantageous to introduce in the model which triggers when the pressure at a junction exceeds the Yield strength of the material considered. A plastic deformation in addition to a more sophisticated shaped base might give a better linearity of the $A_r(N)$ dependence studied in Chapter 5.

In Section 8.2 I did not observe a velocity weakening effect of μ for low v. I would, however, expect the results to be different if I had introduced plastic deformation in the simulations and still treat the area of each junction $A_{\mathrm{r,junction}} = const.$ For low v the slider would now deform because of the

pressure at the junctions, and as more slider spheres comes in contact with the base spheres, more junctions would form, increasing μ. At higher v the slider would not have time to deform in such a way that it would fit on the base, since the shape of the interface changes too fast, and thus μ would not reach the same value as for lower v. In this case the total real area of contact A_r would be a result of the deformations in the system instead of being calculating based on a formula at each junction. I expect that when $v \to 0$ A_r would increase and hopefully give a similar velocity weakening effect and a transition of μ from a static to a dynamic value for low v.

Introducing more frictional interactions

Asperity plowing or wear of surfaces is a frictional interaction that might be introduced in the model. A simplified way of simulating plowing could be to introduce a lowering mechanism of the base asperities spheres slided over. The lowering mechanism could be dependent on for example the pressure at the junction of the base sphere slided over.

Bibliography

[1] Amontons, G., *Histoire de l'Académie Royale des Sciences avec les Mémoires de Mathématique et de Physique*, p.206. (Paris, 1699)

[2] Marone, C., *Laboratory-derived friction laws and their application to seismic faulting* Annu. Rev. Earth Planet. Sci. **26**:643-96 (1998)

[3] Rabinowicz, E., *The nature of the static and kinetic coefficients of friction.* J.Appl.Phys. **22**:1373-1379 (1951)

[4] Rabinowicz, E., *The intrinsic variables affecting the stick-slip process.* Proc. Phys. Soc. **71**:668-675 (London, 1958)

[5] Bowden, F. P. and Tabor, D. *The Friction and Lubrication of Solids:* Part 1. Oxford:Clarendon Press (1950)

[6] Bowden, F. P. and Tabor, D. *The Friction and Lubrication of Solids:* Part II. Oxford:Clarendon Press (1964)

[7] Dieterich, J. H., *Modelling of rock friction: 1. Experimental results and constitutive equations* J. Geophys. Res. 84:2161-68 (1979)

[8] Ruina, A.,*Slip instability and state variable friction laws* J. Geophys. 1983 126:531-54 (1983)

[9] Persson, B. N. J., Totassi, E.,*Theory of friction: Elastic coherence length and earthquake dynamics*. Solid State Communications, 109 (12), p. 739-744. (1999)

[10] Baumberger, T., Berthound, P. and Caroli, C. *Physical analysis of the state- and rate- dependent friction law. II. Dynamic friction* Phys. Rev. B-Condens. Matter **60**:3928-3939. (1999)

[11] Scholz, C. H. and Engelder, T. *Role of aspherity indentation and ploughing in rock friction.* Int. J. Rock Mech. Min. Sci. **13** 149-54 (1999)

[12] Dieterich, J. H. and Kilgore, B. D. *Direct observation of frictional contacts: new insights for state-dependent properties.* Faulting, Friction, and Earthquake Mechanics, Part II, eds. C.J. Marone and M.L. Blanpied. Basel:Birkhauser, pp. 283-302. (1984)

[13] Rubinstein, S. M., Shay, M., Cohen, G., Fineberg, J., *Crack-like processes governing the onset of frictional slip.* MRS Bulletin Vol**33**, p.1181-1189 (2008)

[14] Persson, B. N. J., *Sliding Friction: Physical Principles and Applications* (Springer, Berlin, Heidenberg 1998)

[15] McClelland, G. M., *Adheasion and Friction*, ed. by M.Grunze, H.J. Kreuzer, Springer Ser. Surf. Sci., Vol.**17** (Springer, Berlin, Heidelberg 1989)

[16] Shinjo, K., Hirano, M., Surf. Sci. **283** , 473 (1993)

[17] Braiman Y., Family F., Hentschel G., Phys. Rev. E**53**, R3005 (1996)

[18] Rozman, M. G., Klafter, J., Urbakh, M., *Micro/Nanobiology and its Applications*, ed. by B. Bhushan (Kluwer, Dordrecht 1997)

[19] Elmer, F. J., *Physics of Sliding Friction*, ed. by B.N.J. Persson, E. Tossati (Kluwer, Dordrecht 1997)

[20] Matsukawa, H., Fukuyama, H., Phys. Rev. B **49**, 17286 (1994)

[21] Caroli, C., Noziéres, P., *Physics of Sliding Friction*, ed. by B.N.J. Persson, E. Tosatti (Kluwer, Dordrecht 1996)

[22] Cundall, P. A., Strack, O. D. L., *Discrete numerical-model for granular assemblies* , Geothechnique Vol.**29**, p. 47-65 (1979)

[23] Monette, L. and Anderson, M. P. *Elastic and fracture properties of the two-dimensional triangular and square lattices.* Madelling Simul. Mater. Sci. Eng. **2**, p.53-66. (1994)

[24] Hyun, S. and Robbins, Mark O. *Elastic contact between rough surfaces: Effect of roughness at large and small wavelengths* Tribology International **40**, p.1413-1422 (2007)

[25] Johnson, K. L., *Contact Mechanics* Cambridge University Press (1987)